An analytical model for stiffness degradation of composite laminates with damage under static or cyclic loading

Master of Science Thesis

Carlo Alberto Maria Socci

TUDelft Delft University of Technology

An analytical model for stiffness degradation of composite laminates with damage under static or cyclic loading

Master of Science Thesis

by

Carlo Alberto Maria Socci

to obtain the degree of Master of Science
at the Delft University of Technology,
to be defended publicly on Friday July 19, 2019 at 09:30 AM.

Thesis committee:	Prof. Dr. C. Kassapoglou,	TU Delft, supervisor
	Dr. S. Turteltaub,	TU Delft
	Dr. D. Zarouchas,	TU Delft

An electronic version of this thesis is available at http://repository.tudelft.nl/.

TUDelft
Delft
University of
Technology

No man needs sympathy because he has to work,
because he has a burden to carry.
Far and away the best prize that life offers is
the chance to work hard at work worth doing.

Theodore Roosevelt

Abstract

An analytical model for stiffness degradation of composite laminates with damage under static or cyclic loading is proposed. For static loading, two different modelling approaches have been created. Both account for shear-induced microscopic matrix damage and matrix cracking within each ply orientation of a laminate.

In one approach the residual transverse tensile and shear moduli of a ply are determined by equating the strain energy density of the undamaged ply to that of the ply with damage, for a same applied load. Predictions show excellent agreement with test results for cross-ply laminates, while stiffness degradation is overestimated for shear dominated layups.

The other static approach applies energy equivalence only to the transverse tensile behavior of a ply. For shear behavior, it predicts the residual shear modulus by accounting for the creation of permanent shear strains. Agreement with test results is excellent for cross-ply laminates, and excellent to good for shear dominated layups. The physical foundation behind this model is not as rigorous as the previous one, and as such needs more work.

The proposed fatigue model assumes the matrix strength of a ply to be randomly distributed. Kassapoglou's residual strength model for fatigue loading is used to express fatigue life as a function of matrix strength. The static model is then used to estimate stiffness degradation as a function the same matrix strength. Connecting the two, stiffness degradation as a function of fatigue cycles is obtained. Validation was performed on cross-ply laminates and agreement with results is excellent.

Contents

List of Figures

1
Introduction

The purpose of this research was to create a stiffness degradation model for laminates with damage, under static or fatigue loading. Particular care was put into making sure that the model would be suitable for preliminary design optimization, which requires models to be fast, reasonably accurate, and applicable to a variety of design configurations (meaning little experimental data should be required, and minimal restrictions should be placed on the type of layups being analyzed).

In both industry and academia, there is no shortage of phenomenological models which can predict stiffness degradation for static and fatigue loading, assuming that test data is available for static and fatigue experiments similar in nature to the case they want to predict, as shown in chapter 2. These models might be useful for scenarios like stiffness based structural health monitoring, where the laminate's layup and service spectrum are known in advance and not subject to change. Most of them however may not be suitable for preliminary design, due to the specificity of the experimental data they require to work.

Likewise, there are also many mechanistic models which can predict stiffness degradation for static and fatigue loading extremely accurately, possibly with little need for experimental data. However, it often happens that their computational times are prohibitive for the purposes of preliminary design, or that the model, while fast, is restricted to very specific layups and load-cases.

To fill the gap, static and fatigue models for stiffness degradation are proposed which try to adopt the simplicity and computational speed of phenomenological models without relying on modeling constants or curve fitting parameters. The proposed models also try to follow the mechanistic philosophy of including physics based considerations in the model (eg. for damage initiation), but without modeling damage instances explicitly or undertaking detailed continuum mechanics approaches. Reliance on experimental data is kept to a minimum, with only static tests on ply material and/or standard laminates (eg. [± 45]) being needed. Since the models are fully analytical (and acting at the meso-scale), their computational time is also negligible.

The structure of the report is as follows: a short summary of existing models for stiffness degradation is given in chapter 2. The review is divided into a static and fatigue section. Next, the static models are presented in chapter 3, which ends with extensive validation of the proposed models. Chapter 4 follows with the fatigue model, which is also validated at the end of the chapter. Finally, conclusions and recommendations for future work are given in chapter 5 and chapter 6 respectively.

2

Introduction to stiffness degradation in composite laminates under static or cyclic loading

This chapter serves to provide a brief summary of the literature relevant to this thesis. Since this research investigated stiffness degradation in composite laminates under static or cyclic loading, two sections are present: section 2.1 deals with modeling stiffness degradation under static loading, while section 2.2 covers stiffness degradation under fatigue loading.

2.1. Static Loading

Composite laminates are characterized by the combination of two distinct phases: the fibers and the matrix. The resulting material shows better overall performance (both mechanically and strength-wise) than its constituents alone. Thanks to their directionality (anisotropy), composite materials can also outclass several other (isotropic) materials in terms of strength and stiffness. However, said combination of considerably different materials also results in more complex damage initiation and evolution behavior, which manifests itself in the form of several different types of damage, as opposed to the singular damage type affecting isotropic materials (cracks).

Some of the most common damage types affecting composite laminates are matrix cracking, fiber fractures and delaminations. Unlike the last two, matrix cracking can occur at relatively low loads, well within a structure's "design envelope" [39]. Matrix cracking can significantly reduce a ply's transverse and shear stiffnesses, which in turn can cause degradation of the laminate's overall stiffness and Poisson's ratio [5, 50].

As aircraft manufacturers keep pushing for more efficient designs, stiffness tailoring is likely to become more relevant within the design process, allowing for passive load alleviation, lighter structures, and even wing-morphing in the more distant future. Aircraft operators on the other hand wish to maximize their fleet's useful life. It is therefore likely that future designs will have to account for the interaction of stiffness tailoring and fatigue degradation.

There is no shortage of highly detailed and flexible finite element models, capable of accurately predicting damage propagation and the consequent decay in mechanical properties. The following are examples of finite element models for: matrix cracks [18, 47, 55], delaminations [2, 63], impacts [12, 42, 56] and fatigue [14, 15, 48]. These models are however characterized by long computational times, making them unsuitable for preliminary design and optimization. Likewise, there is no shortage of fast analytical models which can accurately predict specific types of damage, for specific laminate configurations, subject to specific load cases. The following are examples of analytical models for: holes [43, 72], cracks [44], delaminations [49], impacts [16, 17] and fatigue [32, 33, 36]. The obvious downside of such models is that they lack in flexibility, making them once again unsuitable for purposes of design and optimization, which require computational speed just as much as they need flexibility and generality. Additionally, only a portion of the existing stiffness degradation models can account for fatigue. The proposed model is an attempt at closing the gap between flexible but slow FE methods and fast but less accurate analytical ones.

Highsmith and Reifsnider [25] were among the first who tried to rigorously model stiffness degradation due to matrix cracking in off-axis plies. Through a 1D shear lag analysis, the deformation of cracked plies is tied
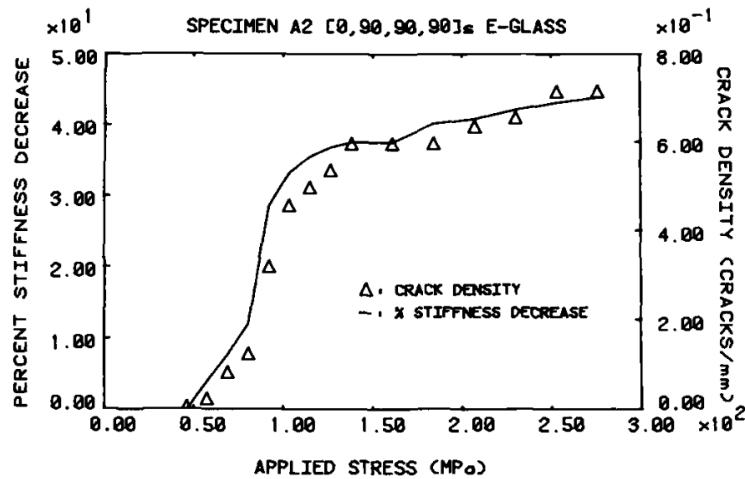
Figure 2.1: Stiffness degradation and matrix crack density as a function of applied stress for a $[0,90_3]_S$ laminate. Taken from [25]

to matrix crack density, which is defined as the number of cracks per unit area within a ply (on the plane perpendicular to fiber direction and aligned with the load). Since only cracks parallel to the fibers are modelled, comparison with experimental results is good for cross-ply laminates under uniaxial tension, but less so for laminates where shear is relevant. A typical stiffness degradation curve for a cross-ply laminate under static tensile loading is shown in fig. 2.1. It can be seen that there is a direct and very close relation between stiffness degradation and matrix crack density. It is typical of cross-ply laminates to show a steep initial drop in stiffness, caused by the rapid appearance of matrix cracks. As the load increases, and with all the weaker regions of the matrix having failed, crack spacing starts stabilizing. Once the distance between matrix cracks is small enough, the stress between them can never be high enough to generate new cracks, causing crack density and stiffness degradation to reach a plateau. This saturation state is known as the characteristic damage state (CDS) [53]

Laws, Dvorak and Hejazi [13, 39] quickly followed. Their model is based on a variant of the self-consistent method, which models cracked ply material as a two-phase medium. The ply's stiffness matrix is expressed as a function of matrix crack density. Unfortunately, according to Hashin [23], the self-consistent scheme assumes the material to be infinite in all directions, negating the possibility of implementing crack opening constraints imposed by adjacent plies, which play an important role in stiffness degradation.

Stiffness degradation due to matrix cracking in cross-ply laminates was treated by Hashin [23, 24]. In the former, Hashin derives the full stress state within cracked off-axis plies by minimizing complementary energy through a variational approach. The laminate's longitudinal stiffness degradation is expressed as a function of matrix crack density, and agreement with experimental stiffness degradation data is excellent. Unfortunately, the model is only applicable to cross-ply laminates under uniaxial tension. In [24] Hashin extends his previous method by allowing cracking (always parallel to the fibers) within the 0° plies. Comparing with the results in [23], the addition of cracks in the 0° plies has almost no effect on the longitudinal stiffness, and a strong effect on the major Poisson's ratio.

Caslini, Zanotti and O'Brien also did interesting work on matrix cracking and stiffness degradation [5]. Their model is much simpler than everything mentioned so far. It is based on a shear lag analysis derived by Ogin et al. in [50], and it relates stiffness degradation to matrix crack density through a closed form expression. Similarly to [23], cracks are only allowed to occur within 90 degree plies embedded in 0° plies. Comparison of predictions with experimental results shows a good match for $[0/90]s$ laminates (predictions are within experimental scatter, but slightly higher than the FEM analysis) and a reasonable match for $[\pm45/0/90]_S$ (where only the 90 degree plies are allowed to crack). While the match is worse than Hashin's, this method is considerably simpler, thus proving that large improvements in simplicity can be obtained with minor compromise in accuracy

Varna, Joffe et al. have also done considerable work in the field [69, 70], based heavily on research by Talreja [59, 61, 62], who developed a synergistic approach to damage modelling combining micromechanics with continuum damage mechanics. The models in [69, 70] rely on material constants which need to be de-

termined from experimental data. Said data should be obtained from a laminate similar to the one being modeled, where all off-axis plies have been substituted with 90 degree plies. For example, validation in [69] was performed on test data from $[0/\pm\theta_4/0_{1/2}]_S$ laminates, where data from a $[0/90_8/0_{1/2}]_S$ laminate was used to determine the model's material constants. The model from [69] gives good predictions for any angle theta where shear stress (and consequently shear damage) is not prevalent, which corresponds to $\theta = 90, 70$ degrees. For $\theta = 55, 40, 25$ degrees predictions are good only when a correction is applied in order to account for unspecified shear damage (assumed by the authors to be of microscopic nature), which requires additional test data from a $[\pm\theta]$ laminate. Hence, aside from the laminate's longitudinal stiffness and Poisson's ratio, the model also tries to predict shear stiffness degradation, albeit in a much more phenomenological fashion. Varna et al. emphasize that shear degradation must be caused by damage modes other than matrix cracking, possibly damage at the fiber-matrix interface [69]. Unlike previous models, [70] also attempts to predict matrix crack density as a function of the applied strains, thus directly linking the decay in laminate's mechanical properties with the applied load. Similarly to what was seen in [69], the match between test data and predictions for the $[\pm\theta/90_4]_S$ laminates analyzed in [70] worsens with the presence of shear stresses, with predictions for $\theta = 40$ degrees being the worst of the group. This emphasizes the presence of damage phenomena (non-linearities) which are exclusive to shear behavior and are absent from 90 degree plies, which experience pure transverse tension (no shear).

Finally, in more recent times, Van Paepegem, De Baere and Degriek modelled the nonlinear shear stress-strain response of GFRP laminates [66, 68]. Their approach, while still making use of continuum damage mechanics, is more phenomenological than the methods presented so far. As such, it requires experimental data from the shear stress-strain response of a $[\pm45]_{2S}$ laminate under tension. The model can predict, for each separate ply, the shear modulus degradation and permanent shear strain due to static loads, regardless of ply orientation. As long as damage is shear dominated, the match with experimental data is excellent. This serves to prove that, with the right choice of experimental data and damage law, it is possible to create a model which is simple, accurate, and reasonably flexible.

From the above literature review, three trends can be discerned. First of all, with the exception of [66, 68, 70], no other work mentioned here makes a direct attempt at linking stiffness degradation to the applied stresses or strains. Instead, stiffness degradation is defined as a function of matrix crack density, which is then left as an independent variable. Obviously, within a design framework, it is desirable to express stiffness degradation as a function of applied stresses or strains. To do that, it would be necessary to perform the extra step of translating the applied loads into matrix crack densities. Apart from being an additional source of error, the extra step could also result in a loss of flexibility. It is pointless to use a flexible and accurate stiffness degradation model if it must be tied to a matrix crack model which is too specific, too inaccurate or too computationally intensive. Secondly, models which require little to no experimental data have to make a tradeoff among accuracy, flexibility and simplicity. Hashin [23, 24] for example sacrifices flexibility and simplicity for the sake of extreme accuracy. Caslini et al. [5] sacrifice some accuracy and some flexibility for the sake of simplicity. Models which require more experimental data can be considerably accurate and simple, like Varna et al. [69, 70] and Van Paepegem et al. [66, 68]. The selection of damage law and type of experimental data can make an enormous difference in the method's flexibility, with Van Paepegem's model being more flexible than Varna's (it is of course noted that they have different scopes).

Finally, relating shear stiffness degradation exclusively to matrix cracking caused by transverse stresses results in poor predictions [25]. When shear stresses are significant, stiffness degradation is more easily associated with other forms of damage, such as fiber matrix debonding [69], driven by shear stresses rather than transverse ones.

The model proposed in this thesis tries to avoid the aforementioned pitfalls, as illustrated in section 3.1, where the model's principles are presented. What is proposed is a "lamina-to-laminate" [51] continuum damage model which, aside from the ply material's mechanical properties, only needs the transverse tensile in situ strength of the ply material (which can be determined from tensile tests of a laminate with 90° plies) and the ply's shear stress-strain curve (monotonic loading up to failure). The model predicts stiffness degradation due to matrix damage caused by static loads, as detailed in chapter 3. For each separate ply, the transverse and shear stiffnesses are modified, according to the ply's stress state and consequent damage level, as discussed in section 3.3 and section 3.4. This makes the model flexible, as it can technically be used for any layup. Moreover, stiffness degradation and applied loads are linked directly, thus avoiding the additional step of having to predict matrix crack density. The updated laminate's stiffness and Poisson's ratios are then derived

through classical laminated-plate theory, as covered in section 3.5. Validation is covered in section 3.6.

2.2. Cyclic Loading

The literature study performed in section 2.1 for stiffness degradation under static loading is now expanded in this section to fatigue loading. The focus remains on stiffness degradation due to matrix damage, and all considerations made in the previous section should be kept in mind.

As stated by Degrieck and Van Paepegem in their extensive review paper on fatigue damage modeling of composite materials [11], fatigue models for composite laminates can be broken down into three main categories: fatigue life models, phenomenological models and mechanistic progressive damage models. The above categories can be defined as follows:

- Fatigue life models only aim to predict fatigue life, usually by means of S-N curves or any other form of diagram which correlates an input parameter (eg. max cyclic stress and stress ratio) to fatigue life by means of extensive experimental data.

- Phenomenological models aim to establish a relation between the degradation of mechanical properties (strength or stiffness) and the application of cyclic loading. They are phenomenological because the model connects fatigue loading to mechanical property degradation without rigorously modeling the actual mechanism (various types of damage) that connects the two.

- Mechanistic progressive damage models aim to rigorously predict the onset and evolution of specific damage (eg. fiber breakage, matrix cracking, delamination...) due to fatigue loading. The degradation in mechanical properties is then associated to the predicted damage state, essentially closing the gap that exists in phenomenological models. These models are usually based on continuum mechanics and micromechanics approaches.

Passipoularidis and Brøndsted [51], who also wrote a detailed review of fatigue evaluation algorithms, broke down existing fatigue models in the same categories. Each of the aforementioned categories has its own benefits and drawbacks. Fatigue life models are clearly the simplest and fastest to implement, but they need for extensive experimental data, which would only be valid for the specific ply material and layup being tested, potentially making the use of fatigue life models prohibitively expensive and time consuming for fatigue oriented preliminary design.

Phenomenological models have the potential of delivering reasonably accurate predictions (especially for preliminary design) while allowing for the fast computation of different design configurations (in terms of load, ply material and layup). A drawback of such models is that there is no clear knowledge of the extent (and possibly type) of damage, only its effect on the modeled properties is known. Moreover, the experimental data needed by the model can often be of the same nature as the data the model is trying to predict (eg. fatigue data is needed, with the same layup and stress-level as the desired prediction). This can be problematic for preliminary design.

Finally, mechanistic progressive damage models can deliver extremely accurate solutions, provided that the material has been properly characterized, and that the layup and load-case are covered by the model. The main downside is the computational time, which is usually too long for such models to be used in preliminary design.

As explained at the end of this section, the proposed fatigue model tries to incorporate the simplicity of phenomenological models with the "physics based approach" of the mechanistic ones. Hence, the remainder of this section will present a representative sample of phenomenological and mechanistic stiffness degradation models.

A good example of a phenomenological model for stiffness degradation is given by Hwang and Han [26, 27]. They devised the concept of fatigue modulus, defined as the secant modulus connecting the origin with the point of applied stress (and resulting strain) at a cycle n. Its degradation rate as a function of cycles was assumed to follow a power law, and the stress-strain relation within a cycle n was assumed to be linear. The last assumption obviously breaks down for materials which experience non-linear behavior upon static loading. While the model gives good predictions for both residual stiffness and fatigue life, it requires the estimation of two material constants through experimental data in order to work. The necessary experimental data is of the same nature (fatigue loading) as the model's predictions, possibly making the model less useful

for preliminary design (since significant changes in layup or materials would require new batches of fatigue tests).

Whitworth [73, 74] proposed stiffness degradation and cumulative damage models for composite laminates, based on the assumption that the stiffness degradation rate is inversely proportional to a power of the residual modulus. The model has three parameters which need to be determined through experimental data, two of which are material dependent, while one is related to the applied cyclic stress. As with many other phenomenological models, the experimental data needed to determine modeling constants is essentially of the same nature as the model's prediction. In this particular case, since one of the constants is stress-dependent, the fatigue data needed for the modeling constants must be obtained at the same applied cyclic stress that the model is trying to predict. The match with experimental data is good, and interestingly the model can also predict the residual strength distribution associated with a specific residual stiffness.

Another phenomenological stiffness degradation proposed by Whitworth [75] follows a degradation law similar in nature to the one shown in his previous work [74], where the rate of degradation of the residual modulus is related to a power of the residual modulus itself. Through the strain failure criterion, Whitworth defined the residual modulus as a function of the ultimate tensile strength and its statistical distribution. This in turn allows to determine the statistical distribution of the residual modulus at any point in fatigue life. Predictions for residual modulus throughout life and its statistical distribution at specific points in life show a good match with experimental data. Similarly to [73, 74], several modeling constants need to be determined through experimental data, under both static and fatigue loading. Some of these constants depend on the applied cyclic stress.

Yang, Jones et al. [76] proposed a phenomenological stiffness degradation model for fiber-dominated composite laminates (exhibiting a linear stress-strain curve). The degradation rate of the residual modulus is assumed to be a function of the pristine modulus and a power function of the number of applied cycles, as well as several modeling constants dependent on environment, stress-ratio, applied stress and frequency. Said constants must be determined through experimental data. The model essentially uses a linear regression to estimate said parameters based on test data from the particular sample being analyzed, covering a portion of its fatigue life. The remaining fatigue life is then predicted by the model. Agreement with a particular sample is good if the experimental data used to determine the model parameters reaches at least the first quarter of the sample's fatigue life. Predictions are otherwise acceptable. The model can also predict the statistical distribution of the residual stiffness at a particular point in fatigue life.

Yang, Lee and Sheu [77] expanded upon the previous model [76] by making it applicable to matrix dominated laminates, which exhibit non-linear stress strain behavior. This was essentially done by substituting the residual modulus in the governing equations of [76] with the fatigue modulus defined in [26, 27]. The same modeling constants used in [76] are present, plus some additional ones to account for the non-linear stress-strain relation of matrix dominated laminates. Similarly to the previous model, stiffness degradation predictions are good if the sample's experiential data covers one fourth of its fatigue life, and acceptable otherwise.

While there are many more phenomenological stiffness degradation models, summarized in [11, 51], they are not going to be discussed here. The ones mentioned so far are already enough to paint a picture of the typical phenomenological stiffness degradation model, since they all share the same benefits and downsides. The main advantage of all models presented so far is their simplicity. Since they do not model the actual damage itself (and its stress-state and growth), only one or two equations are needed to relate the mechanical properties of interest with the independent variable of choice (usually applied load/stress). The direct connection between the residual mechanical properties and the independent variable is particularly convenient for design and optimization purposes. The main downside of all models presented so far is that they always need experimental fatigue data to estimate some modeling constants. The models need to somehow be "grounded in reality", and since that is not done by modeling the damage continuum, it must be done through experimental data. For most models, the necessary fatigue data must be very similar in nature to the very scenario (layup, load-case) that the model is trying to predict. While the fatigue model proposed in this thesis aims to be as simple as the phenomenological ones, all of the test data it requires can be measured experimentally from static tests, none of which need to be carried out on the exact layup being analyzed (although doing so for the transverse tensile in situ strength could benefit accuracy to some extent). No curve fitting or semi-empirical approaches are needed.

A selection of mechanistic models for stiffness degradation will now be presented, followed by a short discussion of their advantages and disadvantages, especially in comparisons with their phenomenological counterparts.

Ogin et al. [50] proposed a mechanistic stiffness degradation model for cross-ply laminates, pointing out that stiffness degradation of such laminates is driven by matrix cracking in the off-axis plies. Through a shear lag analysis, residual stiffness of a cross-ply laminate was expressed as a linear function of matrix crack density (in the off-axis plies). The rate of matrix crack density growth with applied cycles was assumed to depend on the maximum applied cyclic stress and the current crack density. An exact expression for the damage rate was found by incorporating the stored elastic energy between two cracks in the aforementioned assumptions. The linear relation between stiffness degradation and damage (matrix cracks) is then used to define residual stiffness as a function of the applied cycles. Some modeling constants are present, proving that mechanistic methods are not immune to them. They are however much less "aggressive" than their phenomenological counterparts, since (in this case) all constants are load-independent.

Caron and Ehrlacher [4] proposed a micromechanical model for cross-ply laminates where the matrix in the 90 degree plies is discretized into several "cells". The residual strength of each cell is assumed to decay at a rate dependent on the current residual strength, the applied stress range and two modeling constants, which need to be determined through fatigue testing. The initial strength of each cell is assumed to Weibull distributed, with the distribution having to be determined experimentally. The model then starts an iterative process where all cells are loaded. Ff their strength is exceeded, a crack develops, breaking the cell into two sub-cells and redistributing the stresses. If the strength is not exceeded, the strength degradation law is applied. Predictions for the number of matrix cracks as a function of the number of cycles were in excellent agreement with test data. Any existing model relating matrix crack density to stiffness degradation can then be used to find stiffness degradation as a function of the applied cycles (eg. [40]).

Talreja [59, 60] developed a continuum mechanics-based representation of intralaminar (matrix cracks) and interlaminar (delamination) damage, which are represented as vectorial entities, based on their geometrical properties. Some material constants must be determined through experimental data relating residual stiffness properties of a given laminate with its crack density. Stiffness degradation can then be predicted as a function of intralaminar and interlaminar damage, showing an excellent match with test data. Bonora et al. [1] used the continuum approach shown in Talreja's work [59, 60] to predict stiffness degradation due to matrix cracking in a cross-ply laminate under fatigue loads. To do this, matrix crack density (in the 90 degree plies) had to be estimated as a function of applied cycles. Bonora et al. assumed matrix crack density to be related to the applied cycles, the maximum cyclic stress, specimen geometry and some modeling constants, one of which depends on the applied load level. Stiffness degradation of a cross-ply laminate can then be predicted for fatigue loading.

While the match of [1] with experimental data is good, this model shows one of the weaknesses of mechanistic approaches: rather than predicting stiffness degradation directly as a function of the applied load and cycles (like phenomenological models), mechanistic models predict damage (usually crack density) as a function of the applied load and cycles, and then relate said damage to degradation in the laminate's mechanical properties. The extra step (compared to phenomenological models) could introduce "additional points of failure", and could make the less apt to preliminary design optimization, which is usually based on applied loads and displacements, rather than damage states.

While there are a multitude of additional mechanistic stiffness degradation models, they are not presented here (a good review can be found in [11, 51]), since the fatigue model proposed in this research does not base itself on any of them. The goal was to show the advantages and disadvantages inherent of mechanistic models. They all tend to have good accuracy, and if they posses any modeling constants, they are generally less "aggressive" than their phenomenological counterparts (eg. they do not depend on the applied stress level, meaning one batch of test data can be used to predict stiffness degradation at different stress levels). Their main downside is the higher complexity of the method itself, which often needs to dwell into micromechanical, since damage is usually modeled explicitly. Said complexity can results in computationally intensive models, especially when discretization of finite element approaches are necessary.

The proposed fatigue model was created with preliminary design in mind and falls between phenomenological and progressive damage models, similarly to the "lamina to laminate" approaches described in [51]. This is further reinforced by the fact that the fatigue model shown in chapter 4 is based on the proposed static
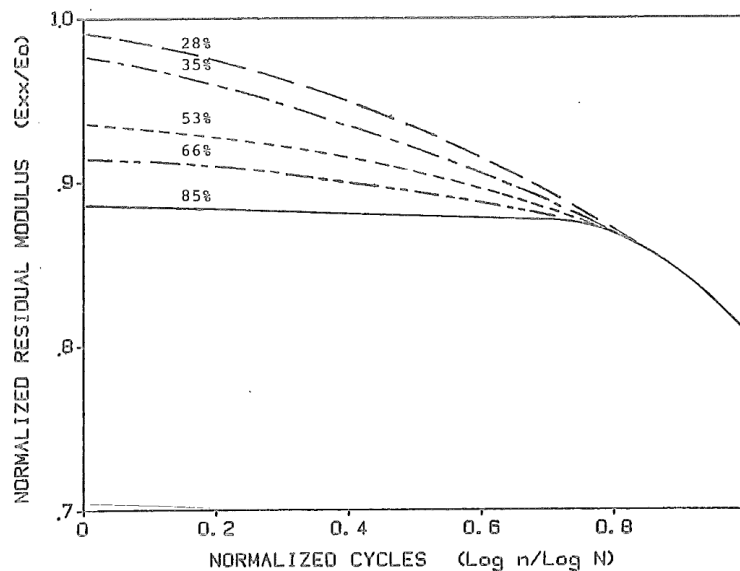
Figure 2.2: Normalized stiffness degradation as a function of normalized fatigue life for $[0,90_2]_S$ graphite/epoxy laminate, according to predictions from [8]. The percentages next to the curves indicate the maximum cyclic stress as a function of static strength.

model from chapter 3, which has been extended to fatigue loading through Kassapoglou's model for residual strength prediction under fatigue loading [30, 32–35]. Both models happen to also be a mix of phenomenological and progressive damage ones. While the proposed fatigue model does not directly predict the precise extent of damage (matrix crack density), or the stress state around said damage, it does base its prediction for the onset of damage and the assumed post-damage behavior on the specific damage type being modeled. Unlike most mechanistic models, the proposed model draws a direct relation between stiffness degradation, applied cycles and cyclic stress level, thus bypassing the additional step of having to predict matrix crack density. Differently from phenomenological models, the proposed fatigue model only needs data which can be measured experimentally from static tests, none of which need to be carried out on the exact layup being analyzed (although doing so for the transverse tensile in situ strength could benefit accuracy to some extent). No curve fitting or semi-empirical approaches are needed. Since the proposed model is fully analytical, and acts at the mesoscale (like the static model) it is also extremely fast.

Finally, it is appropriate to quickly mention literature covering interesting aspects of stiffness degradation during fatigue. Daniel, Lee and Yaniv [8] found that the stiffness degradation curves of cross-ply laminates under uniaxial tensile fatigue loading usually follow a same pattern fig. 2.2. An extremely steep initial drop takes place within the first cycle, due to the formation of transverse matrix cracks (assuming the load is high enough). Then, if the characteristic damage state [53] (CDS) has not been reached within the first cycle, residual stiffness will decrease very gradually with the applied cycles, as the number of matrix cracks slowly increase. If on the other hand the first-cycle load was high enough to reach the CDS, little to no damage (matrix cracks) growth will occur, and the residual stiffness will essentially plateau. At 80% fatigue life point, damage modes other than transverse matrix cracking will kick in, such as longitudinal matrix cracking, delaminations and fiber fractures, causing residual stiffness to degrade quickly, and ultimately resulting in failure.

Another example of typical damage development in a laminate throughout fatigue life is shown in fig. 2.3, [52]. Three phases can be clearly distinguished: a steep initial drop, caused by matrix cracking, which plateaus into a linear more gradual section once the CDS [53] is reached, which ultimately culminates into another steep drop, leading to failure.

Van Paepegem, De Baere et al. [67] took the unusual approach of monitoring the effect of fatigue damage on the Poisson's ratio rather than stiffness. They found that fatigue loading clearly causes the Poisson's ratio to degrade, and that the degradation is clear enough to allow for fatigue damage monitoring through the Poisson's ratio. More interestingly, Van Paepegem, De Baere et al. mention that cross-ply carbon fiber samples with thermoplastic matrix experienced Poisson's ratio degradation under fatigue loading without showing any stiffness degradation, hinting that Poisson's ratio degradation in fatigue may not be exclusively dependent on stiffness degradation. Finally, they also found the Poisson's ratio to be stress dependent, meaning that its

DAMAGE MODES DURING FATIGUE LIFE
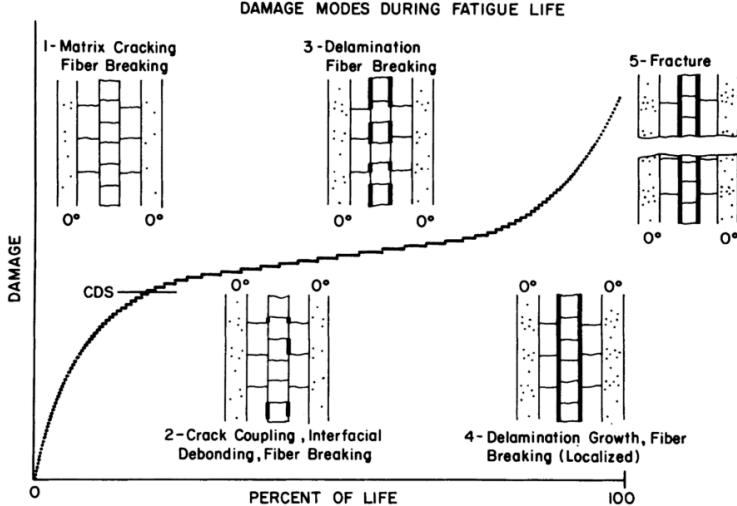
Figure 2.3: Typical damage development phases throughout the fatigue life of a laminate. Residual stiffness is proportional to damage parameter D. Taken from [52]

value during a fatigue cycle will constantly change with the applied load.

Finally, extensive experimental data and observations regarding stiffness degradation and damage development for a wide variety of composite laminates under static or cyclic loading can be found in [28, 54].

Static model

Two models are presented in this chapter, both of which aim to predict stiffness degradation caused by matrix damage under static tensile loading. The models were designed to work with any layup, to be fully analytical, and to require as little experimental input data as possible.

The model's fundamental unit are the unidirectional plies which make up an infinite laminate. Classical laminated plate theory [31] is used to derive laminate properties through the mechanical properties of each single ply.

Stiffness degradation is modeled exclusively through the decay of each ply's transverse and shear moduli (E_{22} and G_{12}), which is assumed to occur due to matrix damage. The residual minor Poisson's ratio v_{21} is also predicted through its dependence on E_{22}. In brief, the model's inputs are the ply material's mechanical properties (E_{11}, E_{22}, G_{12}, v_{12}), the ply material's transverse tensile in situ strength (Y_{is}^T) and its shear stress-strain curve, up to failure. Once the desired layup and longitudinal tensile laminate load N_X have been defined by the user, the chosen model will calculate the residual E_{22} and G_{12} for each ply. Classical laminated plate theory is then used to derive the laminate's new stiffness and Poisson's ratio from the updated ply properties.

The principles behind the design of both models are illustrated in section 3.1, together with a brief introduction. Two different stiffness degradation models have been developed for static loading. While they both handle transverse tension in essentially the same way, they treat shear differently. The first model, presented in section 3.3 allows the matrix to yield due to shear, and to develop matrix cracks due to the combined action of shear and tension. Damage evolution and stiffness degradation is then handled through apportioning of strain energy densities. The second model, shown in section 3.4 takes a more generic approach based on the concept of recoverable and unrecoverable damage, unidentified microscopic shear damage and matrix cracking. Section 3.5 illustrates how the mechanical properties of each single ply are translated into laminate's properties, and also gives a small summary on how the model works in practice. Finally, section 3.6 shows the extensive validation process carried out for both static models.

3.1. Model principles and introduction

The model was created with two goals in mind: preliminary design optimization and cycle-by-cycle fatigue analysis. The former is characterized by the iteration of numerous design configurations. Said configurations could be extremely different from each other, meaning that models used within preliminary design should capitalize on computational speed and generality. Computational speed is also essentially for cycle-by-cycle fatigue analysis, where material properties need to be updated at every cycle to reflect the instantaneous damage state of the structure. The principles below were devised to ensure that the proposed model would be simple enough to be both computationally fast and applicable to a large variety of layups and materials.

- **Rapid evaluation.** The method should be analytical, in order to maximize computational speed and ease of use/implementation.

- **No restrictions to specific layups.** A considerable number of stiffness degradation models constrain the layup to specific configurations (eg. [0/90] cross-ply [5, 23, 24]). While this is done to simplify the damage states being modeled (and provide a stepping stone for future models), it severely limits the spectrum of design configurations that preliminary design optimization can analyze. It should be

noted that while the model can technically be applied to any layup, it has only been validated on balanced symmetric laminates. This should not be an issue since most layups used in practical designs are balanced and symmetric.

- **The model should focus on stiffness degradation only.** As a first step, the model focuses on the effects of matrix damage on ply stiffness, since matrix damage is the first type of damage to occur upon loading, and since degradation upon static or fatigue loading is driven by matrix damage (and possibly fiber-matrix interface damage) [5, 8, 25, 50, 54, 69, 70].

Since plies are the fundamental unit of the model, and since the model should work for any layup and ply material, stiffness degradation needed to be somehow tied to ply quantities which reflected the "mechanical state" of the ply after loading. In this thesis, damage initiation and evolution was tied to Hashin's failure criterion [22], which only requires ply strength and stresses to function. This does not preclude the usage of other failure criteria, stress based or not. Since matrix damage is the first type of damage to occur (at least at ply level), and since it has been shown to have a strong influence on stiffness degradation [5, 8, 25, 50, 54, 69, 70], the proposed method will start with that as a first step.

To minimize the model's complexity, as well as making validation easier, the only load case to be applied to the laminate is uniaxial tension. Because of this requirement, it is convenient to define matrix $\mathbf{T}_{\mathrm{ply}}$, which allows to relate local ply stresses to the in plane distributed load applied to the laminate.

$$\mathbf{T}_{\mathrm{ply}} = \begin{bmatrix} t_{11} & t_{12} & t_{13} \\ t_{21} & t_{22} & t_{23} \\ t_{31} & t_{32} & t_{33} \end{bmatrix} = \mathbf{Q}_{\mathrm{ply}} \cdot \mathbf{N}_{\mathrm{ply}} \cdot \mathbf{S}_{\mathrm{lam}} \tag{3.1}$$

with

$$\underline{\sigma} = \mathbf{T}_{\mathrm{ply}} \cdot \underline{N} \quad \text{or} \quad \begin{bmatrix} \sigma_{11} \\ \sigma_{22} \\ \tau_{12} \end{bmatrix} = \mathbf{Q}_{\mathrm{ply}} \bullet \mathbf{N}_{\mathrm{ply}} \cdot \mathbf{S}_{\mathrm{lam}} \cdot \begin{bmatrix} N_x \\ N_y \\ N_{xy} \end{bmatrix} \tag{3.2}$$

Where $\mathbf{Q}_{\mathrm{ply}}$ is the ply stiffness matrix in the ply coordinate system, $\mathbf{N}_{\mathrm{ply}}$ is the ply strain rotation matrix, $\mathbf{S}_{\mathrm{lam}}$ is the laminate compliance matrix, $\underline{\sigma}$ is the ply stress vector and $\underline{N}$ is the laminate load vector. Note that matrix $\mathbf{T}_{\mathrm{ply}}$ is not symmetric, and has to be defined for each ply orientation. The definitions of $\mathbf{Q}_{\mathrm{ply}}$, $\mathbf{S}_{\mathrm{lam}}$ and $\mathbf{N}_{\mathrm{ply}}$ are shown in eq. (3.3), eq. (3.5) and eq. (3.6) respectively.

$$\mathbf{Q}_{\mathrm{ply}} = \begin{bmatrix} \dfrac{E_{11}}{1 - \nu_{12}\nu_{21}} & \dfrac{\nu_{21}E_{11}}{1 - \nu_{12}\nu_{21}} & 0 \\ \dfrac{\nu_{12}E_{22}}{1 - \nu_{12}\nu_{21}} & \dfrac{E_{22}}{1 - \nu_{12}\nu_{21}} & 0 \\ 0 & 0 & G_{12} \end{bmatrix} \tag{3.3}$$

The lack of out-of-plane components in $\mathbf{Q}_{\mathrm{ply}}$ is due to the plane stress assumption. Moreover, the special orthotropy of the ply material and Maxwell symmetry make it so that $Q_{12} = Q_{21}$, as shown below in eq. (3.4).

$$Q_{12} = Q_{21} \quad \Rightarrow \quad E_{11}\nu_{21} = E_{22}\nu_{12} \tag{3.4}$$

$$\mathbf{S}_{\mathrm{lam}} = [\mathbf{C}_{\mathrm{lam}}]^{-1} \quad \text{with} \quad \mathbf{C}_{\mathrm{lam}} = \frac{1}{T} \sum_{k=1}^{n} \mathbf{M}_k \mathbf{Q}_k \mathbf{M}_k^T t_k \tag{3.5}$$

In the equation for $\mathbf{S}_{\mathrm{lam}}$, $\mathbf{C}_{\mathrm{lam}}$ is the stiffness matrix of the laminate. The subscript k in the equation for $\mathbf{C}_{\mathrm{lam}}$ indicates the current ply number, t_k represents the thickness of the current ply, while T is the thickness of the entire laminate. The stress rotation matrix $\mathbf{M}_{\mathrm{ply}}$ is given in eq. (3.6). The laminate's compliance matrix is limited to its in-plane components since the proposed model has been developed for in-plane loads.

$$\mathbf{M}_{\mathrm{ply}} = \begin{bmatrix} \cos^2\theta & \sin^2\theta & 2\cos\theta\sin\theta \\ \sin^2\theta & \cos^2\theta & -2\cos\theta\sin\theta \\ -\cos\theta\sin\theta & \cos\theta\sin\theta & \cos^2\theta - \sin^2\theta \end{bmatrix}$$

$$\tag{3.6}$$

$$\mathbf{N}_{\mathrm{ply}} = \begin{bmatrix} \cos^2\theta & \sin^2\theta & \cos\theta\sin\theta \\ \sin^2\theta & \cos^2\theta & -\cos\theta\sin\theta \\ -2\cos\theta\sin\theta & 2\cos\theta\sin\theta & \cos^2\theta - \sin^2\theta \end{bmatrix}$$

Where θ is the orientation angle of the ply being analyzed.

3.2. Approximating shear stress-strain behavior

Before diving into the models, it is useful to quickly show how some of the non-linearities associated with shear stress-strain behavior [19, 21] have been simplified. The experimental shear stress-strain curve was approximated by two straight lines (see section 3.6), one representing the "pristine" elastic response, and the other covering plastic behavior.

An example of said approximation is shown in fig. 3.1, where it is possible to see that the stress-strain curve will start out linear (with modulus G_{12}) and then turn plastic when the shear stress equals S_k, following the plastic approximation with slope k until the ultimate stress-strain is reached. The approximation illustrated in this chapter is denoted from hereon as "bilinear approximation".

To find the slope k, some experimental data is required, namely the typical shear stress-strain curve of the material, up to failure. Said experimental data is used to obtain the ultimate shear stress (S_{ult}), ultimate strain γ_{12ult} and strain energy density to failure ($U_{d_{12f}}$), defined in eq. (3.7).

$$U_{d_{12f}} = \int_{0}^{\gamma_{12ult}} \tau_{12}(\gamma)\,\mathrm{d}\gamma \tag{3.7}$$

Slope k should be such that strain energy density to failure for the experimental and approximated shear curves are the same. To restrict all possible solutions of k to a single value, it is imposed that the approximated curve should have the same S_{ult} and γ_{12ult} as the experimental one. Plastic slope k is therefore dependent on a single variable: the damage initiation stress S_k, which should be chosen to comply with the aforementioned energy equivalence. Slope k is defined in eq. (3.8), while an expression for S_k is shown in eq. (3.9)

$$k = \frac{S_{ult} - S_k}{\gamma_{12ult} - \dfrac{S_k}{G_{12}}} \tag{3.8}$$

$$S_k = \frac{2U_{d_{12f}} - S_{ult}\gamma_{12ult}}{\gamma_{12ult} - \dfrac{S_{ult}}{G_{12}}} \tag{3.9}$$

Where S_k represents the shear stress (in the ply) at which shear damage will be initiated. For the energy equivalence model introduced in section 3.3, S_k is associated with shear strength τ_{12y}, which denotes the onset of microscopic matrix damage, illustrated in section 3.3.1. For the recoverable energy model presented in section 3.4, S_k will represent the shear in situ strength S_{IS}, which for that particular model is used to denote the onset of microscopic shear damage. The reason why microscopic shear damage was associated (for the recoverable damage model) with the shear in situ strength S_{IS} and not some other quantity will be made clear at the beginning of section 3.4. Calculating a realistic value for the bilinear approximation's knee is extremely important, since it drives the model's accuracy for scenarios where shear is dominant.

3.3. Energy equivalence model

This is the first of the two proposed models. Two damage phenomena are modeled at ply level: inelastic behavior possibly caused by microscopic damage and matrix cracking. The former is assumed to only occur due to shear, while matrix cracking occurs due to a combination of shear and transverse tensile stresses [37, 69]. All stresses mentioned in this chapter refer ply stresses in the ply's local coordinate system, while "load" refers to the longitudinal tensile load applied to the laminate, unless stated otherwise. The aim of the model is to relate the residual transverse and shear ply moduli ($\overline{E}_{22}$ and $\overline{G}_{12}$) to the applied load (N_X). The initiation and evolution of microscopic matrix damage, as well as its effect on ply stiffness, are covered in section 3.3.1. The same is done for matrix cracking in section 3.3.2. The model is validated in section 3.6.
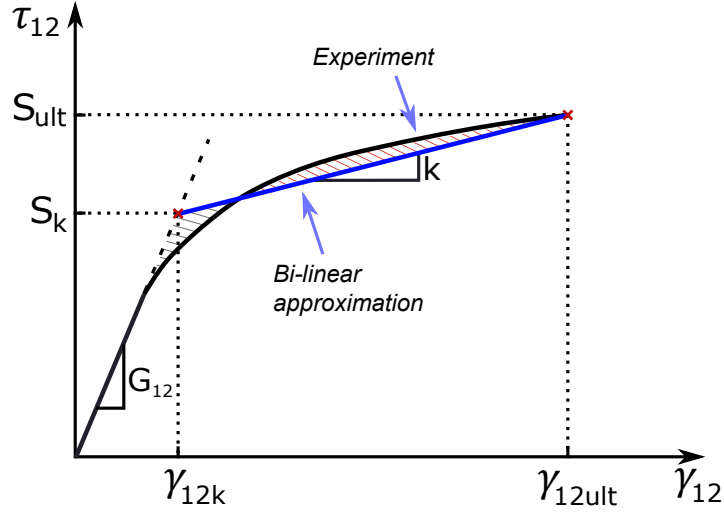
Figure 3.1: Schematic representation of the bilinear shear stress-strain approximation procedure. If the highlighted areas are equal, the experimental and approximated stress-strain curves will have the same strain energy density to failure (area under each curve).

3.3.1. Inelastic matrix behavior in shear

The departure of a ply from linear behavior is postulated to occur when the shear stress exceeds the apparent yield strength τ_{12y}, as shown in eq. (3.10), where shear stress is calculated according to the ply's pristine moduli (no other damage has occurred yet) and yield strength τ_{12y} is assumed to be the knee of the bilinear shear approximation shown in fig. 3.2, since that is the first instance where shear stress-strain behavior will depart linearity.

$$\tau_{12a} = \gamma_{12a} G_{12} = N_X t_{31} \geq \tau_{12y} \tag{3.10}$$

Where τ_{12a} is the applied shear stress, γ_{12a} is the applied shear strain, N_X is the laminate load corresponding to said shear strain assuming the laminate to be pristine and t_{31} was defined in eq. (3.1). At this point, it is convenient to mention a couple of assumptions behind the expected post-damage behavior. For reasons that will be explained in section 3.3.2, matrix cracking is assumed to turn the shear and transverse tensile stress-strain curves perfectly plastic. There exists however an unspecified form of microscopic matrix damage which occurs when shear stresses are dominant. In [37], shear dominated laminates subject to tensile loading exhibited stiffness degradation long before matrix cracks were developed, indicating that non-visible (microscopic) damage must be present. In [69], stiffness degradation of shear dominated laminates occurred without any visible damage, pointing once again at the presence of microscopic damage associated exclusively with shear stresses. It is therefore assumed that the microscopic damage can only be induced by shear stresses, and can only affect shear stress-strain behavior in return. Finally, since microscopic in [37, 69] appeared before matrix cracking (if any), it can be assumed that the first departure of the shear response from elastic behavior must be caused by microscopic damage, which in turn means that the plastic portion of the bilinear shear approximation from section 3.2 can be associated with the microscopic damage.

The evolution of shear damage with the applied load is modeled by imposing an equality between the shear strain energy density that would have been stored had the material stayed intact and the one actually stored in the damaged material.

Looking at fig. 3.2, this is essentially equivalent to stating that areas $OABC$ and $OADE$ should be equal. To derive an equation for the residual shear modulus $\overline{G}_{12}$ it is necessary to find expressions for τ_{12a} and γ_{12a}, which are the shear stress and strain actually applied to the material.

$$\overline{G}_{12} = \frac{\tau_{12a}}{\gamma_{12a}} \tag{3.11}$$

Referring to fig. 3.2, it is easy to derive from geometry an expression relating the applied stress and strain, shown below.

$$\tau_{12a} = \tau_{12y} + k\left(\gamma_{12a} - \frac{\tau_{12y}}{G_{12}}\right) \tag{3.12}$$
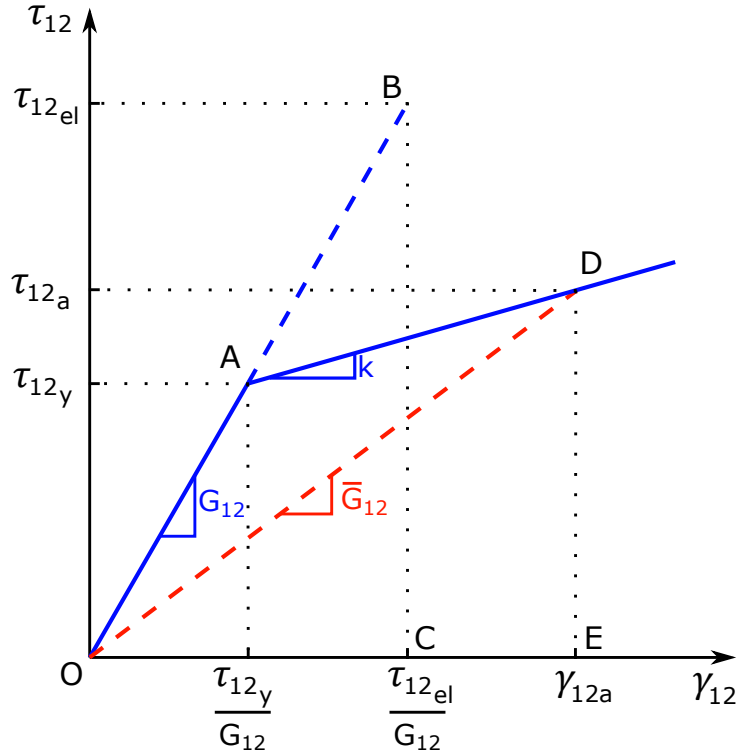
Figure 3.2: Ply material's shear behavior upon appearance of microscopic matrix damage, according to the energy equivalence model.

Enforcing the equality of areas $OABC$ and $OADE$ it is possible to obtain an additional equation containing τ_{12a} and γ_{12a}.

$$\frac{\tau_{12el}^2}{2G_{12}} = \frac{\tau_{12y}^2}{2G_{12}} + \frac{(\tau_{12a} + \tau_{12y})}{2}\left(\gamma_{12a} - \frac{\tau_{12y}}{G_{12}}\right) \tag{3.13}$$

It is obvious that eq. (3.12) and eq. (3.13) constitute a system of two equations in two unknowns, namely τ_{12a} and γ_{12a}. Solving said system yields the following definitions of applied stress and strain:

$$\tau_{12a} = \sqrt{\tau_{12y}^2 + \frac{k}{G_{12}}\left(\tau_{12el}^2 - \tau_{12y}^2\right)} \quad\text{and}\quad \gamma_{12a} = \tau_{12y}\left(\frac{1}{G_{12}} - \frac{1}{k}\right) + \frac{1}{k}\sqrt{\tau_{12y}^2 + \frac{k}{G_{12}}\left(\tau_{12el}^2 - \tau_{12y}^2\right)} \tag{3.14}$$

Where all variables are known apart from τ_{12el}, which is the independent variable, defined as:

$$\tau_{12el} = N_X t_{31} \tag{3.15}$$

Where N_X is the uniaxial longitudinal tensile load currently applied to the entire laminate, thus representing the model's only input and independent variable.

Using eq. (3.14), it is possible to finally write a proper definition for the residual shear modulus under microscopic matrix damage, starting from eq. (3.11):

$$\overline{G}_{12} = \frac{\tau_{12}}{\gamma_{12a}} = \frac{\sqrt{1 + \frac{k}{G_{12}}\left(\frac{\tau_{12el}^2}{\tau_{12y}^2} - 1\right)}}{\frac{1}{G_{12}} - \frac{1}{k} + \frac{1}{k}\sqrt{1 + \frac{k}{G_{12}}\left(\frac{\tau_{12el}^2}{\tau_{12y}^2} - 1\right)}} \tag{3.16}$$

3.3.2. Matrix cracking

Unlike microscopic damage, matrix cracking can be caused by both transverse tension and shear [3, 22], and will consequently affect both the transverse tensile and shear moduli. To predict the onset of matrix cracking, Hashin's criterion for matrix material under transverse tension and shear was used [22], shown in eq. (3.17).

$$\left(\frac{\sigma_{22}}{Y_{IS}^T}\right)^2 + \left(\frac{\tau_{12}}{S_{IS}}\right)^2 = 1 \tag{3.17}$$

Where Y_{IS} and S_{IS} are the transverse tensile and shear in situ strengths respectively. If the in situ strengths are not available, ultimate stresses can also be used, possibly at the expense of modeling accuracy. It should be noted that for particular ply orientations and layups, a small transverse compressive stress might be present, meaning that $t_{21} < 0$. It is known from [10] that, if a unidirectional Glass-Epoxy ply subject is to transverse compression and in-plane shear, small compressive stresses will actually have a beneficial effect on the failure envelope. Since the proposed models are being validated (for now) in uniaxial tension, the compressive stresses will be very small, if any. To be conservative, and to keep the model simple, it is therefore assumed that the effect of transverse compression can be neglected, meaning that whenever $t_{21} < 0$, t_{21} will be set to zero, and the ply will be loaded in pure shear. This applies to all equations within this research where Hashin's criterion is applied, including matrix cracking equations in section 3.4.1 and section 4.3.

Since the presence of microscopic damage affects the shear stress τ_{12}, equations associated with the onset and evolution of matrix cracking are derived for two different cases: one where microscopic damage has occurred before matrix cracking, and one where it has not.

To determine whether microscopic damage will occur before matrix cracking, the critical load for the former should be compared with the cracking one (N_{Xcr}) defined in eq. (3.19). This is shown in eq. (3.18), where t_{31} was used to associate the apparent yield stress with the corresponding laminate load N_X.

$$\frac{\tau_{12y}}{t_{31}} < N_{Xcr} \tag{3.18}$$

If the above condition is true, it means that the load N_X necessary for the shear stress τ_{12a} to exceed τ_{12y} is lower than the load N_{Xcr} necessary to induce cracking, which in turn means that microscopic damage will occur before cracking.

Matrix cracking without microscopic damage

In absence of microscopic damage, the ply material will follow linear elastic behavior for both shear and transverse tension until cracking occurs, meaning that the critical cracking load can be easily found through Hashin's criterion by expressing τ_{12} and σ_{22} as a function of N_{Xcr}, setting the criterion equal to one and then solving for N_{Xcr}, as shown in eq. (3.19)

$$\left(\frac{\sigma_{22}}{Y_{IS}^T}\right)^2 + \left(\frac{\tau_{12}}{S_{IS}}\right)^2 = 1 \quad \Rightarrow \quad N_{Xcr}^2\left[\left(\frac{t_{21}}{Y_{IS}^T}\right)^2 + \left(\frac{t_{31}}{S_{IS}}\right)^2\right] = 1 \quad \Rightarrow \quad N_{Xcr} = \frac{1}{\sqrt{\left(\frac{t_{21}}{Y_{IS}^T}\right)^2 + \left(\frac{t_{31}}{S_{IS}}\right)^2}} \tag{3.19}$$

Once matrix cracking is initiated, ply material behavior is postulated to turn perfectly plastic in both shear and transverse tension. If microscopic damage has not occurred (eq. (3.18) is false), the stress-strain curves for transverse tension and shear will look like fig. 3.3a and fig. 3.3b respectively.

The assumption that the post-cracking stress strain behavior should be perfectly plastic can be justified through the characteristic damage state concept [45, 53]. In brief, once matrix cracking is initiated, the crack pattern (and consequently distance between cracks) will be such that the peak matrix stress between two consecutive cracks will be infinitesimally smaller than the stress which initiated cracking. To make an example: there exists a laminate with 90 degree plies and additional plies in other directions. The laminate is loaded in tension up to the point where matrix cracks appear in the 90 degree plies. The stress in the matrix, between matrix cracks, is infinitesimally smaller than the "critical stress" which induced cracks. Any further increase

(a) Ply material's transverse tensile behavior upon matrix cracking according to the energy equivalence model.

(b) Ply material's shear behavior upon matrix cracking according to the energy equivalence model, assuming that microscopic damage has not occurred.
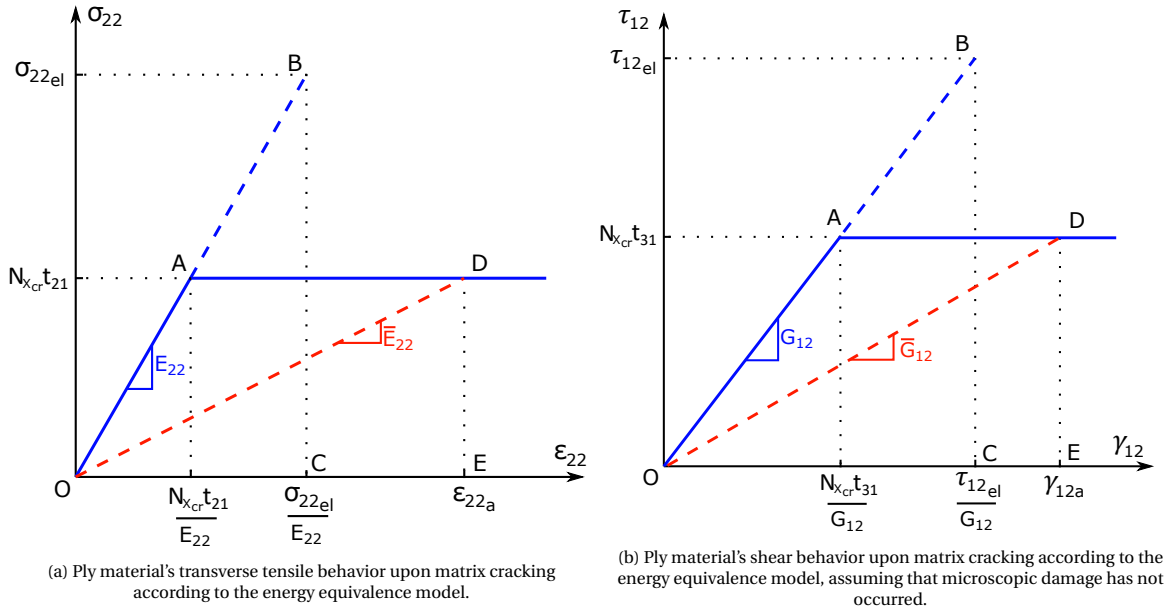
Figure 3.3

in laminate load will induce additional cracks, which will ensure that the stress between them remains infinitesimally smaller than the critical one. It follows that once matrix cracks are initiated, the matrix stress in the cracked ply will stay fixed at its critical value, despite increasing strains, thus justifying the assumption that ply stress-strain behavior turns perfectly plastic right upon matrix cracking. Naturally, this concept does not apply to laminates made exclusively of 90 degree plies, since matrix cracking would be immediately accompanied by failure.

To proceed, the excess strain energy density in a ply associated with the creation of matrix cracks is introduced. The strain energy densities associated with transverse and shear stresses are U_{d22} and U_{d12} respectively:

$$U_{d22} = \frac{\sigma_{22el}^2}{2E_{22}} \quad U_{d12} = \frac{\tau_{12el}^2}{2G_{12}} \tag{3.20}$$

Where the "el" subscript stands for elastic, and indicates that both σ_{22el} and τ_{12el} assume the continuation of elastic behavior. It is acknowledged that in addition to the two expressions in eq. (3.20), there is one more term in the strain energy density which involves σ_{22}. That term, $-\nu_{12}\sigma_{11}\sigma_{22}/E_{11}$ is neglected at this point. Excess strain energy density is defined here as the difference between the strain energy density corresponding to the applied load (assuming the continuation of linear elastic behavior after damage) and the strain energy density corresponding to the load at which, according to the Hashin failure criterion, damage is initiated. Excess strain energy density expressions for the transverse tension and shear portions of the energy density of a ply are given in eq. (3.21)

$$\Delta U_{d22} = U_{d22} - U_{d22cr} = \frac{\sigma_{22}^2 - \sigma_{22cr}^2}{2E_{22}} \qquad \Delta U_{d12} = U_{d12} - U_{d12cr} = \frac{\tau_{12}^2 - \tau_{12cr}^2}{2G_{12}} \tag{3.21}$$

Since the model assumes the laminate to be loaded in uniaxial tension, elastic stresses (σ_{22el}, τ_{12el}) and critical stresses (σ_{22cr}, τ_{12cr}) in eq. (3.21) can be written as a function of t_{21}, t_{31}, N_X, N_{Xcr} and the in situ strengths:

$$\sigma_{22el} = N_X t_{21}, \qquad \sigma_{22cr} = N_{Xcr} t_{21} = \frac{t_{21}}{\sqrt{\left(\dfrac{t_{21}}{Y_{is}^T}\right)^2 + \left(\dfrac{t_{31}}{S_{is}}\right)^2}} \tag{3.22}$$

$$\tau_{12el} = N_X t_{31}, \qquad \tau_{12cr} = N_{Xcr} t_{31} = \frac{t_{31}}{\sqrt{\left(\frac{t_{21}}{Y_{is}^T}\right)^2 + \left(\frac{t_{31}}{S_{is}}\right)^2}} \tag{3.23}$$

Using eq. (3.22) and eq. (3.23) it is possible to rewrite ΔU_{d22} and ΔU_{d12} in eq. (3.21) as follows.

$$\Delta U_{d22} = \frac{1}{2E_{22}} \cdot \frac{t_{21}^2}{\left(\frac{t_{21}}{Y_{is}^T}\right)^2 + \left(\frac{t_{31}}{S_{is}}\right)^2} \Delta H = \frac{\sigma_{22cr}^2 \, \Delta H}{2E_{22}} \tag{3.24}$$

$$\Delta U_{d12} = \frac{1}{2G_{12}} \cdot \frac{t_{31}^2}{\left(\frac{t_{21}}{Y_{is}^T}\right)^2 + \left(\frac{t_{31}}{S_{is}}\right)^2} \Delta H = \frac{\tau_{12cr}^2 \, \Delta H}{2G_{12}} \tag{3.25}$$

where ΔH could be described as the "Hashin failure index", defined in the eq. below:

$$\Delta H = \begin{cases} N_X^2 \left[\left(\frac{t_{21}}{Y_{is}^T}\right)^2 + \left(\frac{t_{31}}{S_{is}}\right)^2 \right] - 1, & \text{if } N_X \geq N_{Xcr} \\ 0, & \text{if } N_X < N_{Xcr} \end{cases} \tag{3.26}$$

With ΔH being equal to zero upon the very first instance of failure ($N_X = N_{Xcr}$). To enforce the equivalence between strain energy density accumulated in the perfectly plastic regime and excess strain energy, it is simply necessary to set the areas OABC and OADE from fig. 3.3b and fig. 3.3a to be equal to each other. By doing so, it is possible to derive the following equation for the residual moduli:

$$\overline{E}_{22} = \frac{\sigma_{22cr}}{\dfrac{\sigma_{22cr}}{E_{22}} + \dfrac{\Delta U_{d22}}{\sigma_{22cr}}} \qquad \overline{G}_{12} = \frac{\tau_{12cr}}{\dfrac{\tau_{12cr}}{G_{12}} + \dfrac{\Delta U_{d12}}{\tau_{12cr}}} \tag{3.27}$$

Using the expressions for the excess strain energy derived in eq. (3.24) and eq. (3.25), it is possible to write the above definitions of the residual moduli in a simpler form, shown below.

$$\overline{E}_{22} = \frac{2E_{22}}{2 + \Delta H} \qquad \overline{G}_{12} = \frac{2G_{12}}{2 + \Delta H} \tag{3.28}$$

Matrix cracking after microscopic damage

If eq. (3.18) is true, microscopic damage will occur before matrix cracking, which means that the τ_{12} used in Hashin's criterion (eq. (3.17)) to determine the onset of cracking is not elastic anymore, and will instead follow the plastic behavior shown in section 3.3.1. An expression for the critical cracking load N_{Xcr_y} accounting for the presence of microscopic damage can therefore be found by taking the post-microscopic damage applied shear stress τ_{12a}, as defined in eq. (3.14), plugging it into Hashin's criterion (eq. (3.17)) and solving for N_X. Since microscopic damage does not affect the traverse tensile response, σ_{22} remain elastic until crack initiation. The final result is shown below:

$$N_{Xcr_y} = \sqrt{\frac{1 - \left(\dfrac{\tau_{12y}}{S_{IS}}\right)^2 \left(1 - \dfrac{k}{G_{12}}\right)}{\left(\dfrac{t_{21}}{Y_{IS}^T}\right)^2 + \dfrac{k}{G_{12}}\left(\dfrac{t_{31}}{S_{IS}}\right)^2}} \tag{3.29}$$

Similarly to the approach followed in the previous section, it is postulated that the excess strain energy generated after matrix cracking (had the material stayed pristine) must be stored within the perfectly plastic portion of the stress-strain curve.

For transverse tension, microscopic damage only affects matrix cracking behavior by changing the critical load at which cracking will occur. This means that fig. 3.3a is still representative of post-microscopic damage matrix cracking for transverse tension, with the caveat that the new critical load will be $N_{Xcr} = N_{Xcr_y}$. This naturally means that the residual modulus $\overline{E}_{22}$ is given by eq. (3.30), which relies on the same derivation shown for eq. (3.31).

$$\overline{E}_{22} = \frac{2E_{22}}{2 + \Delta H} \qquad \text{with} \qquad \Delta H = \begin{cases} N_X^2 \left[\left(\dfrac{t_{21}}{Y_{is}^T} \right)^2 + \left(\dfrac{t_{31}}{S_{is}} \right)^2 \right] - 1, & \text{if } N_X \geq N_{Xcr_y} \\ 0, & \text{if } N_X < N_{Xcr_y} \end{cases} \tag{3.30}$$

For shear, the predicted stress-strain curve for post-microscopic damage matrix cracking is shown in fig. 3.4. The main difference from the case without microscopic damage is the presence of a plastic portion with slope k, following the bilinear approximation, starting at $N_X = \tau_{12y}/t_{31}$ and ending at $N_X = N_{Xcr_y}$. As before, it is postulated that the strain energy density stored after cracking if the material were to be elastic must be equal to its equivalent stored under the perfectly plastic regime. Looking at fig. 3.4, this is equivalent to stating at areas LBCI and HDEG must be equal. From geometry, said equality has been derived in eq. (3.31).

$$\text{LBCI} = \text{HDEG} \quad \Rightarrow \quad \frac{\left(N_X^2 - N_{Xcr_y}^2\right) t_{31}^2}{2G_{12}} = \left(\gamma_{12a} - \gamma_{12cr}\right) \tau_{12cr} \tag{3.31}$$

Where γ_{12a} is the actual shear strain that the ply will experience (accounting for stiffness degradation), γ_{12cr} is the actual shear strain at which matrix cracking was initiated (accounting for stiffness degradation due to microscopic damage) and τ_{12cr} is the shear stress at which matrix cracking was initiated, which naturally corresponds to τ_{12a} shown in fig. 3.4, since stress-strain becomes perfectly plastic upon matrix cracking.

It follows that τ_{12cr} and γ_{12cr} can be found by evaluating eq. (3.14) at N_{Xcr_y}, which is shown below.

$$\tau_{12cr} = \tau_{12y} \sqrt{1 + \frac{k}{G_{12}} \left[\left(\frac{N_{Xcr_y} t_{31}}{\tau_{12y}} \right)^2 - 1 \right]}$$

$$\gamma_{12cr} = \tau_{12y} \left(\frac{1}{G_{12}} - \frac{1}{k} \right) + \frac{\tau_{12y}}{k} \sqrt{1 + \frac{k}{G_{12}} \left[\left(\frac{N_{Xcr_y} t_{31}}{\tau_{12y}} \right)^2 - 1 \right]}$$

$$\tag{3.32}$$

Looking at fig. 3.4, it is obvious that the residual modulus $\overline{G}_{12}$ is given by:

$$\overline{G}_{12} = \frac{\tau_{12a}}{\gamma_{12a}} \tag{3.33}$$

For perfectly plastic behavior due to matrix cracking, it is possible to set $\tau_{12a} = \tau_{12cr}$. Moreover, eq. (3.31) can be used to obtain γ_{12a}, which means the residual shear modulus for post-microscopic damage matrix cracking from eq. (3.33) can finally be defined as:

$$\overline{G}_{12} = \frac{\tau_{12a}}{\gamma_{12a}} = \frac{\tau_{12cr}}{\dfrac{\left(N_X^2 - N_{Xcr_y}^2\right) t_{31}^2}{2G_{12}\tau_{12cr}} + \gamma_{12cr}} =$$

$$= \frac{\tau_{12y} \sqrt{1 + \dfrac{k}{G_{12}} \left[\left(\dfrac{N_{Xcr_y} t_{31}}{\tau_{12y}} \right)^2 - 1 \right]}}{\dfrac{\left(N_X^2 - N_{Xcr_y}^2\right) t_{31}^2}{2G_{12}\tau_{12y} \sqrt{1 + \dfrac{k}{G_{12}} \left[\left(\dfrac{N_{Xcr_y} t_{31}}{\tau_{12y}} \right)^2 - 1 \right]}} + \tau_{12y} \left(\dfrac{1}{G_{12}} - \dfrac{1}{k} \right) + \dfrac{\tau_{12y}}{k} \sqrt{1 + \dfrac{k}{G_{12}} \left[\left(\dfrac{N_{Xcr_y} t_{31}}{\tau_{12y}} \right)^2 - 1 \right]}}$$

$$\tag{3.34}$$
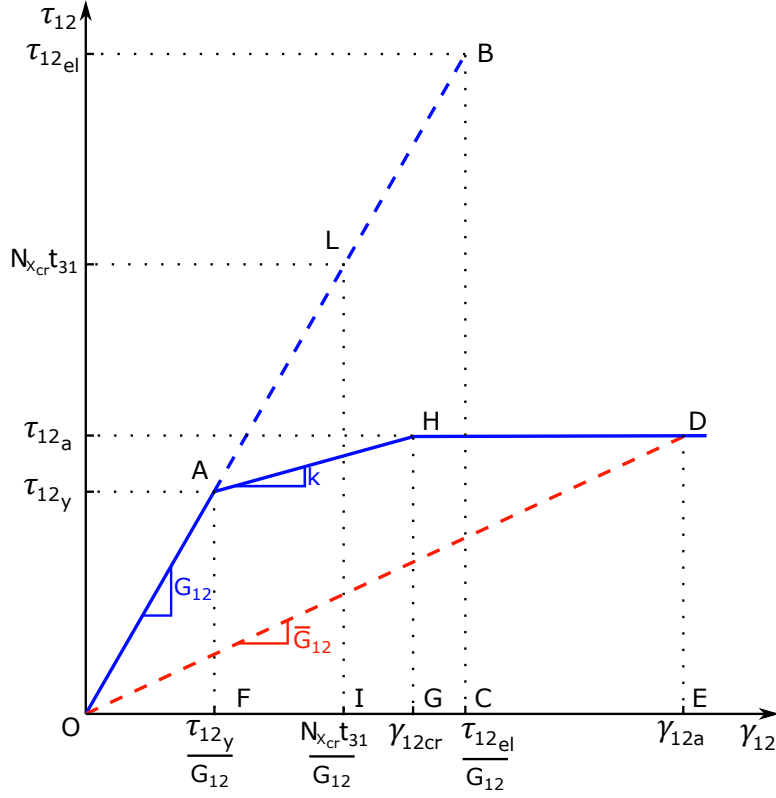
Figure 3.4: Ply material's shear behavior upon matrix cracking according to the energy equivalence model, assuming that microscopic damage has already occurred.

Where τ_{12cr} and γ_{12cr} were filled in from eq. (3.32). While the final definition of the residual shear modulus $\overline{G}_{12}$ shown in eq. (3.34) is unwieldy, it cannot be simplified in any meaningful way (to the author's knowledge).

3.4. Recoverable damage model

This static model differs from the model of section 3.3 mainly in the way shear is handled. It is postulated that transverse tension can only experience matrix cracks, while shear can only experience some unspecified microscopic damage [69]. It is assumed that shear and transverse tensile stresses both contribute towards damage initiation, which is predicted through Hashin's criterion, shown below:

$$\left(\frac{\sigma_{22}}{Y_{IS}^T}\right)^2 + \left(\frac{\tau_{12}}{S_{IS}}\right)^2 = 1 \quad \Rightarrow \quad N_{Xcr}^2\left[\left(\frac{t_{21}}{Y_{IS}^T}\right)^2 + \left(\frac{t_{31}}{S_{IS}}\right)^2\right] = 1 \quad \Rightarrow \quad N_{Xcr} = \frac{1}{\sqrt{\left(\frac{t_{21}}{Y_{IS}^T}\right)^2 + \left(\frac{t_{31}}{S_{IS}}\right)^2}} \quad (3.35)$$

Where the critical load N_{Xcr} is the laminate's longitudinal tensile load at which damage will be initiated, and the in situ shear strength S_{IS} is the knee of the bilinear approximation for shear, as defined in eq. (3.9). Damage evolution and residual modulus prediction is discussed for transverse tension in section 3.4.1 and for shear in section 3.4.2. The model is then validated in section 3.6.

3.4.1. Transverse tensile behavior

Similarly to section 3.3, it is postulated that transverse tension is affected by one damage type: matrix cracks. Again following section 3.3.2, matrix cracking will cause the transverse tensile response to turn perfectly plastic, which means that transverse tension will answer to the same principle of strain energy apportioning used in the aforementioned section. As a result, the final equation predicting the residual transverse tensile mod-
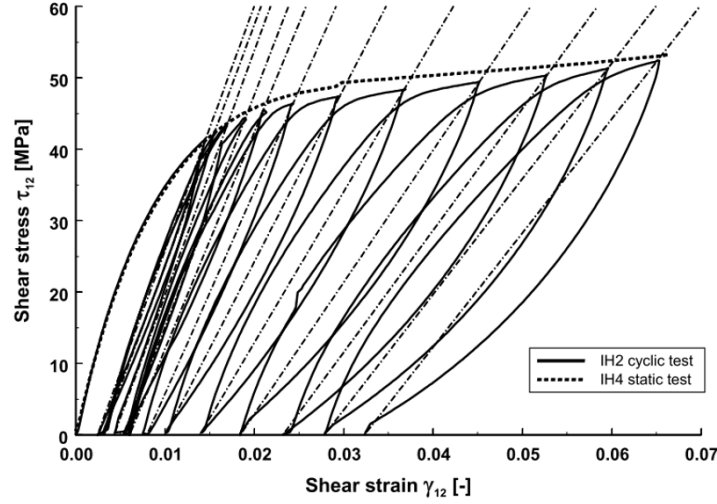
Figure 3.5: Shear stress-strain curve for two $[\pm 45°]_{2s}$ GFRP laminates, one tested under monotonic tension, the other under several loading/unloading cycles. The small differences between the monotonic and cyclic test are due to fact that two separate samples were used. Taken from [68]

ulus $\overline{E}_{22}$ will also be identical to eq. (3.28). The equation is repeated below for convenience.

$$\overline{E}_{22} = \frac{2E_{22}}{2 + \Delta H}$$

$$\text{with} \quad \Delta H = \begin{cases} N_X^2 \left[\left(\frac{t_{21}}{Y_{is}^T} \right)^2 + \left(\frac{t_{31}}{S_{is}} \right)^2 \right] - 1, & \text{if } N_X \geq N_{x_{cr}} \\ 0, & \text{if } N_X < N_{x_{cr}} \end{cases} \tag{3.36}$$

Note that in this case the critical matrix cracking load N_{Xcr} is the one calculated in eq. (3.35), which assumes linear behavior until damage onset.

3.4.2. Shear behavior

Before dwelling into shear behavior under the recoverable damage model, a few points must be mentioned. The "governing equations" provided in this section were based on qualitative assumptions and consideration derived from literature. Several attempts were made to rigorously derive a set of governing equations for the recoverable damage model. Unfortunately, none of them were considered mature enough to be inserted into this text.

What is presented here is therefore one of the "qualitative approaches" that was set up. Before showing any equations, it is useful to mention some important observations derived from literature [37, 38, 66, 68] regarding shear post-damage shear behavior.

1. When a ply is loaded monotonically in shear up to a specific point and then unloaded, the unloading stress strain curve will stop at a specific permanent shear strain γ_{12p}, associated with a specific residual shear modulus G_{12p}. This is the secant modulus between the permanent strain and unloading point, as shown by the straight lines in fig. 3.5.

2. Whenever the ply is reloaded/unloaded, as long as the original unloading load is not exceeded, the stress-strain curve will move along a hysteresis cycle connecting the point of permanent strain with the unloading point.

3. When the unloading point is exceeded, the stress-strain curve will rejoin the monotonic curve as if nothing happened. Hence, the portion of the stress-strain curve past the unloading point follows the same path that the monotonic curve would have followed, had unloading never happened. This is clearly visible in fig. 3.6.

It follows from the first observation that there must be a 1-to-1 correspondence between unloading point and
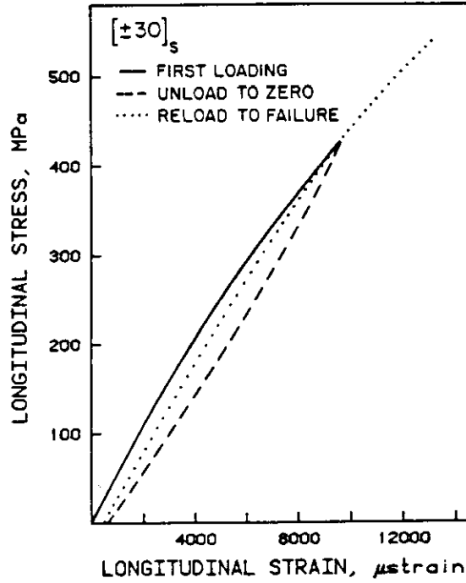
Figure 3.6: Shear stress-strain curve for a $[\pm 30°]_{2s}$ AS1/3501-6 laminate, loaded up to 0.5% strain, unloaded, then reloaded up to failure. Taken from [38]

each permanent strain - residual modulus couple. This means that each unloading point must be associated with a particular damage state.

It is postulated that said damage state is characterized by the presence of two damage types: unrecoverable damage, and recoverable damage. Unrecoverable damage manifests itself in the form of permanent shear strain γ_{12p}, and depends exclusively on the maximum load ever applied in the material's loading history so far (which coincides with the current unloading point). Unrecoverable damage is by definition permanent, since no change in loading condition can decrease the amount of damage.

Recoverable damage on the other hand is exclusively dependent on the load or strain being currently applied, and is associated with the residual modulus G_{12p}, which the model is trying to predict.

Damage associated with the secant modulus of the hysteresis cycle (G_{12p}) must be recoverable since as long as the unloading point is not exceeded, the stress-strain curve will always travel along the hysteresis cycle (observation nr.2). Moreover, once the hysteresis cycle is departed the monotonic curve will be rejoined and continued as if the hysteresis cycle never occurred (observation nr.3), thus proving that no permanent damage was induced within it, and that all of the damage associated with it must be recoverable.

It is recognized here that, while the secant modulus of the hysteresis cycle has just been associated with recoverable damage, there is path dependence within the hysteresis cycle (likely due to viscoelastic effects in the matrix under shear loading) which may or may not be associated with recoverable damage. Since the model is concerned with the secant modulus of the hysteresis cycle, and since the secant modulus is defined exclusively by the only two points on the hysteresis cycle which are path independent, it is assumed that the path dependence of the hysteresis cycle does not preclude the secant modulus G_{12p} from being associated with recoverable damage (for the purposes of this model).

For the proposed model, shear behavior is only affected by unspecified microscopic damage [69], which means that before damage initiation the shear response is elastic, while after damage initiation it will turn plastic (with slope k, according to section 3.2). Damage initiation occurs when $N_X = N_{Xcr}$, as detailed at the beginning of section 3.4. It is now convenient to derive an equation for the secant modulus of a pristine material (no permanent strains) experiencing recoverable damage. The secant modulus G_{12d} must be given by the line connecting the origin (zero stress-strain) with the point of applied stress-strain τ_{12a}-γ_{12a}, as shown in fig. 3.7.

Looking at fig. 3.7, it is apparent that the secant modulus G_{12d} is similar in nature to the residual shear modulus $\overline{G}_{12}$ under microscopic matrix damage from eq. (3.14). The main difference lays in the knee of the bilinear shear approximation. Rather than the apparent yield strength τ_{12y}, in this case it represents the

shear strength $N_{Xcr} t_{31}$, since microscopic shear damage is assumed to contribute towards damage initiation through Hashin's criterion, given in eq. (3.35).

Similarly to what was done for $\overline{G}_{12}$ in section 3.3.1, the residual modulus G_{12d} can be found by equating the excess strain energy density with its counterpart stored within plastic deformation, or in other words, by equating areas $OABC$ and $OADE$ from fig. 3.7. By doing so, and remembering that $\tau_{12el} = N_X t_{31}$, an expression for G_{12d} is obtained:

$$G_{12d} = \frac{G_{12} + \dfrac{k\Delta H}{1 + \sqrt{1 + \dfrac{k}{G_{12}}\Delta H}}}{1 + \dfrac{\Delta H}{1 + \sqrt{1 + \dfrac{k}{G_{12}}\Delta H}}} \tag{3.37}$$

Where ΔH is the Hashin failure index, defined in eq. (3.36). The modulus G_{12d} defined in eq. (3.37) thus represents recoverable damage occurring in a pristine material (no permanent strains). Naturally, the equation for G_{12d} that was just derived assumes the entirety of the applied strain to be recoverable. In other words, eq. (3.37) can predict the secant modulus G_{12d} due to recoverable damage under recoverable strains.

In reality, since the ply material will develop permanent strains once $N_X > N_{Xcr}$, the recoverable strain will only be a portion of the applied one. Looking at figs. 3.5 and 3.6, it can be seen that only the recoverable portion of the applied strain contributes to the load/stress experienced by the ply material within the hysteresis cycle (unloading/reloading). Since the hysteresis cycle was considered to be characterized only by recoverable damage (and some negligible viscoelastic effects), and since the entirety of the recoverable strain (upon unloading/reloading) is contained within the hysteresis cycle, it is assumed that eq. (3.37) should be able to represent the secant modulus of the hysteresis cycle, since the hysteresis cycle itself contains only recoverable damage and recoverable strains, similarly to the pristine material that eq. (3.37) was derived for. The secant modulus of an hysteresis cycle is denoted with G_{12p}, as shown in fig. 3.7.

It has been found in [37] that the ratio of permanent shear strain to applied shear strain increases monotonically with the applied strain. It follows that, as the applied load increases, the percentage of applied strain which is recoverable shrinks. This does not mean that the absolute amount of recoverable strain diminishes with increasing applied load, but only that its percentage compared to the total applied strain does.

To incorporate this observation into eq. (3.37), the load N_X which constitutes ΔH is scaled with the ratio of residual modulus G_{12p} to pristine modulus G_{12}, as shown below:

$$N_{X_s} = N_X \frac{G_{12p}}{G_{12}} \quad \Rightarrow \quad \Delta H_s = \left(\frac{N_X}{N_{Xcr}}\right)^2 \left(\frac{G_{12p}}{G_{12}}\right)^2 - 1 \tag{3.38}$$

Where the s subscript indicates that the quantities account for the aforementioned effects associated with shear. It is then postulated that an expression for G_{12p} can be created, shown in eq. (3.39) and based on eq. (3.37) for G_{12d}.

$$G_{12p} = \frac{G_{12} + \dfrac{k\Delta H_s}{1 + \sqrt{1 + \dfrac{k}{G_{12}}\Delta H_s}}}{1 + \dfrac{\Delta H_s}{1 + \sqrt{1 + \dfrac{k}{G_{12}}\Delta H_s}}} = \frac{G_{12} + \dfrac{k\left[\left(\frac{N_X}{N_{Xcr}}\right)^2 \left(\frac{G_{12p}}{G_{12}}\right)^2 - 1\right]}{1 + \sqrt{1 + \dfrac{k}{G_{12}}\left[\left(\frac{N_X}{N_{Xcr}}\right)^2 \left(\frac{G_{12p}}{G_{12}}\right)^2 - 1\right]}}}{1 + \dfrac{\left[\left(\frac{N_X}{N_{Xcr}}\right)^2 \left(\frac{G_{12p}}{G_{12}}\right)^2 - 1\right]}{1 + \sqrt{1 + \dfrac{k}{G_{12}}\left[\left(\frac{N_X}{N_{Xcr}}\right)^2 \left(\frac{G_{12p}}{G_{12}}\right)^2 - 1\right]}}} \tag{3.39}$$

To the author's knowledge, the expression in eq. (3.39) cannot be solved analytically with respect to G_{12p}. However, since it represents a root finding problem in a single variable, it can solved numerically extremely

Figure 3.7: Ply material's shear behavior upon appearance of microscopic matrix damage, according to the recoverable damage model.

quickly. Looking at eq. (3.39), it can be seen that the scaling performed through eq. (3.38) produced the desired effect. For a same applied N_X, the predicted G_{12p} will be larger than the predicted G_{12d}, since for the former only a portion of N_X is working towards creating recoverable strains. Moreover, as N_X increases, the ratio of recoverable to total applied strain decreases, since the factor $\frac{G_{12p}}{G_{12}}$ will be even lower.

To summarize, an expression relating applied load N_X to recoverable strains and modulus G_{12d} was defined in eq. (3.37). The expression was then expanded to account for the presence of permanent strains within the total applied strain, allowing for the prediction of the secant modulus G_{12p} associated with a hysteresis cycle of unloading/reloading. The fact that only a portion of the applied strain was recoverable was represented by a scaling factor $\frac{G_{12p}}{G_{12}}$ being applied to load N_X, which could also be seen as a measure of the extent of damage.

Finally, from geometry of fig. 3.7, permanent strain γ_{12p} can be defined as:

$$G_{12p}\left(\gamma_{12a} - \gamma_{12p}\right) = \gamma_{12a}G_{12d} \quad \Rightarrow \quad \gamma_{12p} = \gamma_{12a}\left(1 - \frac{G_{12d}}{G_{12p}}\right) \tag{3.40}$$

The proposed model presents two main issues:

- It is implicitly assumed that eq. (3.37), which was derived to estimate the secant modulus G_{12d} due to recoverable damage under recoverable strain in a pristine material, can also predict the secant modulus G_{12p} due to recoverable damage under recoverable strain in a damaged material ($\gamma_{12p} > 0$), as long as the applied load N_X has been scaled to reflect the fact that only a portion of the applied strain is recoverable. There is no hard evidence that the only effect caused by the presence of permanent strains should be a reduction in recoverable strain. The introduction of unrecoverable damage might have other effects that are presently not accounted by eq. (3.39).

- The scaling factor of $\frac{G_{12p}}{G_{12}}$ is arbitrary. It was chosen to represent the fact that the ratio of recoverable strain to total applied strain is directly proportional to damage. There is no particular reason why the scaling factor should not have another form, such as a more generic power law $\left(\frac{G_{12p}}{G_{12}}\right)^c$, where c is some constant.

Unfortunately, at the time of writing, no definitive answer has been reached regarding these issues. The model and ideas proposed in this section should not be seen as definitive or final As seen later in section 3.6.4, where validation is performed, the model proposed in this section achieves a good match with experimental data, better than the energy equivalence method, which is largely based on a similar modeling philosophy (eg. microscopic damage in shear, excess strain energy apportioning). This means that incorporating some of the observations and remarks made here into the energy equivalence model might actually bring drastic improvements to it.

3.5. Ply and laminate level

All theory discussed in section 3.3 and section 3.4 concerned the matrix within individual plies of a laminate. Since the model is designed to be used on laminates with any desired layup, it is necessary to express laminate properties as a function of ply properties. This can be easily done through Classical Laminated Plate Theory [31]. The local stiffness matrix of a pristine ply was defined in eq. (3.3), while an expression for its damaged counterpart is shown in eq. (3.41) below.

$$\underline{\underline{Q}}_{ply} = \begin{bmatrix} Q_{11} & Q_{12} & 0 \\ Q_{21} & Q_{22} & 0 \\ 0 & 0 & Q_{66} \end{bmatrix} = \begin{bmatrix} \dfrac{E_{11}}{1-\nu_{12}\overline{\nu}_{21}} & \dfrac{\nu_{12}\overline{E}_{22}}{1-\nu_{12}\overline{\nu}_{21}} & 0 \\ \dfrac{\overline{\nu}_{21}E_{11}}{1-\nu_{12}\overline{\nu}_{21}} & \dfrac{\overline{E}_{22}}{1-\nu_{12}\overline{\nu}_{21}} & 0 \\ 0 & 0 & \overline{G}_{12} \end{bmatrix} \tag{3.41}$$

Where E_{11} and ν_{12} are the pristine longitudinal stiffness modulus and major Poisson's ratio respectively. $\overline{E}_{22}$ and $\overline{G}_{12}$ (or G_{12p} for the recoverable damage model) are the residual transverse and shear stiffness moduli, while $\overline{\nu}_{21}$ is the residual minor Poisson's ratio, defined in eq. (3.42).

$$\overline{\nu}_{21} = \frac{\nu_{12}\overline{E}_{22}}{E_{11}} \tag{3.42}$$

Compliance of $\overline{\nu}_{21}$ with eq. (3.42) preserves each ply's special orthotropy, by enforcing $Q_{12} = Q_{21}$. To evaluate a laminate's residual stiffness for a specific load N_X, moduli $\overline{E}_{22}$ and $\overline{G}_{12}$ should be evaluated for each ply using the appropriate equations. After enforcing special orthotropy with eq. (3.42), it is possible to assemble the local stiffness matrix of each ply, which can then be assembled into the laminate's ABD stiffness matrix, shown in eq. (3.43).

$$\underline{\underline{ABD}} = \begin{bmatrix} \underline{\underline{A}}_{3x3} & \underline{\underline{B}}_{3x3} \\ \underline{\underline{B}}_{3x3} & \underline{\underline{D}}_{3x3} \end{bmatrix} \text{ with: } \underline{\underline{A}} = \sum_{k=1}^{n} \underline{\underline{C}}_k (z_k - z_{k-1}); \quad \underline{\underline{B}} = \frac{1}{2}\sum_{k=1}^{n} \underline{\underline{C}}_k (z_k^2 - z_{k-1}^2); \quad \underline{\underline{D}} = \frac{1}{3}\sum_{k=1}^{n} \underline{\underline{C}}_k (z_k^3 - z_{k-1}^3) \tag{3.43}$$

The laminate's longitudinal stiffness can be easily obtained through eq. (3.44).

$$E_x = \frac{1}{h} \frac{A_{11} A_{22} - A_{12}^2}{A_{22}} \tag{3.44}$$

Where h is the laminate's thickness. The laminate's major Poisson's ratio can be found through eq. (3.45).

$$\nu_{xy} = \frac{A_{12}}{A_{22}} \tag{3.45}$$

To summarize, the procedure to determine the laminate stiffness properties in the presence of matrix damage in any of its plies is as follows:

1. Obtain the required material properties, which include: the ply material's mechanical properties (E_{11}, E_{22}, G_{12} and ν_{12}), its transverse tensile in situ strength (or alternatively just the standard transverse tensile strength) and the ply material's shear stress-strain curve, up to failure (needed for the bilinear approximation in section 3.2)

2. Use classical laminated-plate theory with pristine material properties to determine the stress-load relations (t_{31} and t_{21}) for shear and transverse stresses in each ply in the local (ply) axis system.

3. For every desired applied load N_X, find the residual E_{22} and G_{12} for each ply, using the appropriate equations from either section 3.3 or section 3.4. All governing equations are closed-form expressions, which means that for each N_X it is possible to immediately calculate the resulting stiffness degradation, without any need to calculate or account for previous loads and without any iteration.

4. With the updated stiffness properties from the previous step, calculate the residual ν_{12} necessary to preserve special orthotropy within each ply, then use classical laminated-plate theory to obtain the laminate's residual axial modulus E_X and residual major Poisson's ratio ν_{xy}.

3.6. Validation

Model validation was performed through experimental data available in literature. All tests involved quasi-static uniaxial tensile loading of laminate coupons and recorded at least one of the following: stiffness degradation (at ply or laminate level), residual Poisson's ratio (at ply or laminate level) and permanent shear strain (at ply level).

To demonstrate the versatility of the model with different materials and layups, test data was selected to cover 5 different ply materials and 13 different layups. Said layup variety is important, since the proposed model predicts damage induced by transverse tension and shear, meaning that there are fundamentally three possible damage scenarios: tension dominated (eg. $[0, 90_2]_S$), shear dominated (eg. $[\pm 45]_{2S}$), and a scenario where the two are comparable (eg. $[\pm 40, 90_4]_S$). All experimental data was obtained from existing literature, namely [25], [70], [69], [65], [66] and [37]. Section 3.6.1 contains an introduction to each separate "batch" of validation data. Validation for cross-ply laminates is illustrated in section 3.6.2, while validation for non-cross-ply laminates is covered in section 3.6.3 and section 3.6.4, with the former using the model from section 3.3 and the latter using the model from section 3.4.

3.6.1. List of sources and ply material data

Comparisons with $[0/90_3]_S$ and $[90_3/0]_S$ glass/epoxy laminates [25]

Data on the glass fiber epoxy unidirectional material used by Highsmith and Reifsnider [25] is summarized in table 3.1. Note that two different transverse in-situ strength values are used here, one for each laminate. These values were obtained by extrapolating data in [25] at the point where the first matrix cracks appeared. As mentioned in [3], in situ strength is dependent on the thickness of the off-axis plies and on the orientation and stiffness of their neighboring plies. The in situ strength is higher when the neighboring plies are stiffer and this would be the case of 90 degree plies embedded in 0 degree plies, as in laminate $[0/90_3]_S$. Outer plies with matrix cracks, as in the $[90_3/0]_S$ laminate, can be seen as an extreme case where one of the adjacent plies has zero stiffness, causing the in situ strength to drop considerably. As a result, the in-situ strength of the $[90_3/0]_S$ laminate is 35% lower than its counterpart with embedded off-axis plies $[0/90_3]_S$.

Laminates were loaded in longitudinal tension. Measurements of the laminate's residual longitudinal stiffness were performed by unloading the laminate and associating the recorded modulus with the stress at which unloading started. The laminate would then be reloaded monotonically until the next (higher) unloading point.

Comparisons between predictions and test data for the laminate's residual longitudinal stiffness can be found in fig. 3.10 for both the $[90_3/0]_S$ and $[0/90_3]_S$ glass/epoxy laminates.

Table 3.1: Required input data Highsmith and Reifsnider 1982 [25]

Property	Value	Source
E_{11} (GPa)	41.70	[25]
E_{22} (GPa)	13.00	[25]
G_{12} (GPa)	3.40	[25]
ν_{12} (-)	0.300	[25]
$Y_{is}^{T}*[0,90_3]_s$ (MPa)	34.05	[25]
$Y_{is}^{T}*[90_3,0]_s$ (MPa)	22.04	[25]
S_k (MPa)	[-]	[-]
k (GPa)	[-]	[-]

*Value derived from data within source.

Comparisons with $[\pm\theta/90_4]_S$ glass/epoxy laminates [70]

Varna, Joffe et al. [70] have carried out tests on $[\pm\theta,90_4]_s$ laminates, with θ = 0, 15, 30 and 40 degrees. The material properties used for the predictions are listed in table 3.2 and were taken from [29] and [58]. The in situ transverse tensile strength and in situ shear strength are also shown in table 3.2. Since they were not explicitly given by the authors, they had to be estimated.

Table 3.2: Required input data for Varna, Joffe et al. 2001 [70]

Property	Value	Source
E_{11} (GPa)	44.73	[29]
E_{22} (GPa)	12.76	[29]
G_{12} (GPa)	5.8	[29]
ν_{12} (-)	0.297	[29]
$Y_{is}^{T}*$ (MPa)	70.96	[70]
S_k^* (MPa)	56.08	[58]
k^* (GPa)	0.56	[58]

*Value derived from data within source.

Before estimating the in situ strengths, it should be noted that Varna, Joffe et al. did not include a monotonic shear stress-strain curve (necessary for the bilinear approximation shown in section 3.2) in any of their papers. Since it was impossible to find the aforementioned data for the material they used (HyE 9082Af, Fiberite), the shear stress-strain curve of a similar material was used instead, namely E-Glass/MY750 from [58]. The shear moduli of the two materials are the same, and other (known) shear properties are also similar. Moreover, Vyas and Pinho [71] use E-Glass/MY750 from [58] to "fill-in" some mechanical properties (including shear ones) missing from HyE 9082Af/Fiberite from Varna, Joffe et al.[69], explicitly stating that the two materials are similar.

Hence, the knee of the bilinear shear approximation is found through the procedure described in section 3.2, eq. (3.9), applied to E-Glass/MY750 test data from [58]. The knee S_k of the curve will then represent the apparent yield strength τ_{12y} for the energy equivalence model in section 3.3 and the shear in situ strength S_{IS} for the model in section 3.4.

The transverse in situ strength can be found by calculating the magnitude of the transverse stress in the 90 plies corresponding to the first instance of stiffness degradation in [70]. Using fig. 3.8 as reference, taken from [70], the first occurrence of matrix cracks can be defined as the intersection between the horizontal line indicating a pristine modulus ($E_X/E_{X0} = 1$) and a second order polynomial fit, based on all experimental data points with residual stiffness lower than one. The applied mechanical strain found at the intersection of the fit and the "horizontal pristine line" is then used to load the laminate. The resulting stress in the 90 plies found through classical laminated-plate theory, represents the transverse tensile in situ strength, listed in Table table 3.2.
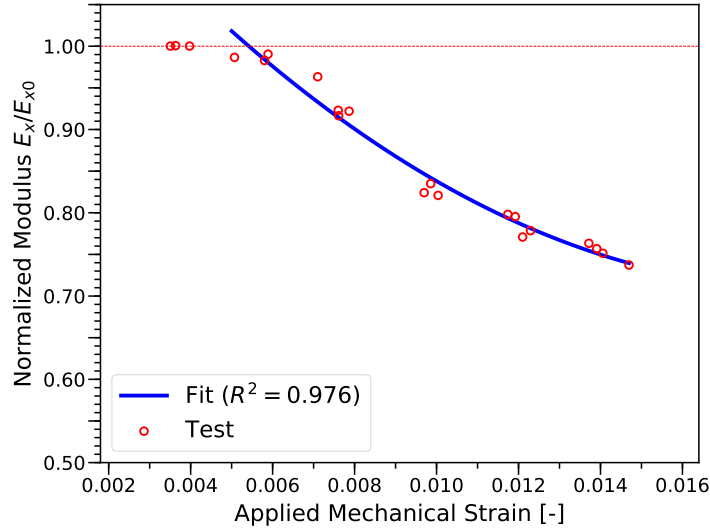
Figure 3.8: Finding transverse tensile in situ strength through first instance of damage within $[0_2, 90_4]_s$ laminate. Test data from [70]

The in situ shear strength for the energy equivalence model can be found through a procedure similar to the one followed for the transverse tensile in situ strength. First, the strain at which damage is initiated is found through experimental data for the $[0, \pm 70_4, 0_{1/2}]_S$ laminate from [69], which uses the same material being covered here (as will be seen in the next section). The axial load corresponding to said strain (for a pristine laminate) is set to be the critical load used in Hashin's failure criterion for matrix cracking, shown in eq. (3.19). Since Y_{IS}^T is known, it is then possible to solve for the shear in situ strength S_{IS} (for the energy equivalence model).

Table 3.3 contains an index associating all tested layups and monitored properties to a specific figure. All four laminates have been tested under quasi-static longitudinal loads. The sample would be loaded up to a specific point, partially unloaded to measure Young's modulus and Poisson's ratio, and then reloaded up to a higher point. The measured residual properties were associated to the axial strain corresponding to the load from which unloading started.

Table 3.3: Index of comparisons for Varna, Joffe et al. 2001 [70]

Layup	E_x/E_{x0}	ν_{xy}/ν_{xy_0}
$[0_2, 90_4]_s$	fig. 3.11	fig. 3.11
$[\pm 15, 90_4]_s$	fig. 3.17	fig. 3.17
$[\pm 30, 90_4]_s$	fig. 3.18	fig. 3.18
$[\pm 40, 90_4]_s$	fig. 3.19	fig. 3.19

Comparisons with $[0/\pm \theta_4/0_{1/2}]_S$ glass/epoxy laminates [69]
The ply material used in Varna, Joffe et al. 1999 [69] for $[0/\pm \theta_4/0_{1/2}]_S$ laminates is identical to the one described in the previous section and used on $[\pm \theta/90_4]_S$ laminates, meaning that all properties listed table 3.2 and all considerations made on both in situ strengths apply to this section as well. Table 3.4 shows which laminates were tested, what properties were monitored, and where to find them. All laminates below have been tested under the same unloading/reloading cyclic loading pattern mentioned in the previous section.

Table 3.4: Index of comparisons for Varna, Joffe et al. 1999 [69]

Layup	E_x/E_{x0}	ν_{xy}/ν_{xy_0}
$[0,90_8,0_{1/2}]_s$	fig. 3.12	fig. 3.12
$[0,\pm25_4,0_{1/2}]$	fig. 3.20	fig. 3.20
$[0,\pm40_4,0_{1/2}]_s$	fig. 3.21	fig. 3.21
$[0,\pm55_4,0_{1/2}]_s$	fig. 3.22	fig. 3.22
$[0,\pm70_4,0_{1/2}]_s$	fig. 3.23	fig. 3.23

Comparisons with $[0/90_2]_S$ [65] and $[\pm45_2]_S$ [66] glass/epoxy laminates

Van Papegem made use of the same glass fiber epoxy material in both [65] and [66], for $[0/90_2]_S$ and $[\pm45_2]_S$ laminates respectively. The ply's stiffness moduli, Poisson's ratio and transverse tensile strength can all be found in [68]. An experimental shear stress-strain curve for the material in question can also be found in figure 3 of [68], which allows to calculate the knee and slope of the bilinear shear approximation by means of eq. (3.9) and eq. (3.8) respectively, both defined in section 3.2. All aforementioned properties are listed in table 3.5.

Table 3.5: Required input data for Van Paepegem 2010 [65] and Van Paepegem et al. 2006 [66]

Property	Value	Source
E_{11} (GPa)	38.90	[68]
E_{22} (GPa)	13.30	[68]
G_{12} (GPa)	5.13	[68]
ν_{12} (-)	0.258	[68]
$Y_{is}^{T}{}^{*}$ (MPa)	36.5	[68]
S_k^{*} (MPa)	45.18	[66]
k^{*} (GPa)	0.1271	[66]

* Value derived from data within source.
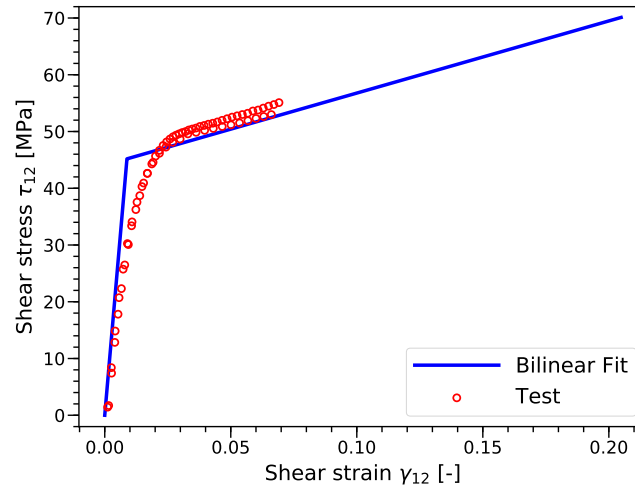
Figure 3.9: Finding in situ shear strength through bilinear approximation of shear stress-strain curve derived from [66]

Looking at the shear bilinear approximation in fig. 3.9, one can see that the experimental curve stops much sooner than its approximation. As stated in [68], the strain gauges used during the test were saturated around 7% strain, meaning that strain at ultimate failure was not recorded. Ultimate shear stress was recorded to be around 70MPa (extrapolated from the sample's failure load). In order to estimate the ultimate shear strain,

a linear fit was run through the last available data points, which show a decidedly linear trend. The ultimate shear strain was then assumed to have the value necessary to reach the ultimate shear stress, resulting an the ultimate shear strain being a little over 20%. While this strain value may seem high, it does yield realistic results, and failure strains around 20% have been observed before for laminates dominated by shear [37].

The $[0, 90_2]_S$ samples were loaded monotonically in longitudinal tension, while the $[\pm 45_2]_S$ samples were subject to quasi-static longitudinal tensile loading, where the residual shear modulus was reported as the secant one during one full unloading/reloading cycle, as shown in **??**.

Comparisons between the model and test data for the $[0, 90_2]_S$ samples' residual Poisson's ratio can be seen in fig. 3.13, while for $[\pm 45_2]_S$ samples predictions of the residual shear modulus and permanent shear strain are shown in fig. 3.24.

3.6.2. Validation of both models for cross-ply laminates

This section contains comparisons between the model's predictions and experimental data for all cross-ply laminates associated with the "batches" of validation data introduced in section 3.6.1. The order of the subsections is the same as section 3.6.1. The last batch of data is not covered since it did not contain any cross-ply laminates.

It should be noted that for cross-ply laminates, due to the complete lack of shear, both static models will give the exact same predictions, since all differences between them are induced by shear. To be precise, the model from section 3.3 will predict the residual transverse modulus through eq. (3.28), while the one from section 3.4 will use eq. (3.36). Since for $t_{31} = 0$ the critical cracking load N_{Xcr} must be identical for both models, it follows that their predictions for cross-ply laminates will be identical.

Comparisons with $[0/90_3]_S$ and $[90_3/0]_S$ glass/epoxy laminates [25]

Plots of normalized stiffness as a function of applied axial stress for the two laminates are shown in fig. 3.10. Very good to excellent agreement with test results is observed with less than 8% discrepancy between tests and predictions. Note that the y axis scale starts from 0.5 instead of 0 in order to magnify the differences. It should be noted that the small horizontal section at prediction's start in fig. 3.10 (left) is due to the choice of in situ strength. When interpolating crack density data from [25] to find the in situ strength for $[0, 90_3]_S$, the very first crack density data-point was excluded, since it occurred at extremely low stresses and was likely caused by material imperfections. If said value is included, the prediction's start will match the test perfectly, at the cost of accuracy closer to failure. This demonstrates that the effect of imperfections on in situ strength evaluation should be minimized. While accounting for them may improve the results for lower loads, it reduces accuracy for higher ones, which are more interesting (from a design perspective) since they are closer to failure.
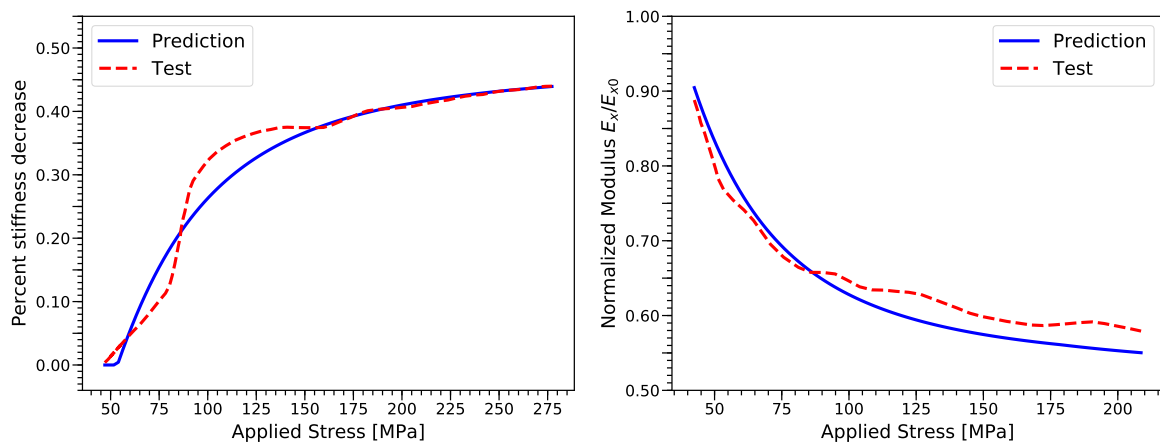
Figure 3.10: Normalized stiffness as a function of applied stress for $[0, 90_3]_S$ (left) and $[90_3, 0]_S$ (right) glass/epoxy laminates. Test data from [25]

Comparisons with $[0_2/90_4]_S$ glass/epoxy laminates [70]
The model's predictions can be found in fig. 3.11. The model shows an excellent match with experimental data for the normalized residual laminate stiffness E_X/E_{X0}. The match with the residual laminate's Poisson's ratio ν_{xy}/ν_{xy0} is also good, although for strains higher than 1.2% the prediction departs the test's mean, while still falling somewhat within experimental scatter. This might be due to additional damage types / non-linearities that appear at higher strains, which the model does not account for.
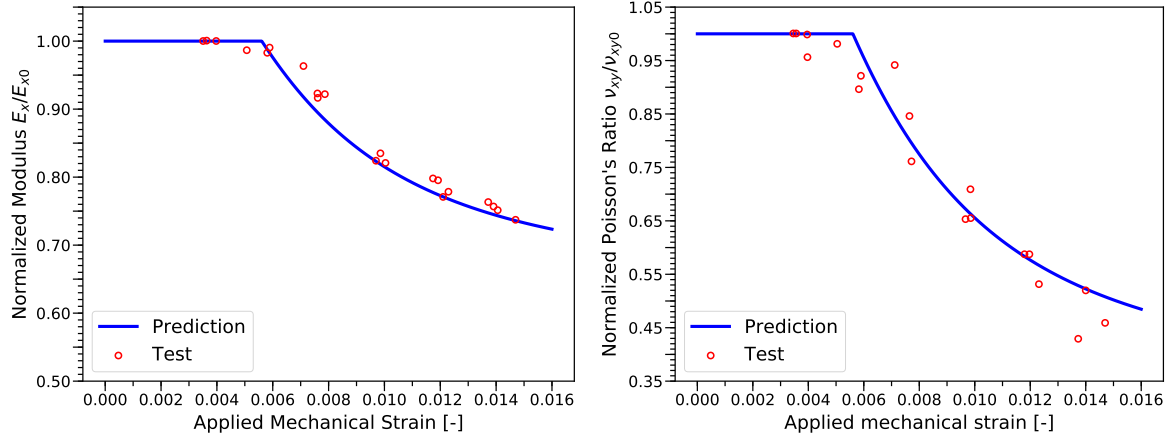
Figure 3.11: Longitudinal stiffness degradation (left) and residual Poisson's ratio (right) predictions for $[0_2, 90_4]_s$ laminate under quasi-static uniaxial tensile loading. Test data from [70]

Comparisons with $[0/90_8/0_{1/2}]_S$ glass/epoxy laminates [69]
The model's predictions can be found in fig. 3.12. Results are excellent for both residual laminate's stiffness and Poisson's ratio. Unlike the previous case, the Poisson's ratio prediction is still excellent for axial strains well above 1.2%.
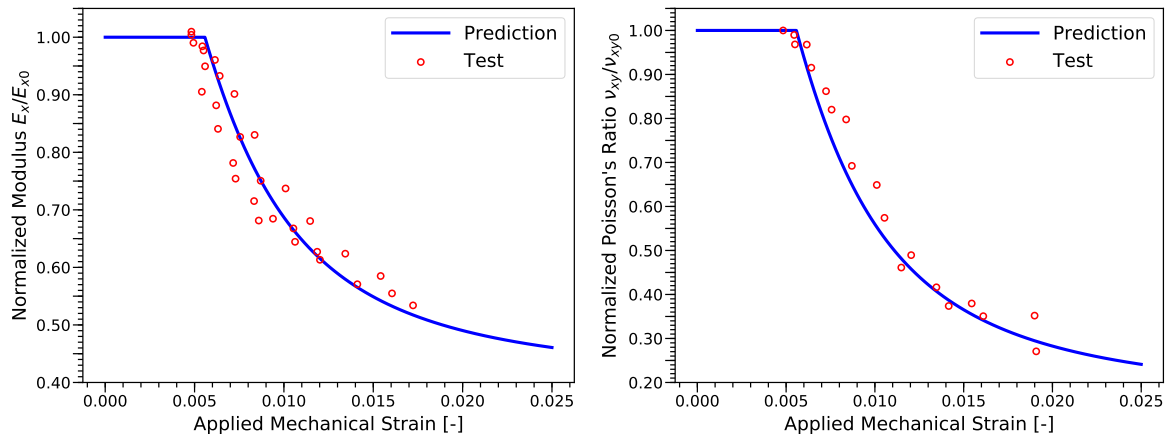
Figure 3.12: Longitudinal stiffness degradation (left) and residual Poisson's ratio (right) predictions for $[0, 90_8, 0_{1/2}]_s$ laminate under quasi-static uniaxial tensile loading. Test data from [69]

Comparisons with $[0/90_2]_S$ glass/epoxy laminates [67]
The comparison between the model's prediction and experimental data is shown in fig. 3.13. Excellent agreement with tests is observed up to a strain of 0.017, after which the prediction departs from experimental data. It should be noted that one of the two test samples from [67] failed at a strain of 0.020 (shown in the figure), and while the strain gauge on the other sample was lost at 0.010 due to debonding, its failure stress was extremely close to the former sample. This indicates that predictions only depart from experimental data close to failure. It is likely that additional damage modes appear close to failure (eg. fiber fracture, delamination) which are not included in the model, thus explaining the discrepancy.

Finally, it should be noted that normalization of test data was performed with the second point of each test curve, corresponding to a Poisson's ratio of around 0.15. The first points can be regarded as outliers, and Van Paepegem himself states that the initial Poisson's ratio can be taken to be ≈ 0.15 [67].
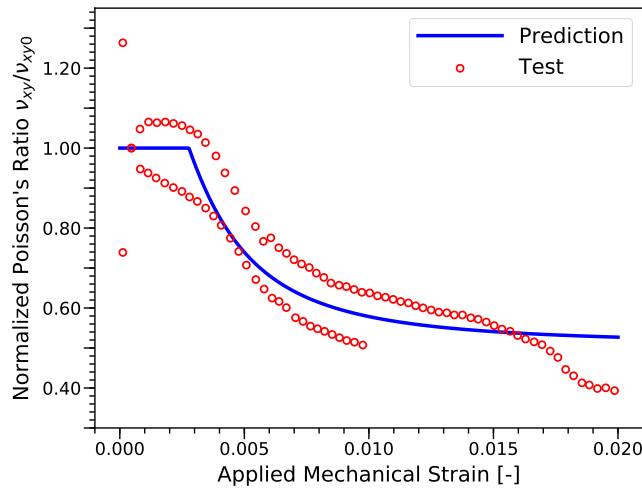
Figure 3.13: Residual Poisson's ratio predictions for $[0, 90_2]_S$ laminate under quasi-static uniaxial tensile loading. Test data from [67]

3.6.3. Validation of the energy equivalence model for selected non-cross-ply laminates

This section contains comparisons between the predictions made with the model from section 3.3 and experimental data for selected non-cross-ply laminates associated with the "batches" of validation data introduced in section 3.6.1. The validation shown here is limited to selected data because the model is known to be (at the moment of writing) too conservative. Since changes will surely be made to the formulas behind the model, it was decided to only show some selected results, representative of the model's strengths and weaknesses.

As stated in section 3.6.2, both models from section 3.3 and section 3.4 achieve the same results when dealing with cross-ply laminates, which are characterized exclusively by transverse tensile damage. All laminates covered here are therefore non-cross-ply.

Comparisons with three laminates will be presented here, starting with the $[\pm30, 90_4]_S$ GFRP laminate from [70], for which the residual axial modulus and residual Poisson's ratio predictions are shown in fig. 3.14. The match with experimental data is very good in both cases. While the model is slightly conservative compared to the test mean, both predictions are within experimental scatter. In both plots, two kinks can be identified: a major one when the strain is equal to 0.006, and a minor one around 0.009. The former is caused by the onset of cracking the 90 degree plies, while the latter is caused by cracking in the 30 degree plies.

Comparisons for the $[0, \pm70_4, 0_{1/2}]_S$ GFRP laminate from [69] are shown in fig. 3.15, which contains predictions of the residual axial modulus and residual Poisson's ratio. The modulus predictions are excellent, with the model matching the test data's mean up to a strain of 0.013, at which point the predictions becomes slightly conservative, falling just short of the experimental scatter. Predictions for the residual Poisson's ratio are completely off the mark, although at the very least damage initiation is predicted appropriately. It is very interesting to see that, for the same laminate, the recoverable damage model from section 3.4 obtains similar results for the modulus degradation, while also matching the Poisson's ratio fairly well.

The residual axial modulus and residual Poisson's ratio of the $[0, \pm40_4, 0_{1/2}]_S$ GFRP laminate from [69] are predicted in fig. 3.16. There is a large discrepancy between predictions and test results. The matrix develops microscopic damage at a strain of around 0.006, as witnessed by the main kink in the residual laminate stiffness curve, and then proceeds to develop cracks around 0.011, as proven by the minor kink in the stiffness degradation curve. This means that shear modulus degradation for the model is too aggressive not only for matrix cracking, but also for microscopic damage, as shown by the poor match with experimental data during the microscopic damage regime.
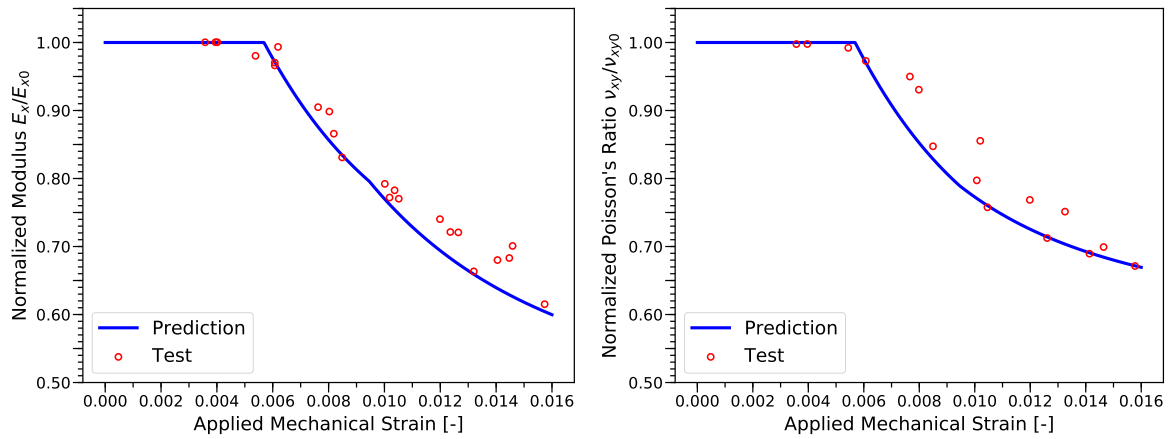
Figure 3.14: Longitudinal stiffness degradation (left) and residual Poisson's ratio (right) predictions for $[\pm30, 90_4]_S$ laminate under quasi-static uniaxial tensile loading, using the model from section 3.3. Test data from [70]
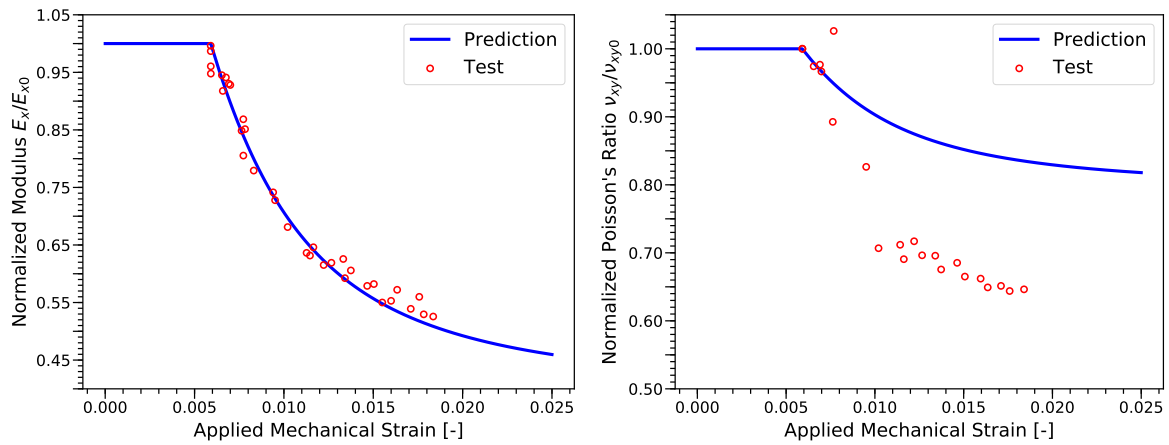
Figure 3.15: Longitudinal stiffness degradation (left) and residual Poisson's ratio (right) predictions for $[0, \pm70_4, 0_{1/2}]_S$ laminate under quasi-static uniaxial tensile loading, using the model from section 3.3. Test data from [69]
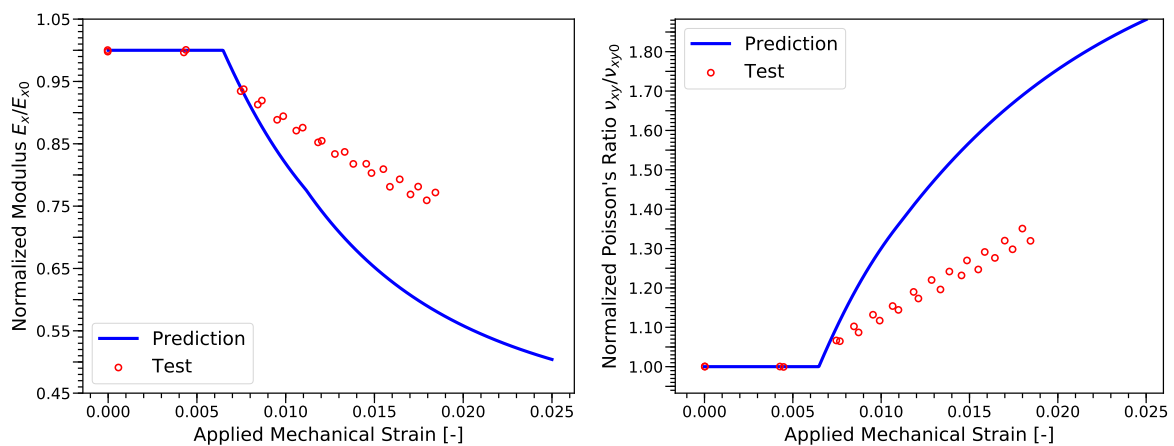
Figure 3.16: Longitudinal stiffness degradation (left) and residual Poisson's ratio (right) predictions for $[0, \pm40_4, 0_{1/2}]_S$ laminate under quasi-static uniaxial tensile loading, using the model from section 3.3. Test data from [69]

3.6.4. Validation of recoverable damage model for non-cross-ply laminates

This section contains comparisons between the predictions made with the model from section 3.4 and experimental data for all non-cross-ply laminates associated with the "batches" of validation data introduced in section 3.6.1. The order of the sub-sections is the same as section 3.6.1. The first batch of data is not covered since it did not contain any non-cross-ply laminates.

Comparisons with $[\pm\theta/90_4]_S$ glass/epoxy laminates [70]

Before discussing each comparison in detail, some general remarks can be made. First of all, the model's predictions show excellent to good match with experimental data. For all residual stiffness comparisons, the model's prediction is always accurate, falling within experimental scatter. For cases with both shear and tensile damage ($[\pm30,90_4]_s$ fig. 3.18 and $[\pm40,90_4]_s$ fig. 3.19) residual stiffness predictions tend to be a little conservative compared to the experimental data's mean, but they always fall within experimental scatter. Predictions of the residual Poisson's ratio are good to acceptable. Unlike the stiffness ones, they do fall just outside of experimental scatter (on the lower side), especially for laminates with a stronger presence of shear damage ($[\pm30,90_4]_s$ and $[\pm40,90_4]_s$) Overall, the results can be regarded as very good, especially when considering the small amount of experimental data required, the model's simplicity and its fast computational speed.

It is interesting to remark that, while in situ tensile strength was predicted using exclusively data from $[0_2,90_4]_s$, damage onset (kink in the prediction curve) is accurately predicted for every single laminate. This goes to show that the in situ strength's variation over different laminates may not be as drastic as implied in [3].

Looking at all results where $\theta > 0$, it can be seen that the model also accounts for damage in the angle-plies (θ). In all cases the 90 degree plies are the first ones to fail, as can be seen by the strong departure from the horizontal line in all plots. Smaller kinks appear around 1.4%, 0.825% and 0.7% strain for θ equal 15, 30 and 40 degrees respectively. The aforementioned smaller kinks represent the onset of damage within non-90 degree plies. As expected, when $\theta = 0$ in fig. 3.11 there are no "secondary" kinks, as matrix stresses are too low to induce any failure in the 0 plies. As θ increases, the strain location of the smaller kink decreases, which is expected since a larger θ means that the matrix is experiencing higher stresses (both transverse tensile and shear).
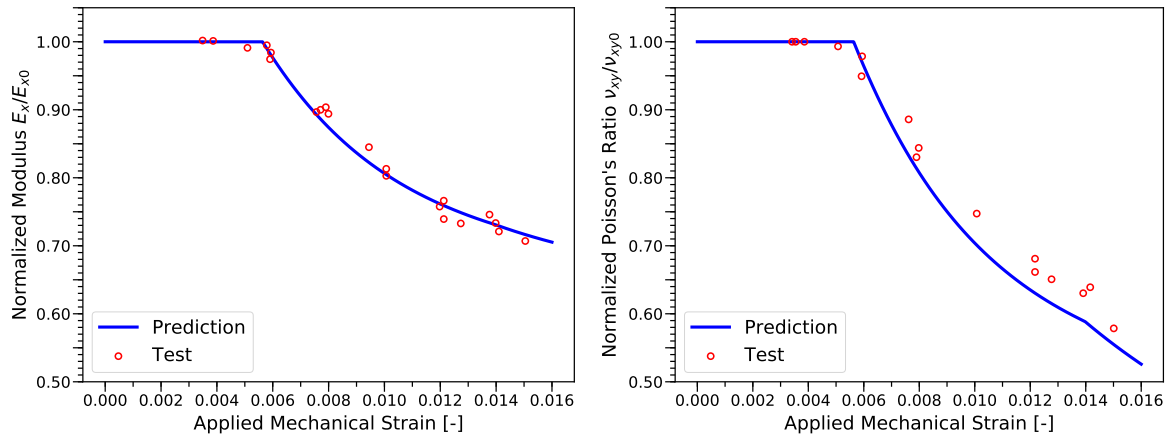
Figure 3.17: Longitudinal stiffness degradation (left) and residual Poisson's ratio (right) predictions for $[\pm15,90_4]_S$ laminate under quasi-static uniaxial tensile loading, using the recoverable damage model from section 3.4. Test data from [70]
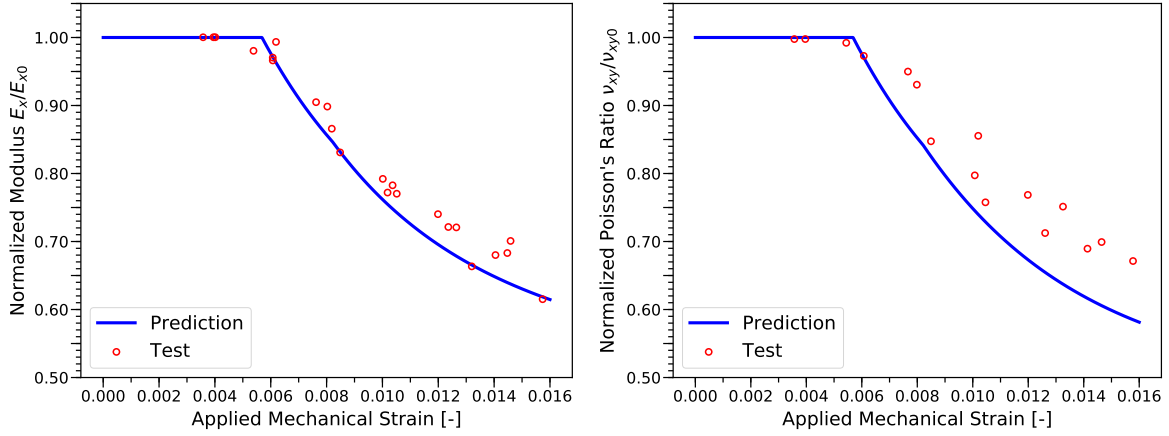
Figure 3.18: Longitudinal stiffness degradation (left) and residual Poisson's ratio (right) predictions for $[\pm 30, 90_4]_s$ laminate under quasi-static uniaxial tensile loading, using the recoverable damage model from section 3.4. Test data from [70]
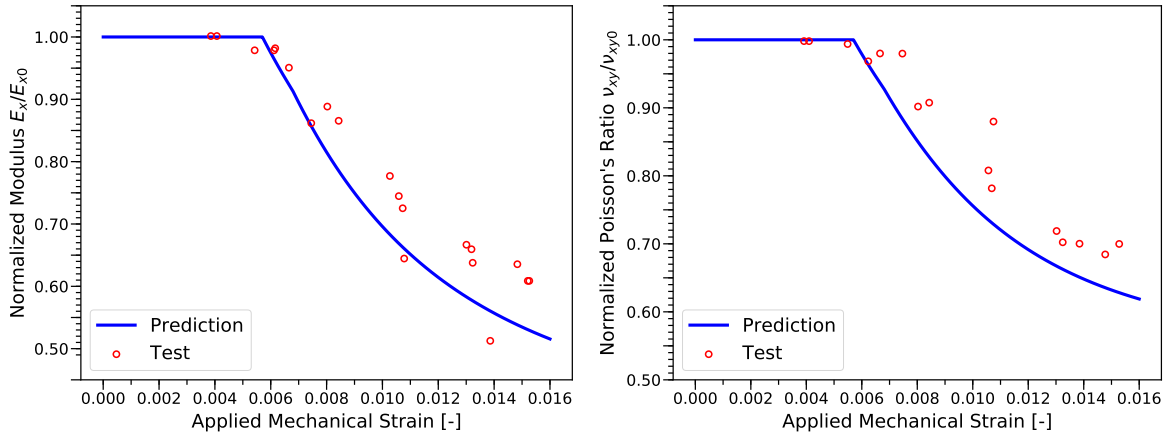
Figure 3.19: Longitudinal stiffness degradation (left) and residual Poisson's ratio (right) predictions for $[\pm 40, 90_4]_s$ laminate under quasi-static uniaxial tensile loading, using the recoverable damage model from section 3.4. Test data from [70]

Comparisons with $[0/\pm\theta_4/0_{1/2}]_S$ glass/epoxy laminates [69]

Compared to the previous section, it is harder to make general remarks on the quality of this batch of comparisons, due to a wider spectrum of model accuracy. Stiffness degradation and residual Poisson's ratio predictions for $[0, \pm 70_4, 0_{1/2}]_s$ are very good, as shown in fig. 3.23.

Residual stiffness predictions for the $[0, \pm 40_4, 0_{1/2}]_s$ and $[0, \pm 25_4, 0_{1/2}]_s$ laminates (fig. 3.21 and fig. 3.20 respectively) are very good. It should be noted that the large scatter associated with the $[0, \pm 25_4, 0_{1/2}]_s$ data makes it hard to estimate the quality of the prediction, although the match with the residual Poisson's ratio of the same laminate is good, despite apparently predicting the onset of damage at higher strains than test data. Finally, predictions for the residual Poisson's ratio of $[0, \pm 40_4, 0_{1/2}]_s$ are acceptable for lower strains.

For the $[0, \pm 55_4, 0_{1/2}]_s$ laminate, shown in fig. 3.22, match with residual stiffness test data is acceptable, while the Poisson's ratio prediction is completely off. It should be noted that Varna, Joffe et al [69] also had some issues matching test data for the $[0, \pm 55_4, 0_{1/2}]_s$ laminate, mentioning that plots of crack density VS applied strain for two samples of said laminate showed two distinct parallel lines, rather than a single one with a common trend-line. Moreover, residual Poisson's data provided has fewer data points than all other laminates and does not show the sample in its pristine form. All of the above considerations hint at the fact that there might be irregularities with the test data of this particular sample.

Overall, comparisons with test data were good. Considering that the match with data for the $[0, 90_8, 0_{1/2}]_s$ (fig. 3.12) laminate of this same batch was excellent, and considering that results for the $[0, \pm 70_4, 0_{1/2}]_s$ lam-

inate are also the best in this section, it follows that the loss of model accuracy might be tied to its shear component. Comparisons with $[0, \pm40_4, 0_{1/2}]_s$ and $[0, \pm25_4, 0_{1/2}]_s$ have indeed shown that the model is currently overshooting the point of damage onset. Using a lower in situ shear strength might considerably improve predictions, but there is no way to justify such a reduction at this point. It is important to keep in mind that the in situ strengths used here, as mentioned in section 3.6.1, were not obtained directly from the $[0, \pm\theta, 0_{1/2}]_s$ laminates, which means some (small) level of mismatch for damage initiation is to be expected.
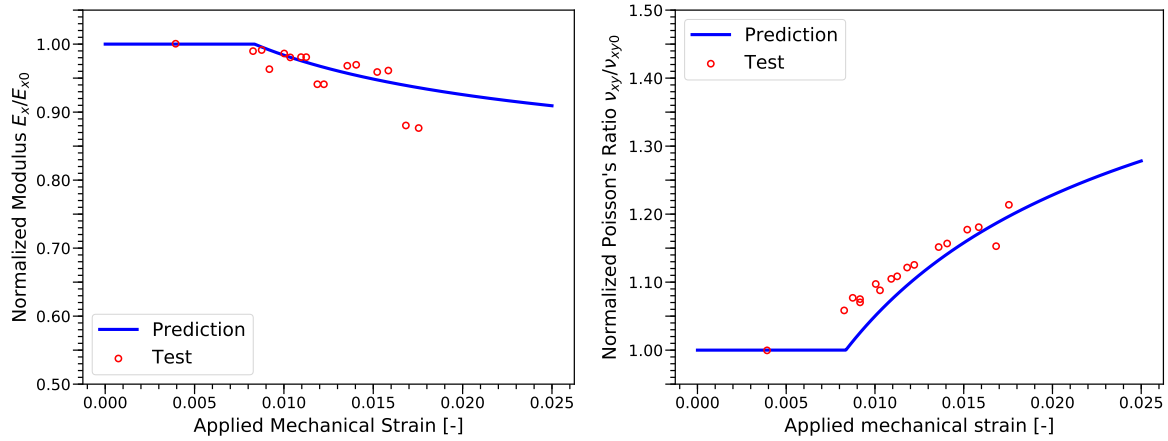
Figure 3.20: Longitudinal stiffness degradation (left) and residual Poisson's ratio (right) predictions for $[0, \pm25_4, 0_{1/2}]_S$ laminate under quasi-static uniaxial tensile loading, using the recoverable damage model from section 3.4. Test data from [69]
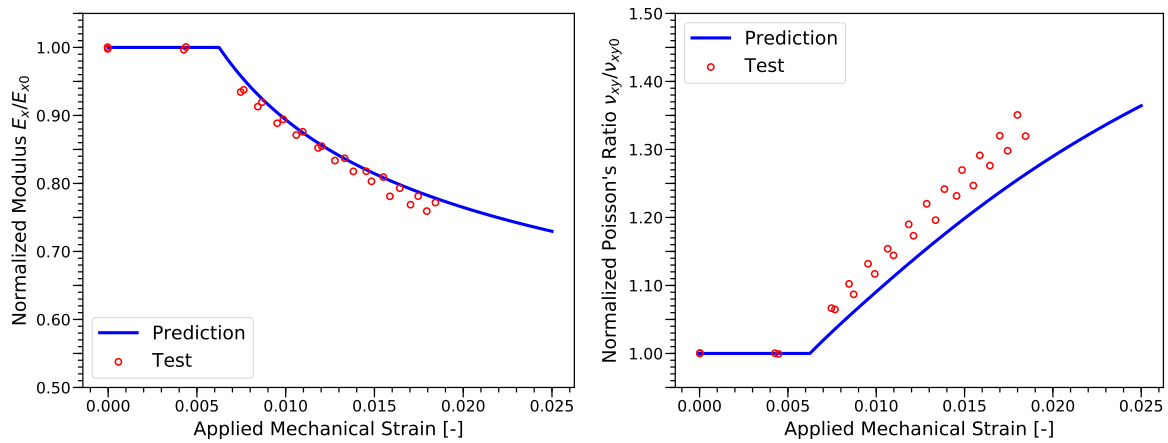
Figure 3.21: Longitudinal stiffness degradation (left) and residual Poisson's ratio (right) predictions for $[0, \pm40_4, 0_{1/2}]_S$ laminate under quasi-static uniaxial tensile loading, using the recoverable damage model from section 3.4. Test data from [69]
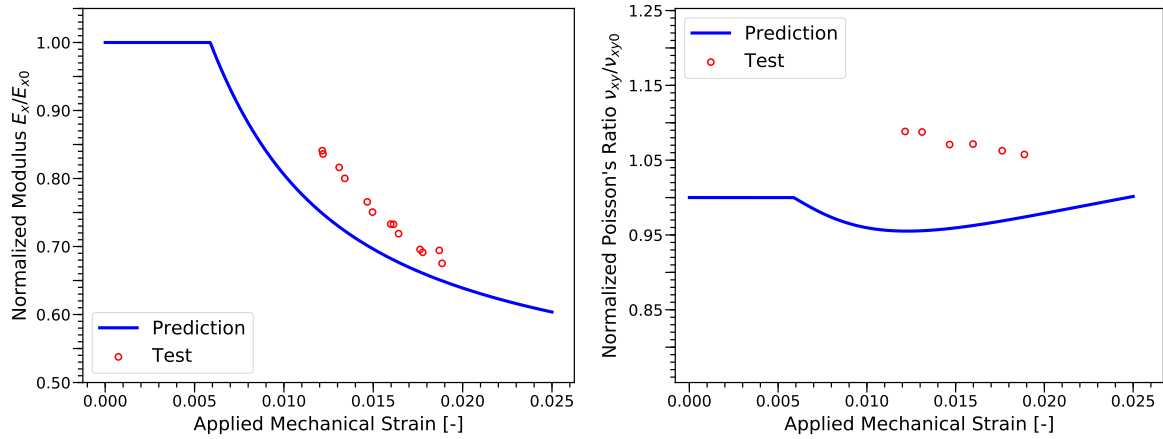
Figure 3.22: Longitudinal stiffness degradation (left) and residual Poisson's ratio (right) predictions for $[0, \pm 55_4, 0_{1/2}]_S$ laminate under quasi-static uniaxial tensile loading, using the recoverable damage model from section 3.4. Test data from [69]
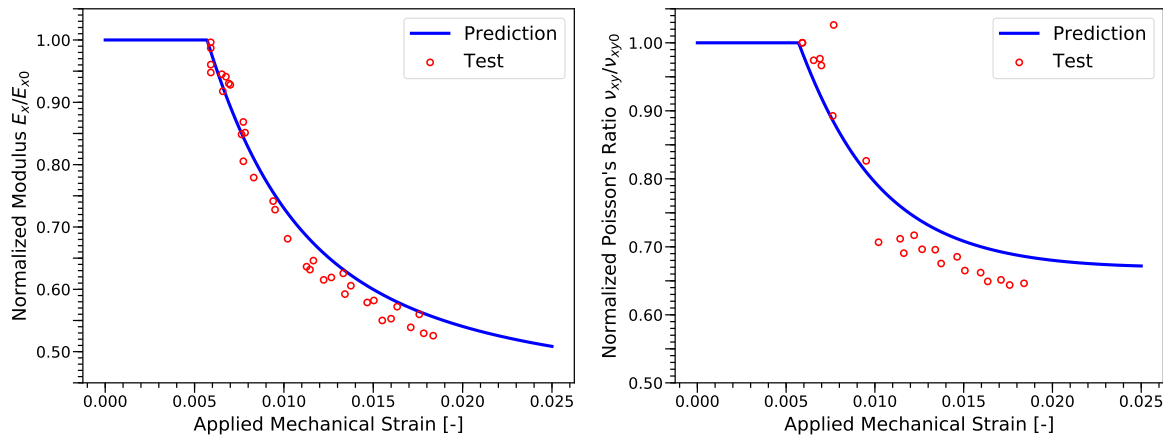
Figure 3.23: Longitudinal stiffness degradation (left) and residual Poisson's ratio (right) predictions for $[0, \pm 70_4, 0_{1/2}]_S$ laminate under quasi-static uniaxial tensile loading, using the recoverable damage model from section 3.4. Test data from [69]

Comparisons with $[\pm 45_2]_S$ glass/epoxy laminates [66]

The match between the model's prediction and experimental data for $[\pm 45_2]_S$ glass/epoxy laminates [66] is good. The normalized residual shear modulus reported in fig. 3.24 refers to the ply's shear modulus, specifically the secant one connecting permanent strain and unloading point, as shown in fig. 3.5. Predictions for the shear modulus fit test data well, falling just outside fo experimental scatter. The predicted permanent strain is higher than the test data's mean, which might be due to the slight overestimation of stiffness degradation.
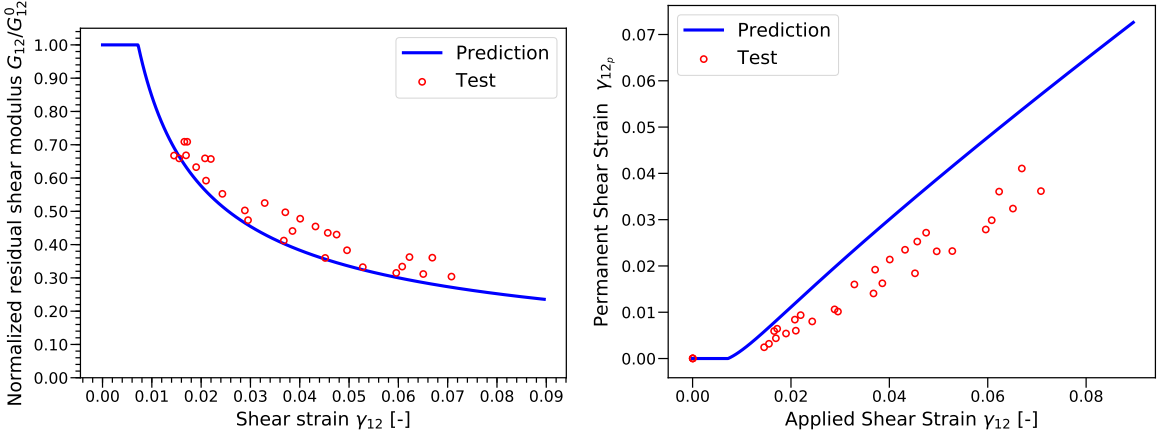
Figure 3.24: Ply's shear modulus degradation (left) and ply's permanent shear strain (right) predictions for $[\pm 45_2]_S$ laminate under quasi-static uniaxial tensile loading, using the recoverable damage model from section 3.4. Test data from [66]

4

Fatigue Model

The model presented in this chapter aims to predict stiffness degradation caused by matrix damage under cyclic tensile loading in cross-ply laminates. The model is based on the static models shown in chapter 3. The proposed fatigue model and its principles are introduced in section 4.1. The model draws a relation between stiffness degradation and applied fatigue cycles by integrating the static models with Kassapoglou's model for cycles to failure and residual strength under fatigue loading [30, 32–35], which is introduced in section 4.2. The actual manner in which the residual strength model for fatigue and the residual stiffness model for static loading are related to each other is illustrated in section 4.3. Finally, validation is performed in section 4.4.

4.1. Model principles and introduction

Since the fatigue model is based on its static counterparts, it follows that the same exact modeling principles illustrated in section 3.1 apply to the fatigue one as well, with two caveats:

- **Application to cross-ply laminates.** The static models predicted stiffness degradation cross-ply laminates excellently, while some issues were encountered with shear dominated laminates, which have been detailed in sections 3.3 and 3.4.2 and chapter 5. Since the fatigue model is based on the static one, it was decided, as a first step, to apply it exclusively to cross-ply laminates. This will ensure that results are reliable, which in turn will allow to truly verify whether the methodology used to extend the static model to fatigue is effective. As mentioned in chapters 5 and 6, as soon as the issues with shear in the static model are addressed, the fatigue model will be updated to work with all laminates.

- **No experimental fatigue data required.** The proposed fatigue model is based on integrating the static models from chapter 3 with Kassapoglou's model for cycles to failure and residual strength under fatigue loading [30, 32–35]. The aforementioned residual strength model predicts the initiation and evolution of damage due to fatigue loading, and has the added benefit not needing any experimental fatigue data to do so. For cross-ply layups under uniaxial tension, the only experimental data needed is the coefficient of variation of the ply material's transverse tensile strength distribution, under static loading. Since the static and fatigue models were designed with preliminary design optimization in mind, not needing fatigue experimental data is particularly convenient, since fatigue data is harder to obtain.

The other principles listed in section 3.1 still apply (namely, the need for simplicity while minimizing loss of accuracy, and the model's focus on stiffness degradation only).

Similarly to the static model, the fatigue model's fundamental scale are the unidirectional ply which compose an infinite laminate, with classical laminated plate theory being used to draw mechanical relations between the single plies and the laminate. It is assumed that only longitudinal tensile cyclic loads are applied $0 \leq R < 1$ and that the amplitude is kept constant.

4.2. Summary of Kassapoglou's [30, 32–35] model for cycles to failure and residual strength under fatigue loading

The stiffness degradation model for fatigue loads proposed here is based on Kassapoglou's model for cycles to failure and residual strength under fatigue loading, which has been illustrated in great detail in [30, 32–35], and which from here on will be referred to as the "residual strength model". This section provides a summary

of the elements of the residual strength model which are relevant to the proposed fatigue model for stiffness degradation.

The model analytically predicts the strength degradation of a laminate under fatigue loading starting with static test data and updating the prediction of cycles to failure as the scatter of the residual strength distribution changes. For example, prediction of strength degradation under cyclic uniaxial tension will require as a starting point the statistical distribution of failure under quasi-static uniaxial tension.

According to the residual strength model, for a maximum (in magnitude) applied stress σ with a corresponding fatigue life of N cycles, the residual strength σ_r of a sample after n cycles can be written as:

$$\sigma_r = \sigma^{\frac{n}{N-1}} \sigma_{sf}^{\frac{N-n-1}{N-1}} \tag{4.1}$$

Where σ_{sf} is the static failure strength of the pristine sample. The above equation was obtained by assuming that the residual strength must change non-linearly with the amount of applied cycles.

Assuming that σ_{sf} follows a two parameter Weibull distribution with scale parameter β and shape parameter α, and assuming that the residual strength σ_r is decaying nonlinearly as shown in eq. (4.1), it can be shown that the residual strength σ_r is also a two parameter Weibull distribution, with scale parameter β_r and shape parameter α_r defined as:

$$\beta_r = \beta^{\frac{N-n-1}{N-1}} \sigma^{\frac{n}{N-1}}$$
$$\alpha_r = \alpha \frac{N-1}{N-n-1} \tag{4.2}$$

The probability of failure under stress σ at cycle n can be expressed as:

$$p(\sigma, n) = 1 - e^{-\left(\frac{\sigma}{\beta_r}\right)^{\alpha_r}} \tag{4.3}$$

Where β_r and α_r refer to the residual strength Weibull distribution, and are given in eq. (4.2). It can be demonstrated that, for a residual strength which is Weibull distributed and decays non-linearly (eq. (4.1)), the cycle-by-cycle probability of failure is constant. This means that for a certain maximum applied stress σ, the probability of failure in eq. (4.3) should be independent of n (which ranges between 0 and N). It is easy to see that the final expression of the cycle-by-cycle failure probability is given by

$$p = 1 - e^{-\left(\frac{\sigma}{\beta}\right)^{\alpha}} \tag{4.4}$$

which is independent of the number of cycles n. This will turn out to be very useful later on. It can then be shown [30, 35] that fatigue life N for an applied cyclic stress σ is then given by:

$$N = -\frac{1}{\ln(1-p)}, \quad R = 0 \tag{4.5}$$

Where p is the static probability of failure for an applied maximum cyclic stress σ, given by eq. (4.3). It should be noted that until now the stress-ratio R has been assumed to be equal to zero. A method to use eq. (4.5) for cases where $0 < R < 1$ is covered at the end of this section. For eq. (4.5) to be valid, the damage must not to change with cycles. If the damage changes, the value of p must be calculated again through eq. (4.4) and the cycles to failure N are updated with eq. (4.5). In the limiting case, this should be done every cycle. Thanks to the way the residual strength model is integrated with the static one, it will not be necessary to update p at every cycle. In fact, it will be possible to predict stiffness degradation after any arbitrary number of cycles n without ever needing to update p, and without any loss in accuracy, as explained at the end of section 4.3

To use eq. (4.5), loading has to be restricted to a single type: either tension or compression. This is due to the fact that eq. (4.5) accepts a single value of p, while mixed tension-compression would result in two separate

values of p: one for the tension and one for compression. This assumption can be relaxed to allow mixed tension-compression ($R < 0$), as shown in [35].

Finally, it is necessary to account for the fact that for increasing values of the stress-ratio R, the predictions should be less conservative, since the load excursion that the material experiences is diminishing, which in turn means that any damage that should have developed between zero load and the minimum stress does not occur [35].

According to [35], the above can be done by shifting the 1% value of the static failure distribution closer to the mean, while keeping the 99% fixed. The resulting skewed distribution is assumed to be a Weibull distribution. If the original static strength distribution is a normal one, the 1% and 99% values (x_1 and x_2 respectively) are defined as:

$$x_1 = X_m - 2.326s$$
$$x_2 = X_m + 2.326s \tag{4.6}$$

Where X_m and s are the normal distribution's mean and standard deviation respectively. The new location of the 1% (x_1^*) can be found through:

$$x_1^* = X_m - r(X_m - x_1) \tag{4.7}$$

Where r is a factor dependent on the stress ratio R, defined below:

$$r = 1 - R, \quad 0 < R < 1$$
$$r = 1 - \frac{1}{R}, \quad R > 1 \tag{4.8}$$

Since the skewed distribution is assumed to be a Weibull one, and since its 1% and 99% CDF values should correspond to x_1^* and x_2 respectively, the following system of two equations in two variables must be enforced:

$$\begin{cases} 1 - e^{\left(\frac{x_1^*}{\beta}\right)^\alpha} = 0.01 \\ 1 - e^{\left(\frac{x_2}{\beta}\right)^\alpha} = 0.99 \end{cases} \tag{4.9}$$

Solving the system of equations in eq. (4.9) for α and β will give the shape and scale parameters (respectively) of the skewed Weibull distribution. Hence, to predict fatigue life for a maximum cyclic stress σ with $R > 0$, the cycle-by-cycle probability of failure p should be calculated through eq. (4.4), where α and β have been obtained from eq. (4.9), which assumes the starting (unskewed) distribution to be normal.

4.3. Stiffness degradation model for cyclic loading

Fundamental assumptions

To integrate the static stiffness degradation model with the residual strength model, it is necessary to enforce four assumptions regarding matrix strength within each ply:

1. The static strength of a region of matrix material is randomly distributed, signifying that while the region will have a specific mean strength, some of the material may fail at a static stress below or above said mean. It follows that the residual strength model (section 4.2) can be used to predict the fatigue life of said matrix region under cyclic loading, where the end of fatigue life denotes the appearance of matrix cracks.

2. The mean strength of matrix material is inhomogenous and changes across the matrix. It follows that different matrix regions will have different mean strengths. However, for any chosen matrix region, the scatter of randomly distributed matrix strength with respect to the mean must be constant across the entire material. For example, if matrix strength were to be normally distributed, n matrix regions will have n different mean strengths, but their standard deviations must be such that the coefficient of variation is the same for all regions.

3. Mean matrix strength has a lower limit, meaning there is a tensile laminate load N_X below which matrix cracking will never occur.

4. Matrix strength is continuous, meaning that there are infinite matrix strength values between two arbitrarily chosen limits.

To summarize the above assumptions, any particular matrix region will have randomly distributed strength, with a specific mean strength characteristic of that particular region. The mean strength must be higher than (or equal to) the minimum one, which will be defined later, and a scatter such that the distribution's coefficient of variation is equal to the material's (hence the coefficient of variation is a material constant).

Foundation for damage initiation, evolution, and stiffness degradation

It is now necessary to define matrix strength for the fatigue model, and associate it with a particular load type and damage mode. For now, the application will be to cross-ply laminates under uniaxial tension.

It follows that the fatigue model is based on any of the two static models presented in section 3.3 and section 3.4 respectively, since in the absence of shear they both behave identically. Referring to section 3.3.2 (subsection: Matrix Cracking without Yielding, specifically eq. (3.19)), it follows that for pure transverse tension ($t_{21} > 0$ and $t_{31} = 0$) Hashin's criterion for matrix damage under transverse tension and shear will degenerate to a maximum stress one, which in turn means that the critical laminate load N_{Xcr} which will induce matrix cracking can be defined as:

$$N_{Xcr} = \frac{Y_{IS}^T}{t_{21}} \tag{4.10}$$

Which in turn makes the "Hashin failure index", originally defined in eq. (3.26), equal to:

$$\Delta H = \begin{cases} N_X^2 \left(\dfrac{t_{21}}{Y_{is}^T} \right)^2 - 1, & \text{if } N_X \geq N_{Xcr} \\ 0, & \text{if } N_X < N_{Xcr} \end{cases} \tag{4.11}$$

It should be noted that the Hashin failure index can still be used, since the maximum stress criterion can be seen as a special case of Hashin's criterion. The resulting expressions for the residual transverse ($\overline{E}_{22}$) and shear ($\overline{G}_{12}$) moduli after matrix cracking are be identical to those shown in eq. (3.28), which is repeated below for convenience.

$$\overline{E}_{22} = \frac{2E_{22}}{2 + \Delta H} \qquad \overline{G}_{12} = \frac{2G_{12}}{2 + \Delta H} \tag{4.12}$$

While an expression for $\overline{G}_{12}$ is provided for the sake of completion, its value will not affect any of the predictions, since the longitudinal modulus of a cross-ply laminate is unaffected by the shear moduli of its plies (according to CLPT, and assuming that the load is aligned with the zero degree plies).

Looking at the three equations above, and remembering the assumptions listed at the beginning of this section, the "matrix strength" referenced so far must be the transverse tensile in situ strength Y_{IS}^T, and the random distribution of matrix strength will follow whatever statistical distribution is associated with Y_{IS}^T. It follows from these considerations that the minimum mean matrix strength mentioned in the third assumption must necessarily be the Y_{IS}^T derived from static testing of a pristine material, since the static model will not predict any matrix cracking for $\sigma_{22} < Y_{IS}^T$, or alternatively $N_X < N_{Xcr}$ (from eq. (4.10)).

Extension of the stiffness degradation for static model to cyclic loading

The extension of the aforementioned static foundation to cyclic loading can be conveniently explained by showing the steps that the model will follow.

It is assumed that static test data of the ply material in transverse tension proves the transverse tensile in situ strength to be normally distributed, with mean $X_{m_1} = Y_{IS}^T$ and coefficient of variation CV_Y. It follows that the standard deviation can be defined as $s_1 = X_{m_1} \cdot CV_Y$. Recalling the findings from the last paragraph of the previous section, the aforementioned static distribution will also be the weakest one (as denoted by the subscript "1"), meaning matrix regions with said strength distributions will be the first ones to develop cracks under static loading, due to their shorter fatigue lives.

According to the second assumption made at the beginning of section 4.3, there must be regions of the matrix which will have mean X_{m_c} and standard deviation s_c defined as:

$$\begin{cases} X_{m_c} = c \cdot X_{m_1} \\ s_c = X_{m_c} \cdot CV_Y = c \cdot X_{m_1} \cdot CV_Y = c \cdot s_1 \end{cases} \tag{4.13}$$

Where $c > 1$, since according to the third assumption, X_{m_1} is the lower limit for mean matrix strength. For a same applied stress σ, the estimated fatigue life N_c of a matrix region with mean strength X_{m_c} will grow monotonically with the value of c. This can be proven through eqs. (4.4), (4.5) and (4.9) of the residual strength model, and is in compliance with the equal rank assumption [20], which states that "for a given specimen its rank in static strength is equal to its rank in fatigue life" [7].

It is reinforced here that the proposed fatigue model does not attempt to predict ultimate failure of the laminate or ply. Failure here (and consequently reaching the end of fatigue life) is considered to be the appearance of matrix cracks.

The pristine cross-ply laminate starts being loaded cyclically with longitudinal tensile load N_X, with $0 < R < 1$ (eg. $R = 0.1$). For a generic matrix region, which has a normally distributed transverse tensile in situ strength for static loading, with mean $X_{m_c} = Y_{IS}^T \cdot c$ and standard deviation CV_Y (known from test data), fatigue life N_c can be calculated through the following steps. The procedure below applies to $0 < R < 1$. Alternate steps in for cases where $R = 0$ are provided after the procedure.

1. Turn the normal distribution with mean X_{m_c} and standard deviation s_c into a Weibull one with shape and scale parameters α and β, found by following equations 4.6 through 4.9.

2. Use eq. (4.4) to evaluate the cycle-by-cycle probability of failure p of the resulting Weibull distribution for the applied maximum stress given by eq. (4.14)

$$\sigma = \sigma_{22} = N_X t_{21} \tag{4.14}$$

Where the cycle-by-cycle probability of failure p is then found through:

$$p\left(\sigma = N_X t_{21}\right) = 1 - e^{-\left(\frac{N_X t_{21}}{\beta}\right)^{\alpha}} \tag{4.15}$$

3. Use the newfound probability of failure p with eq. (4.5) to estimate the fatigue life of the chosen matrix region:

$$N = -\frac{1}{\ln\left(1 - p\right)} = -\frac{1}{\ln\left[1 - \left(1 - e^{-\left(\frac{N_X t_{21}}{\beta}\right)^{\alpha}}\right)\right]} = \frac{1}{\ln\left[e^{-\left(\frac{N_X t_{21}}{\beta}\right)^{\alpha}}\right]} = \frac{1}{\left(\frac{N_X t_{21}}{\beta}\right)^{\alpha}} \tag{4.16}$$

Where fatigue life of the chosen region is therefore dependent on the maximum applied cyclic transverse tensile stress in the ply ($\sigma_{22} = N_X t_{21}$). Fatigue life is also dependent on the scale and shape parameters of the adjusted Weibull distribution, which are in turn dependent on the region's mean strength ($X_{m_c} = X_{m_1} \cdot c = Y_{IS}^T \cdot c$) and fatigue stress ratio R.

The steps shown above are only valid for $0 < R < 1$. In cases where $R = 0$, a similar procedure should be followed. The only difference is that the first step can be skipped, and the cycle-by-cycle probability of failure for the maximum applied stress can be found through the normal distribution directly. For the cycle-by-cycle probability of failure of a normal distribution to be constant throughout the entire fatigue life, it is necessary to assume that residual strength must degrade linearly with the amount of applied cycles, rather than non-linearly. A detailed explanation can be found in [35].

Since the fatigue life N_c of a generic matrix region with mean strength X_{m_c} has been defined as a function of the applied cyclic load N_X, it is now necessary to derive a relation between the initiation of damage in the region and the resulting stiffness degradation.

The static model gives stiffness degradation as a function of an applied static load, while the fatigue model outputs fatigue life as a function of an applied cyclic load. If the two models are set up to "create" the same damage state, the stiffness degradation associated with said damage state must also be equal for both models, which in turn would establish a relation between the static model and the fatigue one.

For the generic matrix region with mean strength $X_{m_c} = c \cdot Y_{IS}^T$, the applied cyclic stress $\sigma_{22} = N_X t_{21}$ will induce failure after N_c cycles. It was proven previously in this section that all matrix regions with mean strength $X_{m_h} = h \cdot Y_{IS}^T$ where $X_{m_1} < X_{m_h} \leq X_{m_c}$ (consequently $1 \leq h < c$) will have already failed by the time X_{m_c} fails, since for a same applied stress (or load), their lives are shorter. This means that right when $n = N_c$, matrix cracks will appear for the first time in all matrix regions with mean strength $X_{m_c} = c \cdot Y_{IS}^T$, and they will have already appeared at $1 < n < N_c$ in all weaker regions.

The equivalent static damage state must then be one where the equivalent static load N_{X_s} is such that cracks in a material with strength $X_m = X_{m_c} = c \cdot Y_{IS}^T$ would have been initiated right at the applied N_{X_s}. Any matrix material with strengths lower than X_{m_c} that should have already failed at loads lower than the applied N_{X_s}. Recalling eq. (4.10) and eq. (4.11), it can safely stated that the equivalent static load representing said damage state should then be given by $N_{X_s} t_{21} = c \cdot Y_{IS}^T$.

It follows that, for the static model, the damage state corresponding to a matrix region with mean strength $X_{m_c} = c \cdot Y_{IS}^T$ having just reached the end of its fatigue life $n = N_c$ is one where the applied static load N_{X_s} is given by:

$$N_{X_s} = \frac{c \cdot Y_{IS}^T}{t_{21}} \tag{4.17}$$

Which means that degradation of the ply's transverse modulus can be expressed as:

$$\overline{E}_{22} = \frac{2E_{22}}{2 + \Delta H} = \frac{2E_{22}}{2 + N_{X_s}^2 \left(\dfrac{t_{21}}{Y_{is}^T}\right)^2 - 1} = \frac{2E_{22}}{1 + c^2} \tag{4.18}$$

To summarize, for any ply in a cross-ply laminate under longitudinal cyclic tensile load N_X, with $0 \leq R < 1$, the residual modulus $\overline{E}_{22}$ as a function of the applied cycles can be found by assuming a value of c, finding the corresponding $\overline{E}_{22}$, calculating the fatigue life N_c for a matrix region with mean $X_{m_c} = c \cdot Y_{IS}^T$ and associating the passage of $n = N_c$ cycles with the previously found value of $\overline{E}_{22}$.

All equations provided here are closed-form equations, meaning that no iteration is required, and that the number of values c being sampled will not improve the solution's accuracy (although it will give a better idea of the stiffness degradation's shape). Naturally, it makes sense to start with $c = 1$, and increase it until the laminate's fatigue life is reached, at which point ultimate failure would occur. The prediction of the laminate's fatigue life and ultimate failure is not addressed at this point.

The residual stiffness in eq. (4.18) refers to the ply material. The properties of the entire laminate can be derived through section 3.5. Since cross-ply laminates are being analyzed in this case, it is possible to conveniently derive an expression for the residual stiffness of the entire laminate, shown in eq. (4.19).

$$\overline{E}_X = \frac{1}{\mu(a+b)} \left[aE_{11} + b\overline{E}_{22}\frac{\mu}{\overline{\mu}} - \frac{v_{12}^2\left(aE_{22} + b\overline{E}_{22}\dfrac{\mu}{\overline{\mu}}\right)^2}{aE_{22} + bE_{11}} \right] \tag{4.19}$$

$$\text{where} \qquad \mu = 1 - v_{12}v_{21} \qquad \overline{\mu} = 1 - v_{12}^2\frac{\overline{E}_{22}}{E_{11}}$$

Where a and b are the number of 0 and 90 degree plies respectively, E_{11} and E_{22} are the longitudinal and transverse moduli of the pristine ply material, $\overline{E}_{22}$ is the residual transverse stiffness of the damaged 90 degree plies, as predicted in eq. (4.18), and v_{12} and v_{21} are the major and minor Poisson's ratios (respectively) of the pristine ply material.

Table 4.1: Required input data for comparisons with test data from [8], section 4.4.1

Property	Value	Source
E_{11} (GPa)	142.0	[9, 40]
E_{22} (GPa)	10.3	[9, 40]
G_{12} (GPa)	7.6	[9, 40]
ν_{12} (-)	0.27	[9, 40]
Y_{IS}^{T}* (MPa)	49.31	[8]
CV_Y (-)	12.1%	[64]

*Value derived from data within source.

4.4. Validation

Unfortunately, the amount of data available for the fatigue model's validation is considerably smaller than its static counterpart. The main culprits are the restrictions that the model is affected by (only cross-ply laminates, only $R \geq 0$, only constant amplitude loading...) and the fact that statistical distributions of the ply material's transverse tensile strength are required (which have been rarely reported in papers covering stiffness degradation due to fatigue loading). The three following sections show comparisons with test data from three different sources. The model's prediction quality was found to be excellent as long as the dominant damage mode (driving stiffness degradation) is matrix cracking in the 90 degree plies.

4.4.1. Comparisons with $[0/90_2]_S$ AS4/3501-6 laminates from [8]

Introduction and experimental data

Daniel, Lee and Yaniv [8] performed longitudinal tensile fatigue tests on graphite epoxy $[0/90_2]$ laminates, for which they recorded (among other things) stiffness degradation as a function of the applied normalized cycles. Three different cyclic stresses were applied: 28% of the static failure stress, 53% and 85%. A stiffness degradation curve was generated for each loading type. Since they do not mention the R ratio at which the tests were performed, it is assumed that $R = 0$. The ply's mechanical properties are not provided in [8], and neither is the ply material's exact name. In other works by the same authors [9, 40, 41], the ply material is always AS4/3501-6, and it is always used to make the exact same laminates that are shown in [8]. The laminates undergo the same tests, and the stress-strain curves presented for them are identical to those shown in [8]. It can therefore be safely assumed that AS4/3501-6 is being used in [8]. Its properties are given in table 4.1.

The transverse in situ strength was obtained by fitting 4th order polynomials through the data points showing the relation between applied longitudinal tensile stress and crack density for a $[0/90_2]_S$ graphite/epoxy laminate (fig. 4.1), where all matrix cracks are contained within the off-axis plies. The intersection with the stress axis gives the applied longitudinal stress at which matrix cracks were initiated. The data point at the bottom was considered an outlier, since it does not follow the trend shown by all other points. It is likely due to the presence of imperfections in the matrix. The longitudinal stress at which matrix cracks are initiated was found to be 260.69MPa, which through CLPT was related to a transverse tensile stress in the 90 degree plies of 49.21MPa, which is therefore selected as the in situ strength Y_{IS}^{T} shown in table 4.1.

The coefficient of variation of the material's static failure distribution under transverse tension was found in [64], where it was obtained through tensile tests of $[90]_8$ AS4/3501-6 laminates. Two alternative values were available, dependent on whether the ply material had been bled or not. The CV of the bled material was selected (12.1%), since the corresponding ply properties were closer to the ones in table 4.1 than the unbled one.

In order to compare the model's predictions with the published results, for which cycles have been normalized with fatigue life, it is necessary to know the fatigue life of the sample Since [8] does not provide the fatigue life of the samples under the three different loading, it had to be estimated through [41], which is a paper by the same authors providing fatigue life predictions for $[0/90_2]_S$ AS/3501-6 laminate (identical to those used in [8]). Referring to fig. 4.2, it is possible to estimate that an AS4/3501-6 $[0/90_2]_S$ laminates loaded with a maximum normalized cyclic stress of 85%, 53% and 28% static failure stress will have fatigues lives of $10^{4.6676}$, $10^{10.668}$ and $1.13 \cdot 10^{14}$ cycles respectively.
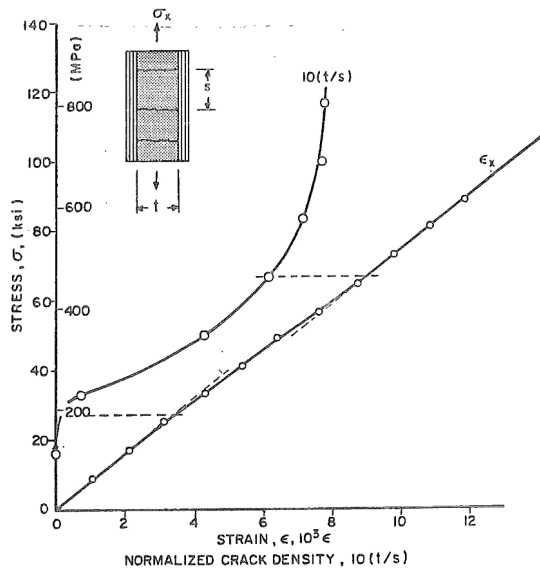
Figure 4.1: Applied longitudinal stress as a function of either applied longitudinal strain or normalized matrix crack density (in the off-axis plies) for a $[0/90_2]_S$ laminate [8]
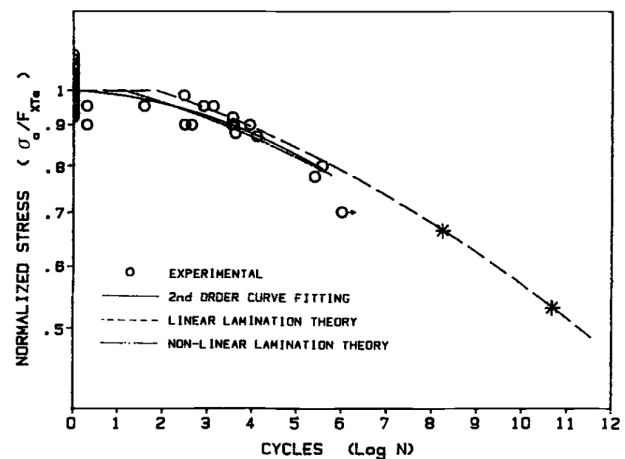
Figure 4.2: Fatigue life as a function of the maximum applied cyclic stress (normalized with static strength) for a $[0/90_2]_S$ AS4/3501-6 laminate.[41]

Finally, since the applied stress is normalized, it is necessary to know what the static failure stress is. Daniel reports the tensile strength of an AS4/3501-6 $[0/90_2]_S$ laminate under tension to be 779MPa [9].

Comparison between predictions and experimental data

Knowing all of the aforementioned data, it is then possible to generate predictions for the laminate's residual stiffness under cyclic fatigue loading, as shown in fig. 4.3, fig. 4.4 and fig. 4.5. Since in this case $R = 0$, cycle-by-cycle probability of failure can be found directly from the starting normal distribution, without any need of conversion to Weibull distributions.

Results for the sample under 28%, shown in fig. 4.3 are very good. While the prediction does exactly match the mean of the test data, it does follow it closely enough, and it always falls within experimental scatter. A few interesting observations can be made: according to the predictions, stiffness degradation does not start at the first cycle due to the stress being too low to immediately generate (statically) any matrix cracks. While test data does show an immediate drop, it is very small (2.5%), especially for a cross-ply laminate, and it is followed by a second steeper decline in stiffness degradation. Recalling the typical trend of stiffness degradation in laminates under fatigue loading, it is not unreasonable to assume that the (few) matrix cracks responsible for the first immediate drop might have originated from imperfections, due to the drop's low magnitude, its flatness, and the fact that it is followed by a steeper drop (starting at 10% life) with a different slope. Test data stops at 0.4 normalized life due to the authors stopping the test before failure (the estimated life shows a prohibitive amount of cycles needed to break the sample).

Results for the sample under 53% load, shown in fig. 4.4 are excellent. The initial stiffness drop due to static loading is matched accurately, the predictions closely follow the test data's mean and always falls within experimental scatter.

Predictions for the laminate under 85% load, shown in fig. 4.5, are acceptable. The initial drop in stiffness, due to "static cracking" within the first cycle is captured quite well. The model follows the trend of the data's mean up to 80% normalized fatigue life, with the prediction falling just short of experimental scatter. According to [8], for the 85% load the sample is saturated with matrix cracks within the first cycle, with little to no growth in the number of matrix cracks after that. At 80% normalized life new types of damage appear, namely longitudinal cracking, delamination and fiber fracture. These damage types drive stiffness degradation between 80% normalized life and failure. Since the aforementioned damage types are not part of the proposed model (for now), the predictions is not expected to provide a good match between 80% normalized life and failure. The fact that the prediction is close to test data until 80% normalized life, even following the trend of the small decay in stiffness occurring until then, should be proof of the model's validity.
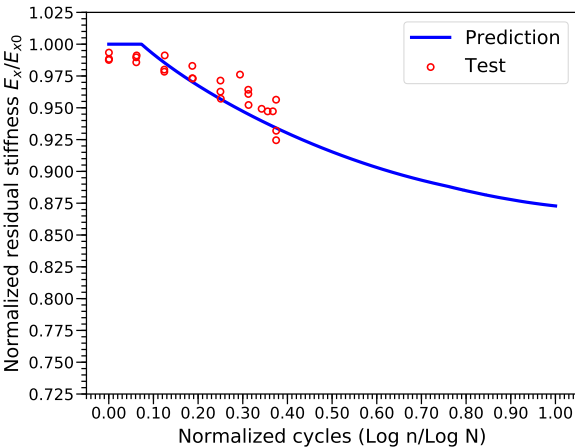
Figure 4.3: Normalized longitudinal stiffness degradation for a $[0/90_2]_S$ AS4/3501-6 laminate under a maximum cyclic stress of 28% of its static strength. Data taken from [8]
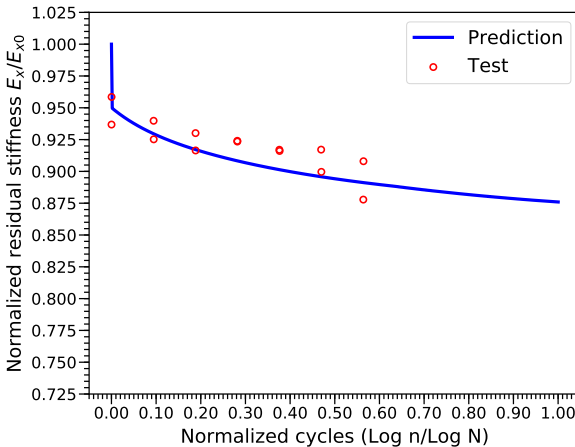
Figure 4.4: Normalized longitudinal stiffness degradation for a $[0/90_2]_S$ AS4/3501-6 laminate under a maximum cyclic stress of 53% of its static strength. Data taken from [8]
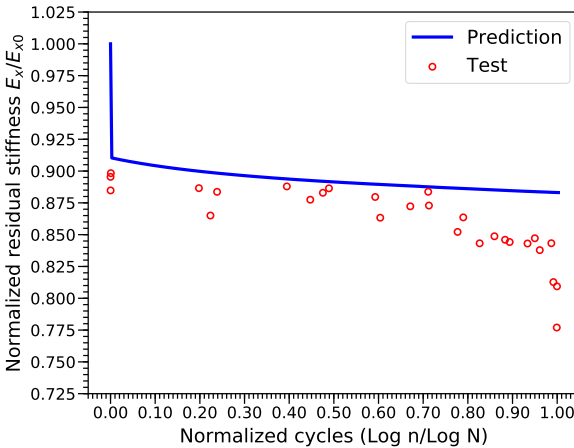
Figure 4.5: Normalized longitudinal stiffness degradation for a $[0/90_2]_S$ AS4/3501-6 laminate under a maximum cyclic stress of 85% of its static strength. Data taken from [8]

Finally, to provide a small overview on the quality of predictions, the model has given good results as long as matrix cracking was the main damage mode occurring in the sample. For the sample under 28% load, it was observed that in [8] that very few matrix cracks will appear in the first cycle, and that at the millionth cycle their number had increased but was still very far from reaching the characteristic damage state (CDS, originally introduced in [53] and essentially representing the point where the matrix has been saturated with cracks). This indicates that throughout the entire test matrix cracks were the main damage mode. Similar observation were made for the case of 53% load, mentioning a larger number of initial matrix cracks, but still not reaching CDS. In the 85% case on the other hand, CDS was basically reached within the first cycle, meaning that the matrix was almost immediately saturated with cracks, and that no additional matrix cracks (at least in the off-axis plies) were created. This is was probably the cause of the relatively flat stiffness degradation plot until 0.8 normalized life is reached. At that point (according to [8]) longitudinal matrix cracking will appear (in the 0 degree plies), leading to delaminations at the intersection between longitudinal and transverse cracks, followed by fiber fractures. From the above discussion it can be concluded that the model works very well, since it only tries to model stiffness degradation due to matrix cracking, and it generated good predictions whenever matrix cracks were dominant.

4.4.2. Comparisons with Charewicz and Daniel STP907 1986 [6]

Introduction and experimental data

Charewicz and Daniel [6] performed fatigue tests on several AS4/3501-6 crossply laminates. Stiffness degradation data was reported only for a $[0/90_4]_S$ laminate, which was tested under a maximum applied longitudinal stress of 345MPa, with $R = 0.1$.

Since the authors did not report any of the material properties other than the name, and since the same material and layups used in this paper were also used in [8, 9, 40], which were also authored by Daniel, it was assumed that the ply properties provided by the aforementioned sources, which were also used in section 4.4.1 also apply in this case. The ply's mechanical properties can be found in table 4.1.

Since the in situ strength Y_{IS}^T shown in table 4.1 was obtained from a $[0/90_2]_S$ laminate it needs to be updated for the $[0/90_4]_S$ laminates covered in this comparison. As shown by Camanho, Davila et al in [3], changes in the number of adjacent 90 degree plies (which in this case doubled) could have a very strong influence on the in situ strength.

Charewicz and Daniel [6] mention that static loading of the $[0/90_4]_S$ laminate has a linear stress-strain response up to an applied stress of 166MPa, with no matrix cracks appearing. Beyond said stress, there is a rapid increase in matrix cracking, and the response turns non-linear. Through CLPT, the transverse stress in the 90 degree plies was found to be 46.44MPa, which is very close to the value of 49.31MPa obtained for $[0/90_2]_S$ in table 4.1. Finally, since the test data was plotted against normalized fatigue cycles, the sample's fatigue life is necessary, which was estimated to be $1.22 \cdot 10^7$ cycles through an S-N curve provided in [6].

Comparison between predictions and experimental data

A comparison between the proposed model's predictions and test data is shown fig. 4.6. The $[0/90_4]_S$ laminate was tested under a maximum applied longitudinal stress of 345MPa, with $R = 0.1$. The match is good up to about 40% of the fatigue life. After that, the test data show a rapid decrease in stiffness associated with failure modes not captured by the model in its current form, namely dispersed longitudinal cracking and local delamination [6]. The case shown in fig. 4.6 is similar to the one covered in fig. 4.5 of section 4.4.1. The "static" stiffness drop experienced in the first cycle is predicted very accurately, just like figs. 4.4 and 4.5. The plateau predicted after the first couple of cycles is also to be expected, since according to Charewicz and Daniel [6] the sample reaches its characteristic damage state (CDS) [53] practically immediately, meaning that the matrix is saturated with cracks within the first few cycles, and that little stiffness degradation (due to matrix cracking) is to be expected after that.
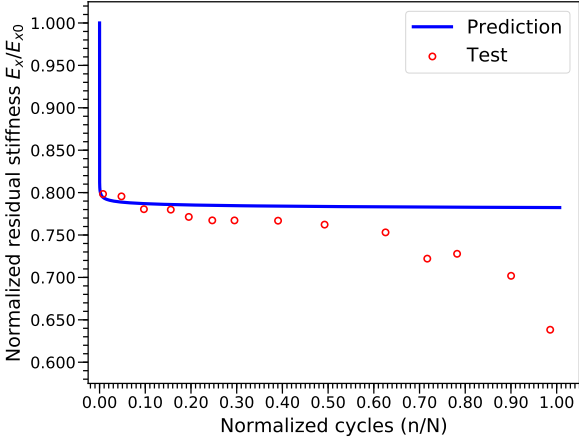
Figure 4.6: Normalized longitudinal stiffness degradation for a $[0/90_4]_S$ AS4/3501-6 laminate under a maximum cyclic stress of 345MPa, $R = 0.1$. Data taken from [6]

4.4.3. Comparisons with Ryder and Crossman 1983 [54]

Additional comparisons for T300/5208 $[0_2/90_4]_S$ laminates from [54] are provided in appendix A. Lack of some input data for the model meant that the CV of transverse tensile failure had to be taken from 90 degree flexure tests, rather than a conventional monotonic static test on a $[90]$ laminate. As such, the predictions are not considered of sufficient quality to be included in the main text.

5

Conclusions

The goal of this research was to create a stiffness degradation model for laminates under static and cyclic loading. As mentioned in chapter 1, the models were created with preliminary design optimization in mind, which is characterized by the iteration of numerous design configurations. It follows that the proposed models should be computationally fast and valid for any (realistic/practical) laminate. Naturally, the predictions should also be as close to experimental data as possible. A brief discussion follows on how the models fared in terms of computational speed, generality and accuracy.

Regarding computational speed, the models are fully analytical, making them inherently fast. Moreover, all the static and fatigue model equations are closed-form expressions, meaning no numerical iteration is required, with the exception of eqs. (3.39) and (4.9), which have to be solved numerically but are not computationally intensive. Finally, since the damage and corresponding stiffness degradation are modeled at ply level, and since interaction of damage between different plies is not yet included in the model, the static and fatigue models only need to be run once per ply orientation. For example, a laminate with n plies, all being oriented at 0, 90 or ±45 degrees will require the model to run only 4 times to fully characterize stiffness degradation under static or cyclic uniaxial tension (due to symmetry, results from the -45 and $+45$ plies would be identical, so the model could technically run just 3 times). This makes the model even more computationally efficient, especially since in actual structural designs there is a finite and small number of unique ply orientations being used within a same laminate. It can be concluded that the proposed models are likely fast enough to be used for any practical optimization purpose, and that efforts to improve the models should be focused on other areas (discussed below).

Regarding model flexibility and applicability to several design configurations, it should be mentioned that the model was only applied to uniaxial loading in order make its development easier, and to provide a stepping stone for its expansion to additional load cases. The static models can technically be applied to any laminate, and they have been validated for realistic/practical laminates (symmetric and balanced, not completely unidirectional). While there are no restrictions on the laminate's layup, results have been shown to worsen for layups containing shear dominated plies. This issue is minor for the recoverable damage model (section 3.4), and more pronounced for the energy equivalence model (section 3.3). The accuracy of these models is discussed in more detail in the next paragraph. The fatigue model was only applied to cross-ply laminates due to the aforementioned accuracy issues with shear dominated plies. As soon as the accuracy of the static model is improved, the fatigue model can be expanded to all layups. It can be concluded that there is currently no indication that the model could not be expanded to account for additional loads cases, layups and damage modes, as discussed in chapter 6. This is especially true when considering that the predictions are based on ply stresses, that excellent to good match has been obtained for predictions based on transverse and shear stresses, and that the applied load case and ply orientation are only used to determine ply stresses, and nothing else. Finally, it should be noted that both the static and fatigue models need remarkably little experimental data to run, especially compared to many of their counterparts mentioned in chapter 2. All necessary data can be measured experimentally from static tests, none of which need to be carried out on the exact layup being analyzed (although doing so for the transverse tensile in situ strength could benefit accuracy to some extent). No curve fitting or semi-empirical approaches are needed.

Regarding the energy equivalence model in particular (from section 3.3): the model has achieved an excellent match with test data from cross-ply laminates, while it tends to overestimate stiffness degradation in laminates with shear dominated plies. The fact that the energy equivalence method worked extremely well with transverse tension might be an indication that the principle of energy equivalence is indeed valid, and

that the problem with shear lays in the way strain energy is assumed to be stored within the damaged ply. Accounting for the presence of permanent strains [37, 38, 66, 68], possibly by adopting some of the observations made in the recoverable damage model (section 3.4) might help. The damage sequence presented by the model (microscopic matrix damage only if the ply is shear dominated, followed by matrix cracking) is consistent with available literature [37, 38, 69], and the derivation of all equations governing shear behavior is rigorous and "mathematically sound", unlike its recoverable damage model counterparts. It can be concluded that the energy equivalence model represents a solid foundation for predicting stiffness degradation due to matrix damage under static loading in any (realistic) layup. Its shortcomings have been identified, and once the alleviating effect of permanent shear strain on the residual modulus is accounted for, model accuracy should drastically improve.

Regarding the recoverable damage model (from section 3.4): The model has achieved an excellent match with test data from cross-ply laminates, and an excellent to good match for laminates with shear dominated plies. Unlike the energy equivalence method, the equations used to predict the residual shear modulus are not backed by a rigorous mathematical derivation. Rather, they were established through the qualitative assumptions and observations discussed in section 3.4.2 (based on literature [37, 38, 66, 68]). While the results shown by the recoverable damage model are very good, they cannot be backed (for now) by a rigorous derivation. However, considering that the recoverable damage and energy equivalence models share many modeling choices (microscopic shear damage, matrix cracking, excess strain energy apportioning...) it is not to be excluded that taking some of the concepts used in the recoverable damage model (especially unloading/reloading behavior, hysteresis), and implementing them into the energy equivalence model might result in drastic improvements,

Finally, regarding the fatigue model (from chapter 4): The model has achieved an excellent match with test data from cross-ply laminates, up to a point where rapid damage propagation sets in, which is not yet included in the present model. The excellent results prove that fatigue life and residual stiffness can be successfully related by equating the predicted damage state between the residual strength (fatigue) model and the static stiffness degradation model. The same procedure should be followed again once the issues experienced by the static model with shear are addressed. Moreover, the excellent match with the initial stiffness drops (in the first cycle) is further proof of the static model's validity (for cross-ply laminates). While fatigue predictions do diverge at some point from test data in figs. 4.5 and 4.6, it was proven in both cases that this was caused by the presence of damage modes other than matrix cracking (eg. delamination and fiber fracture). These damage modes only become relevant close to the end of fatigue life, especially for low cycle fatigue, as discussed in chapter 6. The fatigue model was only applied to cross-ply laminates due to the issues experienced by the static models with shear laminates. As soon as those are resolved, the fatigue model can be expanded to more generic laminates. It can be concluded that the proposed fatigue model is a step in the right direction, matching test data perfectly (as long as matrix cracks were the dominant damage mode), and that the updated static model should be extended to fatigue in the same fashion presented in section 4.3 for cross-ply laminates.

Based on the conclusions reached in this chapter, recommendations for future work are given in chapter 6.

<div align="right">6</div>

Recommendations for future work

The recommendations below are arranged in descending order of priority, where priority is determined by the impact that each new feature would have on the model's completeness, versatility and usefulness.

- **Modify the energy equivalence model from section 3.3 to reduce/eliminate overestimation of stiffness degradation within shear dominated laminates.** Accounting for the presence of permanent shear strains might induce the desired alleviating effect on predictions for shear dominated laminates, as suggested by existing literature [37, 38, 66, 68] and by the validation results of the recoverable damage model, shown in section 3.6.4. To this end, it would benefical to make use of the knowledge gained from the development of the recoverable damage model (section 3.4.2).

- **Devise a rigorous derivation for the residual shear modulus equations provided in section 3.4.2, which has shown excellent predictions, but needs a solid theoretical backing.** Since the energy equivalence model has a stronger foundation than the recoverable damage one, this step should only be taken if the previous one does not work.

- **Expand the fatigue model to handle non-cross-ply laminates**. This should preferably be done by integrating the chosen static model with the residual strength model for fatigue (section 4.2), in a manner analogous to the one shown in section 4.3, which has been proven to work excellently for cross-ply laminates. This task can only be carried out once one of first two points has been successfully addressed.

- **Validate the preferred static model using purely UD** [0] **laminates, non-symmetric laminates and unbalanced laminates.** While the static models can already be applied to such laminates, validation did not include any of them, due to their infrequent use in actual structural designs and in published test data. For the same reasons, if validation of such laminates does not yield positive results, there would be no strong need to modify the model, especially since the issue might be due to the driving damage modes not being captured by the model. This is covered in the next point.

- **Introduce additional damage modes to the fatigue model** (eg. fiber fracture, fiber-matrix debonding, longitudinal splitting, delamination) to improve the match between predictions and experimental data for the final portion of fatigue life, where such damage modes will be prevalent [8, 52, 57] and figs. 2.2 and 2.3

- **Expand the fatigue model to handle spectrum (variable amplitude) loading.** To this end, the approaches for spectrum loading shown in [32, 35] should be tried first, since they were successfully applied to the residual strength fatigue model that has been used in this research (section 4.2). Spectrum loading should only be implemented after that the fatigue model has produced reliable predictions for the entirety of fatigue life (including the final portion).

- **Expand the static model to handle loads other than longitudinal tensile loading** (eg. longitudinal compression, or biaxial loading, bending). This should only be done once the model has been proven to work reliably for any layup under uniaxial tension. It would be particularly interesting to check the quality of predictions when different load cases are applied to the same sample in succession (eg. uniaxial loading, followed by biaxial loading, followed by shear loading.). The new static model should then be implemented within the fatigue one.

Fatigue model validation with data from Ryder and Crossman [54]

This appendix contains comparisons for the residual stiffness predicted by the fatigue model, and the one measured experimentally in [54] for T300/5208 $[0_2/90_4]_S$ laminates. Lack of some input data for the model meant that the CV of transverse tensile failure had to be taken from 90 degree flexure tests, rather than a conventional monotonic static test on a [90] laminate. As such, the predictions are not considered of sufficient quality to be included in the main text.

Introduction and experimental data

Ryder and Crossman performed extensive fatigue testing for stiffness degradation of various T300/5208 laminates, as documented in [54]. The only cross-ply laminate they used is $[0_2/90_4]_S$. Fatigue tests were performed using three different maximum applied loads, corresponding to a longitudinal applied strain (on the pristine laminate, upon the first loading) of 0.005, 0.006 and 0.0065. The ply properties of unidirectional T300/5208 material are reported in table A.1.

Since the statistical distribution of ply material failure under transverse tensile stresses was not reported, it had to be assumed. The distribution was assumed to be normal, with mean Y_{IS}^T given by the transverse stress at which matrix cracks will first appear. Said stress was found through fig. A.1, which shows that matrix cracks will occur around 0.00475 applied longitudinal strain (sample A1).

The point was chosen to represent the onset of substantial matrix cracking. While samples A1, A2 and A3 all exhibit matrix cracks before 0.00475 strain, the stability and high value of their crack spacing indicates that they must be due to local phenomena (eg. imperfection) rather than the global stress-state of the laminate. Sample A1 was the only one with enough data points to make it possible to clearly pinpoint the sudden increase in matrix cracks which indicates the point where all regions in the matrix will start cracking (in order to start attaining the characteristic damage state [53]). Through CLPT, it was possible to calculate the transverse stress in the 90 degree plies corresponding to an applied longitudinal strain of 0.00475 to an $[0_2/90_4]_S$ T300/5208 laminate, which was found to be 44.33MPa.

The coefficient of variation associated with the aforementioned normal distribution for traverse tensile failure had to be found from additional sources. A CV of 13.3% was found for 90-degree flexure tests of T300-3K/5208 coupons, from [46]. Since Ryder and Crossman [54] did not specify the fiber grade, it is not possible to verify

Table A.1: Required input data for comparisons with test data from [54], section 4.4.3

Property	Value	Source
E_{11} (GPa)	163.40	[54]
E_{22} (GPa)	10.20	[54]
G_{12} (GPa)	6.48	[54]
ν_{12} (-)	0.30	[54]
Y_{IS}^T* (MPa)	44.33	[54]
CV_Y (-)	13.3%	[46]

*Value derived from data within source.
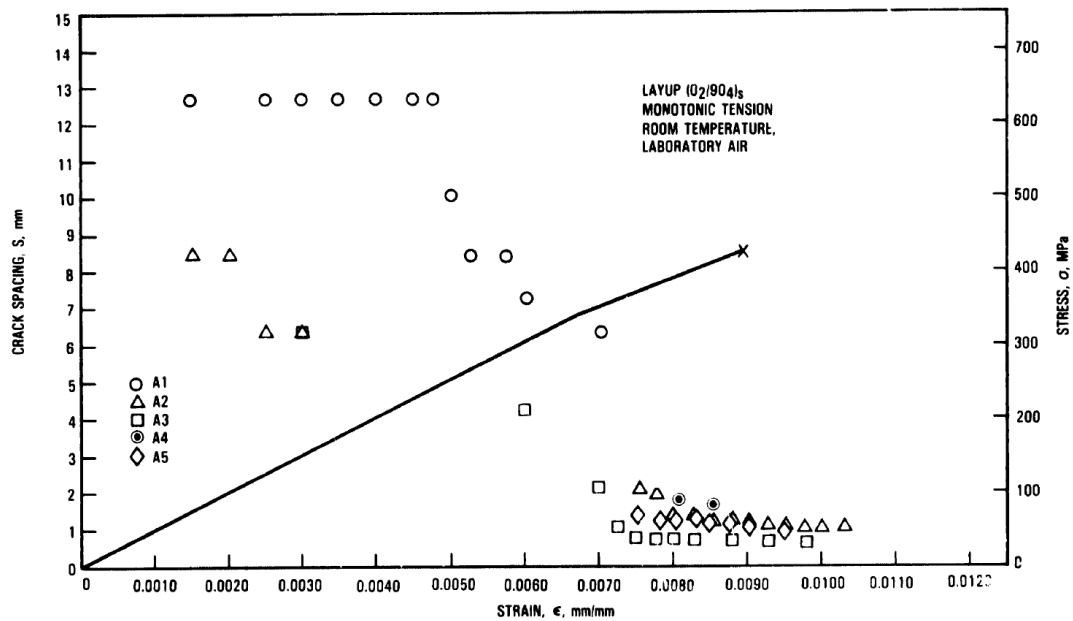
Figure A.1: Crack spacing and longitudinal stress as a function of applied longitudinal strain for a $[0_2/90_4]_S$ T300/5208 laminate [54]

whether they used T300-3K, and [46] does not provide ply properties. However, since transverse tensile failure is mostly matrix dominated, the fiber grade issue is considered to be negligible. It is recognized that ideally the CV value should have been obtained through longitudinal tensile tests of $[90]_S$ coupons, but the value just provided was the only one available in literature. The value of 13.3% does not seem unreasonable (AS4/3501-6 after bleeding has a value of 12.1%). Predictions with different CV values have been plotted in fig. A.5 to show that the accuracy of the CV is not the most critical variable for prediction accuracy (that would likely be the mean transverse in situ strength).

Unlike in section 4.4.1, no coupon fatigue life estimate was needed to plot the comparisons with test data, since Ryder and Crossman [54] plotted stiffness degradation against the actual number of cycles, not the normalized one.

Comparison between predictions and experimental data

Comparisons between the model's prediction and test data from [54] can be found in fig. A.2, fig. A.3 and fig. A.4, which depict stiffness degradation for a maximum applied cyclic load corresponding to a longitudinal applied strain (on the pristine laminate, upon the first loading) of 0.005, 0.006 and 0.0065 respectively.

Since the test data presents a considerable amount of scatter (Ryder and Crossman reported the fatigue life scatter to be greater than two orders of magnitude), it is difficult to make precise statements. As a general observation, it can be stated that the predictions are good. While they do not perfectly match the mean they do follow its trend, laying right outside of experimental scatter.

The large plateau in the prediction curves is caused by matrix crack saturation. While the predicted stiffness drop associated with saturation is slightly conservative for these particular predictions, the number of cycles at which the plateau occurs is predicted fairly accurately.

The model also predicted matrix cracking in the 0 degree plies (splitting), although its effect on the laminate's residual longitudinal stiffness is negligible. The sample tested in [54] also underwent said splitting and found it not to have a measurable effect on longitudinal laminate stiffness, which was also confirmed by [28].

Finally, to show the influence of the coefficient of variation on the model, the predictions from fig. A.2 were ran again with the standard CV value of 13.3% and two additional values, chosen arbitrarily to be 10.0% and 16.6%. The results are shown in fig. A.5. While the CV does have an influence, it is not a particularly strong one. Hence, the uncertainty surrounding the value of 13.3%, obtained from 90 degree flexural tests in [46], should not detract from the proposed model and the quality of its predictions. If anything, the value of 13.3% seems a little high, compared to its 12.1% and 10.0% counterparts for AS4/3501-6 (depending on bleeding)

[64], and as seen in fig. A.5, a lower CV would actually benefit the predictions.
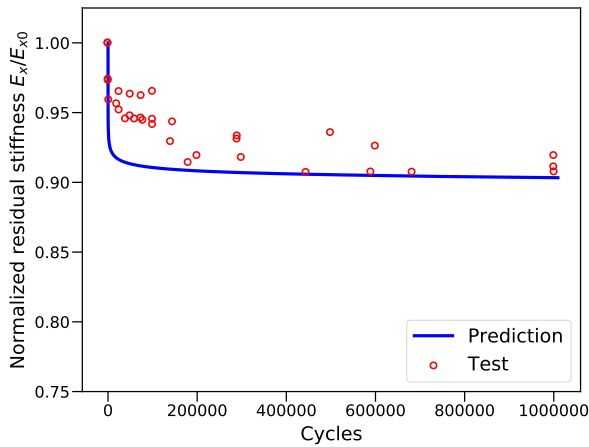
Figure A.2: Normalized longitudinal stiffness degradation for a $[0_2/90_4]_S$ laminate under a maximum cyclic stress equivalent to an applied 0.005 longitudinal strain on the pristine laminate, $R = 0.1$. Data taken from [54]
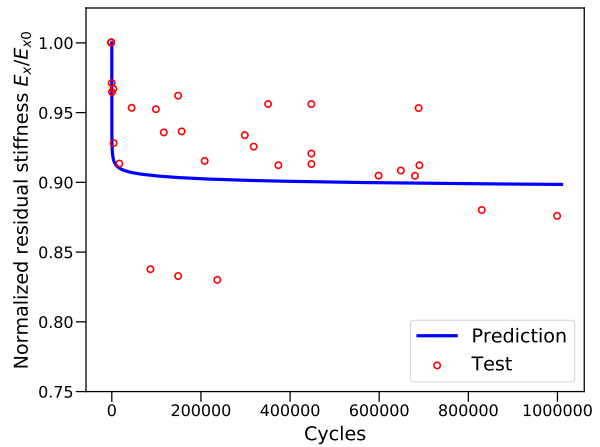
Figure A.3: Normalized longitudinal stiffness degradation for a $[0_2/90_4]_S$ T300/5208 laminate under a maximum cyclic stress equal to an applied 0.006 longitudinal strain on the pristine laminate, $R = 0.1$. Data taken from [54]
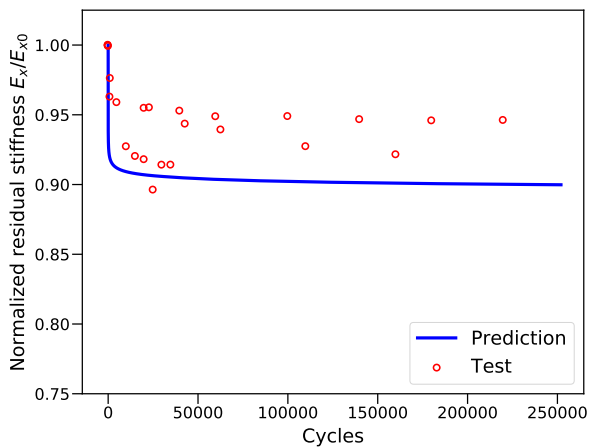
Figure A.4: Normalized longitudinal stiffness degradation for a $[0_2/90_4]_S$ T300/5208 laminate under a maximum cyclic stress equal to an applied 0.0065 longitudinal strain on the pristine laminate, $R = 0.1$. Data taken from [54]
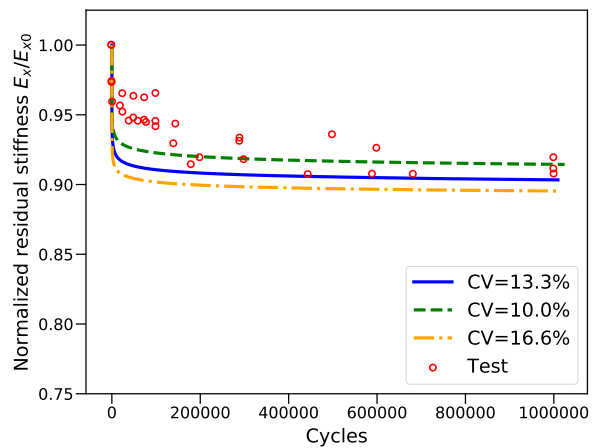
Figure A.5: Predictions based on the case from fig. A.2, using different coefficients of variation for the normally distributed transverse tensile strength. The "standard value" is 13.3%, as reported in table A.1. Data taken from [54]

Bibliography

[1] Bonora, N., La Barbera, A., Marchetti, M., and Milella, P. (1993). Experimental verification and theoretical simulation of fracture behaviours of composite materials. *Composite Structures*, pages 87–97.

[2] Camanho, P. and Davila, C. (2003). Numerical Simulation of Mixed-mode Progressive Delamination in Composite Materials. *Journal of Composite Materials*, 37(16):1415–1438.

[3] Camanho, P. P., Dávila, C. G., Pinho, S. T., Iannucci, L., and Robinson, P. (2006). Prediction of in situ strengths and matrix cracking in composites under transverse tension and in-plane shear. *Composites Part A: Applied Science and Manufacturing*, 37(2):165–176.

[4] Caron, J. F. and Ehrlacher, A. (1999). Modelling of fatigue microcracking kinetics in crossply composites and experimental validation. *Composites Science and Technology*, pages 1349–1359.

[5] Caslini, M., Zanotti, C., and O'Brien, T. K. (1987). Study of Matrix Cracking and Delamination in Glass/Epoxy Laminates. *Journal of Composites Technology and Research*, 9(4):121–130.

[6] Charewicz, A. and M., D. I. (1986). Damage mechanisms and accumulation in graphite/epoxy laminate. *Composite Materials: Fatigue and Fracture, ASTM STP 907*, pages 274–297.

[7] Chou, P. C. and Croman, R. (1978). Residual Strength in Fatigue Based on the Strength-Life Equal Rank Assumption. *Journal of Composite Materials*, pages 177–194.

[8] Daniel, I. M., Lee, J. W., and Yaniv, G. (1987). Damage mechanisms and stiffness degradation in graphite/epoxy composites. In *ICCM and ECCM (Sixth International Conference on Composite Materials and Second European Conference on Composite Materials)*, volume 4, pages 4.129–4.138.

[9] Daniel, I. M. and Lee, J, W. (1990). Damage Development in Composite Laminates Under Monotonic Loading. *Journal of Composites Technology and Research*, 12(2):98–102.

[10] Dávila, C. G., Camanho, P. P., and Rose, C. A. (2005). Failure criteria for FRP laminates. *Journal of Composite Materials*, 39(4):323–345.

[11] Degrieck, J. and Van Paepegem, W. (2001). Fatigue damage modeling of fibre-reinforced composite materials: Review. *Applied Mechanics Reviews*, 54(4):279.

[12] Donadon, M., Iannucci, L., Falzon, B., Hodgkinson, J., and de Almeida, S. (2008). A progressive failure model for composite laminates subjected to low velocity impact damage. *Computers & Structures*, 86(11-12):1232–1252.

[13] Dvorak, G. J., Laws, N., and Hejazi, M. (1985). Analysis of progressive matrix cracking in composite laminates I. Thermo elastic properties of a unidirectional composite with cracks. *Journal of Composite Materials*, 19(May 1985):216–234.

[14] Eliopoulos, E. N. and Philippidis, T. P. (2011a). A progressive damage simulation algorithm for GFRP composites under cyclic loading. Part I: Material constitutive model. *Composites Science and Technology*, 71(5):742–749.

[15] Eliopoulos, E. N. and Philippidis, T. P. (2011b). A progressive damage simulation algorithm for GFRP composites under cyclic loading. Part II: FE implementation and model validation. *Composites Science and Technology*, 71(5):750–757.

[16] Esrail, F. and Kassapoglou, C. (2014a). An efficient approach for damage quantification in quasi-isotropic composite laminates under low speed impact. *Composites Part B*, 61:116–126.

[17] Esrail, F. and Kassapoglou, C. (2014b). An efficient approach to determine compression after impact strength of quasi-isotropic composite laminates. *Composites Science and Technology*, 98:28–35.

[18] Farrokhabadi, A., Mohammadi, B., and Hosseini-Toudeshky, H. (2016). A simplified micromechanics model for predicting the stiffness degradation in symmetric composite laminates. *Fatigue & Fracture of Engineering Materials & Structures*, 38(11):1334–1346.

[19] Hahn, H. T. (1973). Nonlinear behavior of laminated composites. *Journal of Composite Materials*, 7(April 1973):257–271.

[20] Hahn, H. T. and Kim, R. Y. (1975). Proof Testing of Composite Materials. *Journal of Composite Materials*, pages 297–311.

[21] Hahn, H. T. and Tsai, S. W. (1973). Nonlinear Elastic Behavior of Unidirectional Composite Laminae. *Journal of Composite Materials*, 7(1):102–118.

[22] Hashin, Z. (1980). Failure Criteria for Unidirectional Fiber Composites. *Journal of Applied Mechanics*, 47(June 1980):329–334.

[23] Hashin, Z. (1985). Analysis of cracked laminates: a variational approach. *Mechanics of Materials*, 4:121–136.

[24] Hashin, Z. (1987). Analysis of Orthogonally Cracked Laminates Under Tension. *Journal of Applied Mechanics*, 54:872–879.

[25] Highsmith, A. L. and Reifsnider, K. L. (1982). Stiffness-Reduction Mechanisms in Composite Laminates. *Damage in Composite Materials, ASTM STP 775*, pages 103–117.

[26] Hwang, W. and Han, K. S. (1986a). *Cumulative Damage Models and Multi-Stress Fatigue Life Prediction*, volume 20.

[27] Hwang, W. and Han, K. S. (1986b). Fatigue of Composites—Fatigue Modulus Concept and Life Prediction. *Journal of Composite Materials*, 20(2):154–165.

[28] Jamison, R. and Reifsnider, K. (1982). Advanced Fatigue Damage Development in Graphite Epoxy Laminates. interim report for period 1 april 1981 to 1 december 1982. Technical report, AFWAL TR-82-3103.

[29] Joffe, R., Krasnikovs, A., and Varna, J. (2001). COD-based simulation of transverse cracking and stiffness reduction in [S/90n]s laminates. *Composites Science and Technology*, 61(5):637–656.

[30] Kassapoglou, C. (2007). Fatigue life prediction of composite structures under constant amplitude loading. *Journal of Composite Materials*, (22):2737–2754.

[31] Kassapoglou, C. (2010a). *Design and analysis of composite structures: With applications to aerospace structures*. Wiley.

[32] Kassapoglou, C. (2010b). Fatigue of composite materials under spectrum loading. *Composites Part A: Applied Science and Manufacturing*, 41(5):663–669.

[33] Kassapoglou, C. (2011). Fatigue model for composites based on the cycle-by-cycle probability of failure: Implications and applications. *Journal of Composite Materials*, 45(3):261–277.

[34] Kassapoglou, C. (2012). *Predicting the Structural Performance of Composite Structures Under Cycling Loading*. PhD thesis, Delft University of Technology.

[35] Kassapoglou, C. (2015). *Modeling the Effect of Damage in Composite Structures: Simplified Approaches, Chapter 6*. Wiley.

[36] Kassapoglou, C. and Kaminski, M. (2011). Modeling damage and load redistribution in composites under tension-tension fatigue loading. *Composites Part A: Applied Science and Manufacturing*, 42(11):1783–1792.

[37] Lafarie-Frenot, M. C. and Touchard, F. (1994). Comparative in-plane shear behaviour of long-carbon-fibre composites with thermoset or thermoplastic matrix. *Composites Science and Technology*, 52(3):417–425.

[38] Lagace, P. A. (1984). Nonlinear stress-strain behavior of graphite/epoxy laminates. In *25TH structures, structural dynamics and materials conference*, pages 63–73.

[39] Laws, N., Dvorak, G., and Hejazi, M. (1983). Stiffness changes in unidirectional composites caused by crack systems. *Mechanics of Materials*, 2:123–137.

[40] Lee, J. and Daniel, I. M. (1990). Progressive Transverse Cracking of Crossply Composite Laminates. *Journal of Composite Materials*, 24:1225–1243.

[41] Lee, J. W., Daniel, I. M., and Yaniv, G. (1989). Fatigue Life Prediction of Cross-Ply Composite Laminates. *Composite Materials: Fatigue and Fracture, Second Volume, ASTM STP 1012*, pages 19–28.

[42] Lopes, C., Camanho, P., Gürdal, Z., Maimí, P., and González, E. (2009). Low-velocity impact damage on dispersed stacking sequence laminates. Part II: Numerical simulations. *Composites Science and Technology*, 69(7-8):937–947.

[43] Mar, J. W. and Lin, K. Y. (1977a). Fracture mechanics correlation for tensile failure of filamentary composites with holes. *Journal of Aircraft*, 14:703–704.

[44] Mar, J. W. and Lin, K. Y. (1977b). Fracture of boron/aluminum composites with discontinuities. *Journal of Composite Materials*, 11:405–421.

[45] Masters, J. E. and Reifsnider, K. L. (1982). An Investigation of Cumulative Damage Development in Quasi-Isotropic Graphite/Epoxy Laminates. *Damage in Composite Materials, ASTM STP 775, K. L. Reifsnider, Ed., American Society for Testing and Materials*, pages 40–62.

[46] McKague, L., Reynolds, J., and Fruit, J. (1982). Mechanical Characteristics of T300-6K/V378A Graphite/Polyimlde. *Composite Materials: Testing and Design (Sixth Conference) ASTM STP 787*.

[47] Montesano, J., McCleavea, B., and Singh, C. V. (2018). Prediction of ply crack evolution and stiffness degradation in multidirectional symmetric laminates under multiaxial stress states. *Composites Part B*, 133:53–67.

[48] Naderi, M. and Maligno, A. R. (2012). Finite element simulation of fatigue life prediction in carbon/epoxy laminates. *Journal of Composite Materials*, 47(4):475–484.

[49] O'Brien, T. K. (1982). Characterization of delamination onset and growgth in a composite laminate. *Damage in Composite Materials, ASTM STP 775*, pages 140–167.

[50] Ogin, S. L., Smith, P. A., and Beaumont, P. W. R. (1985). Matrix cracking and stiffness reduction during the fatigue of a (0/90)s GFRP laminate. *Composites Science and Technology*, 22(1):23–31.

[51] Passipoularidis, V. A. and Brøndsted, P. (2009). *Fatigue Evaluation Algorithms : Review; Risø-R-Report 1740*.

[52] Reifsnider, K. L. (1990). *Composite materials series, Fatigue of composite materials (Vol. 4), Damage and damage mechanics (Ch. 2)*.

[53] Reifsnider, K. L. and Talug, A. (1980). Analysis of fatigue damage in composite laminates. *International Journal of Fatigue*, 2(1):3–11.

[54] Ryder, J. T. and Crossman, F. W. (1983). A Study of Stiffness, Residual Strength and Fatigue Life Relationships for Composite Laminates. Technical report, NASA & Lockheed-California Company.

[55] Sadeghi, G., Hosseini-Toudeshky, H., and Mohammadi, B. (2014). An investigation of matrix cracking damage evolution in composite laminates – Development of an advanced numerical tool. *Composite Structures*, 108:937–950.

[56] Shi, Y., Swait, T., and Soutis, C. (2012). Modelling damage evolution in composite laminates subjected to low velocity impact. *Composite Structures*, 94(9):2902–2913.

[57] Shirazi, A. and Varvani-Farahani, A. (2010). A stiffness degradation based fatigue damage model for FRP composites of $(0/\theta)$ laminate systems. *Applied Composite Materials*, 17(2):137–150.

[58] Soden, P. D., Hinton, M. J., and Kaddour, A. S. (1998). Lamina properties, lay-up configurations and loading conditions for a range of fibre-reinforced composite laminates. 58.

[59] Talreja, R. (1985). A continuum mechanics characterization of damage in composite materials. In *Proceedings of the Royal Society of London. Series A, Mathematical and Physical Sciences*, volume 399, pages 195–216.

[60] Talreja, R. (1986). Stiffness properties of composite laminates with matrix cracking and interior delamination. *Engineering Fracture Mechanics*, 25(5-6):751–762.

[61] Talreja, R. (1990). Internal variable damage mechanics of composite materials. *In: Yielding, damage and failure of anisotropic solids, London.*

[62] Talreja, R. (1996). A synergistic damage mechanics approach to durability of composite material systems. *In: Cardon A, Fukuda H, Reifsnider K, editors. Progress in durability analysis of composite systems. Rotterdam: A.A. Balkema.*

[63] Turon, A., Camanho, P. P., Costa, J., and Dávila, C. G. (2006). A damage model for the simulation of delamination in advanced composites under variable-mode loading. *Mechanics of Materials*, 38:1072–1089.

[64] United States Department of Defense (2012). *Composite Materials Handbook-17 (CMH-17-2G) Volume 2 - Polymer Matrix Composites - Material Properties.*

[65] Van Paepegem, W. (2010). Fatigue damage modelling of composite materials with the phenomenological residual stiffness approach. *Fatigue Life Prediction of Composites and Composite Structures*, pages 102–138.

[66] Van Paepegem, W., De Baere, I., and Degrieck, J. (2006a). Modelling the nonlinear shear stress-strain response of glass fibre-reinforced composites. Part II: Model development and finite element simulations. *Composites Science and Technology*, 66:1465–1478.

[67] Van Paepegem., W., De Baere, I., Lamkanfi, E., and Degrieck, J. (1990). Monitoring quasi-static and cyclic fatigue damage in fibre-reinforced plastics by Poisson's ratio evolution. *International Journal of Fatigue*, 32(1).

[68] Van Paepegem, W., Debaere, I., and Degrieck, J. (2006b). Modelling the nonlinear shear stress-strain response of glass fibre- reinforced composites. Part I: Experimental results. *Composites Science and Technology*, 66:1455–1478.

[69] Varna, J., Joffe, R., Akshantala, N. V., and Talreja, R. (1999). Damage in composite laminates with off-axis plies. *Composites Science and Technology*, 59:2139–2147.

[70] Varna, J., Joffe, R., and Talreja, R. (2001). A synergistic damage-mechanics analysis of transverse cracking $[\pm\Theta/90_4]$ laminates. *Composites Science and Technology*, 61(5):657–665.

[71] Vyas, G. M. and Pinho, S. T. (2012). Computational implementation of a novel constitutive model for multidirectional composites. *Computational Materials Science*, 51(1):217–224.

[72] Whitney, J. M. and Nuismer, R. J. (1974). Stress fracture criteria for laminated composites containing stress concentrations. *Journal of Composite Materials*, 8:253–265.

[73] Whitworth, H. (1990). Cumulative damage in composites. *Journal of Engineering Materials . . .*, pages 3–6.

[74] Whitworth, H. A. (1987). Modeling Stiffness Reduction of Graphite/Epoxy Composite Laminates. *Journal of Composite Materials*, 21(4):362–372.

[75] Whitworth, H. A. (1998). A stiffness degradation model for composite laminates under fatigue loading. *Composite Structures*, 40(2).

[76] Yang, J. N., Jones, D. L., Yang, S. H., and Meskini, A. (1990). A Stiffness Degradation Model for Graphite/Epoxy Laminates. *Journal of Composite Materials*, 24:753–769.

[77] Yang, J. N., Lee, L. J., and Sheu, D. Y. (1992). Modulus reduction and fatigue damage of matrix dominated composite laminates. *Composite Structures*, 21:91–100.